
# DISSERTATION

# Control of the plate motion and camber in a reversing rolling mill with edger rolls

Ausgeführt zum Zwecke der Erlangung des akademischen Grades eines
Doktors der technischen Wissenschaften (Dr. techn.)

unter der Leitung von
Univ.-Prof. Dipl.-Ing. Dr. techn. Andreas Kugi
E376
Institut für Automatisierungs- und Regelungstechnik

eingereicht an der
Technischen Universität Wien
Fakultät für Elektrotechnik und Informationstechnik

von
Dipl.-Ing. Christopher Pietschnig
Matrikelnummer: 1125819

Wien, November 2022

| | |
|---|---|
| Studiendekan: | Univ.-Prof. Dr.sc. Silvan Schmid |
| Betreuer: | Univ.-Prof. Dipl.-Ing. Dr. techn. Andreas Kugi |
| Tag des Rigorosums: | 02.12.2022 |
| Prüfungsvorsitzender: | O.Univ.-Prof. Dipl.-Ing. Dr. techn. Manfred Schrödl |
| Erster Gutachter: | Univ.-Prof. Dr. Ian K. Craig |
| Zweiter Gutachter: | Assoc.-Prof. Dipl.-Ing. Dr. techn. Andreas Steinböck |

# Vorwort

Die vorliegende Arbeit entstand im Rahmen meiner Tätigkeit als wissenschaftlicher Mitarbeiter im CD-Labor für Modellbasierte Prozessregelung in der Stahlindustrie am Institut für Automatisierungs- und Regelungstechnik (ACIN) der Technischen Universität Wien in Zusammenarbeit mit der Firma voestalpine Stahl GmbH. Ermöglicht wurde dieses Projekt durch die finanzielle Unterstützung von Seiten der Christian Doppler Forschungsgesellschaft und der voestalpine Stahl GmbH.

Ich bedanke mich an dieser Stelle sehr herzlich bei Univ.-Prof. Dipl.-Ing. Dr. techn. Andreas Kugi und Associate Prof. Dipl.-Ing. Dr. techn. Andreas Steinböck für das Ermöglichen und die hervorragende wissenschaftliche Betreuung dieser Arbeit sowie die durchgehende Unterstützung und fachliche Expertise. Vielen Dank, dass ihr Beiden stets eine offene Tür und ein offenes Ohr für uns Mitarbeiter habt wenn wir es brauchen!

Bedanken möchte ich mich auch bei allen Mitarbeitern der voestalpine Stahl GmbH die an diesem Projekt beteiligt waren. Mein besonderer Dank gilt hier Dipl.-Ing. Dr. techn. Florian Schausberger und Dipl.-Ing. (FH) Clemens Göttfert für die sehr enge und unkomplizierte Zusammenarbeit. Ohne ihr persönliches Engagement und das große Vertrauen in meine Arbeit wäre die Umsetzung der entwickelten Regelungskonzepte an der Industrieanlage der voestalpine in dieser Form wohl nicht möglich gewesen.

Ein herzliches Dankeschön geht zudem an alle aktuellen und ehemaligen Kolleginnen und Kollegen am ACIN. Vielen Dank für die unzähligen fachlichen Diskussionen, für das ausgezeichnete Arbeitsklima sowie gemeinsame Kipferlfrühstücke, Kaffeerunden und private Gespräche. Vielen Dank für die unvergessliche, gemeinsame Zeit! Auch wenn sich unsere Wege als Kollegen trennen mögen, mögen sie sich hoffentlich als Freunde schon bald wieder kreuzen.

Ganz besonders bedanke ich mich außerdem bei meiner Familie. Wenngleich sie während meines Studiums nicht immer genau wussten welchen Tätigkeiten ich an der Universität genau nachgehe, haben sie mir dennoch stets uneingeschränkt

vertraut und mich unterstützt. Ohne eure Unterstützung wäre all dies nicht möglich gewesen.

Zu guter Letzt danke ich dir liebe Verena. Danke für deine liebevolle Unterstützung, deine ruhigen und besonnene Art und deine Begleitung auf diesem Weg.

Wien, im November 2022 Christopher Pietschnig

# Abstract

In flat steel rolling, reversing hot rolling mills are typically used to reduce the thickness of steel slabs or plates. Some reversing rolling mills are equipped with edger rolls to adjust the width of the rolled plate. At best, the plate passes the roll gap laterally centered and has a perfect cuboid shape with defined geometries. In reality, lateral nonuniformities like temperature gradients and thickness inhomogeneities cause the plate to drift in a lateral direction. This can result in a camber or thickness wedge or both. These effects deteriorate the product quality and can also entail collisions with the mill stand or other equipment along the roller table. To prevent such problems, active control of the lateral position and contour shape is indispensable.

In this work, a reversing roughing mill of voestalpine Stahl GmbH, Linz, Austria is considered. The roll gap adjustment works electromechanically and self-retaining, meaning that it can only be adjusted between two consecutive rolling passes. The industrial plant is further equipped with edger rolls, originally intended to counteract spreading in forward rolling passes. This work, is dedicated to the question if these edger rolls are also suitable as an alternative control input to control the lateral position and centerline shape of the plate during the rolling passes by moving them in a lateral direction.

To this end, a dynamic model of the lateral plate motion during the rolling pass as well as for the resulting shape of the plate is derived and validated by measurement data, recorded at the industrial plant of voestalpine Stahl GmbH. The suitability of the edger rolls as an alternative control input for the plate motion and camber is then discussed based on the validated model.

For monitoring purposes and for feedback control, the industrial plant is equipped with two camera systems on the entry and exit side of the roll gap. With the camera systems, the plate motion in the field of view and its shape are recorded while passing through the roll gap. Clearly, plastic deformation takes place in the roll gap, which is inaccessible to machine vision or sensor systems.

Because the exit side camera is located a few meters downstream of the roll gap, the measurement of the plate shape is subject to a transport delay. However, the measured shape of the whole plate is available after every rolling pass is finished.

After discussing why edger rolls are a feasibility alternative control input, three control concepts are elaborated and their suitability for the industrial plant is examined. First, a linear quadratic regulator (LQR), which uses the lateral force applied by the edger rolls as a control input, is examined. For safety reasons, it is used in a cascade control structure with a subordinate admittance control. The lateral forces required by the outer control loop are thus converted into lateral edger positions by the inner control loop. For the second control strategy, the lateral force/position relation is considered in the mathematical model. This has the advantage that the inner control loop of the first strategy can be omitted. With this model, a two-degrees-of-freedom control strategy, which consists of an optimal feedforward control and a feedback controller with Smith predictor, is designed. In the previous concepts, only forward rolling passes (where edger rolls are active) and only one pass at a time are taken into account. The third and final extension uses the optimal feedforward controller and additionally predicts the optimal edger trajectories and roll gap tilts for all remaining rolling passes. These three concepts are then extensively discussed in simulation studies based on the validated mathematical model.

The thickness profile of the plate and the roll gap under load are not measured at the industrial plant. This makes it difficult to identify the sensitivity of this control input. Further, the impact of an incoming wedge and the roll gap tilt cannot be separated because both are assumed to be constant throughout the rolling pass and both have a similar influence on the shape of the outgoing plate centerline. Thus, the second approach is the most promising and feasible concept and was implemented at the industrial plant. The corresponding measurements show a significant improvement of the plates' final shape while ensuring a safe plate motion throughout the rolling pass.

# Kurzzusammenfassung

Beim Walzen von Stahl wird die Dicke von Stahlbrammen oder Vorstreifen üblicherweise zuerst in Reversierwalzgerüsten reduziert. Einige Reversierwalzgerüste sind mit Staucherwalzen ausgestattet, um die Breite der gewalzten Vorstreifen einzustellen. Im besten Fall durchlaufen Vorstreifen den Walzspalt mittig und verlassen ihn mit perfekter quaderförmiger Geometrie. In der Realität allerdings bewirken laterale Inhomogenitäten wie Temperaturgradienten und Dickeninhomogenitäten, dass sich der Vorstreifen in lateraler Richtung bewegt. Dies kann zu einer Krümmung, einem Dickenkeil oder beidem führen. Beide Effekte verschlechtern die Produktqualität und können im schlimmsten Fall zu Kollisionen mit dem Walzgerüst oder anderen Komponenten entlang des Rollgangs führen. Um solche Problemen zu vermeiden, ist eine Regelung der lateralen Position und Vorstreifenform unabdingbar.

In dieser Arbeit wird das Vorgerüst, ein Reversierwalzgerüst der voestalpine Stahl GmbH, Linz, Österreich, betrachtet. Die Walzspaltverstellung erfolgt elektromechanisch und selbsthaltend. Dies hat zur Folge, dass sie nur zwischen zwei aufeinanderfolgenden Walzstichen verstellt werden kann, nicht jedoch während eines Walzstiches. Das Vorgerüst ist außerdem mit Staucherwalzen ausgestattet. Diese sind ursprünglich dazu gedacht, der Verbreiterung des Vorstreifens in Vorwärtsstichen entgegenzuwirken. Diese Arbeit widmet sich nun der Frage, ob diese Staucherwalzen auch als alternativer Stelleingang geeignet sind, um die laterale Position und Mittellinienform des Vorstreifens während der Walzstiche zu regeln, indem sie in lateraler Richtung bewegt werden.

Dazu wird ein dynamisches Modell der lateralen Vorstreifenbewegung während des Walzstichs sowie der resultierenden Vorstreifenform erstellt und anhand von Messdaten validiert, welche am Vorgerüst der voestalpine Stahl GmbH aufgenommen wurden. Anschließend wird anhand des validierten Modells die Eignung der Staucherwalzen als alternativer Stelleingang für die Vorstreifenbewegung und die Krümmung diskutiert.

Zur Messung und Regelung von Position und Form der Vorstreifen ist das Vorgerüst mit zwei Kamerasystemen auf der Einlauf- und Auslaufseite des Walzspalts ausgestattet. Mit den Kamerasystemen wird die Vorstreifenbewegung im Sichtfeld und deren Form erfasst. Plastische Verformung findet im Walzenspalt statt. Dieser ist allerdings für Sensorsysteme und Messungen unzugänglich. Da sich die auslaufseitige Kamera einige Meter hinter dem Walzenspalt befindet, unterliegt die Messung der Vorstreifenform einer Transportverzögerung. Die gemessene Form des gesamten Vorstreifens steht jedoch nach Abschluss jedes Walzstichs zur Verfügung.

Nach der Diskussion, warum Staucherwalzen ein geeigneter alternativer Stelleingang sind, werden drei Regelungskonzepte ausgearbeitet und auf ihre Eignung für das Vorgerüst untersucht. Zunächst wird ein linear-quadratischer Regler (LQR) entworfen, welcher die von den Staucherwalzen aufgebrachte laterale Kraft als Stelleingang verwendet. Aus Sicherheitsgründen wird eine kaskadierte Regelung mit unterlagerter Admittanzregelung eingesetzt. Die vom äußeren Regelkreis geforderten lateralen Kräfte werden somit vom inneren Regelkreis in laterale Staucherpositionen umgerechnet. Für die zweite Regelungsstrategie wird die laterale Kraft/Positionsbeziehung im mathematischen Modell berücksichtigt. Dadurch ergibt sich der Vorteil, dass der innere Regelkreis der ersten Strategie entfallen kann. Mit diesem Modell wird eine Regelungsstrategie mit zwei Freiheitsgraden entworfen, die aus einer optimierungsbasierten Vorsteuerung und einem Regler mit Smith-Prädiktor besteht. Bei den bisherigen Konzepten werden nur Vorwärtsstiche (bei denen Staucherwalzen aktiv sind) und jeweils nur ein einzelner Stich berücksichtigt. Die dritte und letzte Erweiterung nutzt die optimierungsbasierte Vorsteuerung und berechnet die optimale Stauchertrajektorie und Walzspaltneigungen für alle verbleibenden Walzstiche im voraus. Diese drei Konzepte werden anschließend ausführlich in Simulationsstudien basierend auf dem validierten mathematischen Modell diskutiert.

Das Dickenprofil des Vorstreifens und der Walzspalt unter Last werden am Vorgerüst nicht vermessen. Dies macht es schwierig, die Sensitivität dieser Systemeingänge zu identifizieren. Außerdem kann der Einfluss eines einlaufenden Dickenkeils und die Walzspaltneigung nicht getrennt erfasst werden, da angenommen wird, dass beide während des gesamten Walzstichs konstant sind und beide einen ähnlichen Einfluss auf die Form der Mittellinie des auslaufenden Vorstreifens haben. Somit ist der zweite Ansatz das vielversprechendste Konzept und wurde am Vorgerüst implementiert. Die entsprechenden Messungen zeigen eine signifikante Verbesserung der finalen Vorstreifenform bei gleichzeitiger Gewährleistung einer sicheren Vorstreifenbewegung während des gesamten Walzstichs.

# Contents

# List of symbols

### General notation

| | |
|---|---|
| AC | admittance control |
| AWP | anti-wind-up |
| CCD | charge coupled device |
| CMOS | complementary metal oxide semiconductor |
| DLL | dynamic link library |
| FEM | finite element method |
| FOV | field of view |
| LQR | linear quadratic regulator |
| MPC | model predictive control |
| TCP | transmission control protocol |

### Latin symbols

| | |
|---|---|
| $\Delta\bar{w}$ | mean width change due to edge rolling |
| $\Delta w_{DS}$, $\Delta w_{OS}$ | width change on the drive and operator side |
| $\Delta X$ | lateral offset due to asymmetric edge rolling |
| $\Delta z^{-}$ | spatial step size |
| $\Delta\mathbf{U}$ | input vector |
| $\mathcal{O}$ | observability matrix |
| $\mathcal{R}$ | controllability matrix |
| $\tilde{F}$ | force related to the admittance controller |
| $\tilde{h}^{-}$ | thickness profile of the plate after edge rolling |
| $\mathbf{1}$ | vector of ones |

| | |
|---|---|
| $\mathcal{U}$, $\mathcal{Y}$ | extended input and output vector |
| $\mathbf{A}$, $\mathbf{B}$ | dynamic and input matrix of the position-input model |
| $\mathbf{cl}$ | discretized vector of the plate centerline |
| $\mathbf{CL}^-$ | discretized incoming plate centerline |
| $\mathbf{CL}_{\Delta hH}$ | discretized changes of the plate centerline due to thickness wedge and roll gap tilt |
| $\mathbf{C}$ | output matrix |
| $\mathbf{DD}$ | matrix for numerical approximation of the second derivative |
| $\mathbf{D}$ | input matrix |
| $\mathbf{d}$ | vector of exogenous inputs |
| $\mathbf{F}_x$, $\mathbf{F}_u$ | matrices for the MPC |
| $\mathbf{F}_{\Delta h}$, $\mathbf{F}_{\Delta H}$ | matrices for the MPC |
| $\mathbf{F}_{\Delta u}$, $\mathbf{F}_{cl}$ | matrices for the MPC |
| $\mathbf{G}$, $\mathbf{H}$ | input matrix for exogenous inputs |
| $\mathbf{K}_x$, $\mathbf{K}_d$ | control gain matrix |
| $\mathbf{P}$ | matrix of the discrete algebraic Riccati equation |
| $\mathbf{Q}$, $\mathbf{R}$ | weighting matrices |
| $\mathbf{S}$ | rotation and translation matrix |
| $\mathbf{u}$ | input vector of the position-input model |
| $\mathbf{x}$ | state vector of the position-input model |
| $\mathbf{Y}$ | output vector |
| $\mathbf{y}$ | output vector |
| $\mathbf{z}$ | discretized vector of the plate length |
| $a$ | lateral acceleration of the edger rolls |
| $A_s$ | shear area of the plate |
| $b_1^-$, $b_2^-$, $b_1^+$ | abbreviation in the force-input model |
| $cl$ | centerline |
| $cl^-$, $cl^+$ | centerline of the incoming and outgoing plate |
| $cl_{x,u}$ | changes of the plate centerline due to changes of the edger rolls' lateral position |
| $d^-$, $d^+$ | abbreviation in the force-input model |
| $E$ | Young's modulus |
| $e$ | control error |
| $E_h$, $E_l$ | nominal and reduced Young's modulus in the roll gap |
| $e_{rms}$ | shape error |
| $F$ | lateral force applied to the plate |
| $F_\Sigma$ | sum of the roll forces on the drive side and operator side |

| | |
|---|---|
| $F_R$ | roll force |
| $F_u$ | lateral force on a single edger roll |
| $F_u^\Sigma$ | sum of the edger forces on the drive side and operator side |
| $f_{E_l}$, $f_{K_\Sigma}$, $f_{\Delta hH}$ | normalizing factors for the parameter estimation |
| $F_{u,fric}$ | lateral friction force on a single edger roll |
| $G$ | shear modulus |
| $G_h$, $G_l$ | nominal and reduced shear modulus in the roll gap |
| $G_{a,b}$ | transfer function from input $a$ to output $b$ |
| $H$ | height of the roll gap |
| $h$ | thickness of the plate |
| $h_0^-$ | initial plate thickness, before edge rolling |
| $h_n$ | height of the neutral plane |
| $H_W$ | additional height, caused by mill stretch |
| $H_{adj}$ | adjusted roll gap height |
| $I_y$ | area momentum of inertia of the beam |
| $J$ | cost function |
| $k^+$ | stiffness related to the force on the exit side |
| $k^-$ | stiffness related to the force on the entry side |
| $k^P$, $k^I$ | control parameter |
| $k_1^d$, $k_2^d$ | parameters for the admittance controller |
| $K_\Sigma$ | sensitivities $K_{\Sigma^-}^-$, $K_{\Sigma^+}^-$, $K_{\Sigma^-}^+$ and $K_{\Sigma^+}^+$ |
| $K_h^+$, $K_H^+$ | sensitivity |
| $K_h^-$, $K_H^-$ | sensitivity |
| $k_r$ | residual term |
| $k_W$ | asymmetric mill stretch |
| $K_{\Sigma^-}^+$, $K_{\Sigma^+}^+$ | sensitivity |
| $K_{\Sigma^-}^-$, $K_{\Sigma^+}^-$ | sensitivity |
| $k_{fm}$ | mean yield stress of the plate material |
| $k_{u^\pm}$ | eigenvalue of the position-input model |
| $L$ | length of the neutral plane |
| $L^-$, $L^+$ | length of the incoming and outgoing plate |
| $l_e$ | distance between the edger rolls and the roll gap |
| $l_{FOV}$ | distance between the field of view and the roll gap |
| $M$ | bending moment |
| $m^d$, $d^d$, $k^d$ | desired mass, damping and stiffness for the admittance controller |
| $m_0$, $d_0$, $k_0$ | nominal mass, damping and stiffness for the admittance controller |

| | |
|---|---|
| $m_{\Delta,G}$, $m_{\Delta,M}$ | mill and material modulus |
| $N$ | number of discretization steps |
| $P$ | control gain |
| $Q$ | shear force |
| $q_{roll}$ | local roll force per unit width |
| $R_e$ | radius of the edger rolls |
| $r_v$, $r_C$, $r_H$, $r_{off}$ | model parameters for friction force of the edger rolls |
| $RP$ | number of rolling passes |
| $s$ | Laplace variable |
| $s_1$, $s_2$ | scalar parameter |
| $T$ | scalar weighting factor |
| $t$ | time |
| $T_s$ | sampling time |
| $u$ | lateral position of the edger rolls |
| $u_r$ | circumferential speed of the work rolls |
| $V$ | material velocity profile |
| $v$ | lateral velocity of the edger rolls |
| $v_0$ | model parameter for friction force of the edger rolls |
| $V_1$ | gain parameter |
| $v_{en}$ | mean entry velocity of the plate |
| $W$ | lateral position of the plate in the roll gap |
| $w$ | lateral position of the plate |
| $w_0$, $w_1$ | width of the incoming plate before and after edge rolling |
| $W_{0,offset}$ | offset value for the initial plate position in the roll gap |
| $w_{cyl}$ | distance between the cylinders on the drive side and operator side |
| $X$ | Lagrangian coordinate in lateral direction |
| $x$, $y$, $z$ | Cartesian coordinate frame located at the center of the mill stand |
| $Y$ | Lagrangian coordinate in transversal direction |
| $z_{in}$ | processed plate length |

### Greek symbols

| | |
|---|---|
| $\chi_F$, $\chi_{cl}$ | scalar weighting parameters |
| $\Delta$ | difference value |
| $\gamma$ | small angle of plate rotation |
| $\kappa$ | curvature of the beam |

| | |
|---|---|
| $\kappa_{x,u}$ | changes of the curvature of the beam due to changes of the edger rolls' lateral position |
| $\lambda$ | ratio of the mean input and mean output plate thickness |
| $\lambda_{1,2}^{-}$ | eigenvalues of the specialized model |
| $\lambda_{u^{\pm}}$ | eigenvalues of the position-input model |
| $\mu$ | mean value of the plate centerline |
| $\nu$ | Poisson's ratio |
| $\omega$ | angular velocity of the plate in the roll gap |
| $\Phi$ | angular displacement of the plate in the roll gap |
| $\Sigma$ | tensile stress |
| $\varphi$ | angular displacement of the plate |
| $\vartheta$ | represents $\Sigma^{-}$, $\Sigma^{+}$, $H$ or $h^{-}$ |
| $\boldsymbol{\chi}_{\mathcal{U}}$, $\boldsymbol{\chi}_{\mathcal{Y}}$ | weighting matrices |
| $\boldsymbol{\chi}_{Y}$, $\boldsymbol{\chi}_{\Delta u}$ | weighting matrices |
| $\boldsymbol{\Phi}$, $\boldsymbol{\Gamma}$ | discretized dynamic and input matrix |
| $\zeta$ | independent variable for the length of the outgoing plate |

**Subscripts**

| | |
|---|---|
| 0 | usually designating an initial value |
| $\alpha$ | represents quantities on the input, output or both sides of the roll gap $\{i, o, b\}$ |
| $\Delta H$ | quantity belonging to the roll gap tilt |
| $\Delta h$ | quantity belonging to the thickness wedge |
| $\Delta hH$ | quantity belonging to the linear combination of the thickness wedge and roll gap tilt |
| $\kappa$ | quantity belonging to the curvature |
| $b$ | quantity of backward rolling passes |
| $DS$, $OS$ | quantities on the drive or operator side |
| $F$ | quantity of the force-input model |
| $f$ | quantity of forward rolling passes |
| $k$ | index |
| $max$ | maximum value |
| $meas$ | measured quantity |
| $par$ | quantity of the parameter estimation |
| $s$ | stationary value |

### Superscripts

| | |
|---|---|
| $*$ | optimal value |
| $+$ | quantities on the exit side of the roll gap |
| $-$ | quantities on the entry side of the roll gap |
| $(j)$ | $j$-th rolling pass |
| $cam$ | quantity determined based on the lateral position obtained by the camera measurement |
| $cl$ | quantity determined based on the plate centerline obtained by the camera measurement |
| $d$ | desired value |
| $DS$, $OS$ | quantities on the drive or operator side |
| $FB$ | feedback |
| $FF$ | feedforward |
| $meas$ | measured quantity |

### Diacritics

| | |
|---|---|
| $\bar{(\cdot)}$ | mean value |
| $\breve{(\cdot)}$ | estimated version of the corresponding parameter |
| $\tilde{(\cdot)}$ | rotated and shifted version of the corresponding plate centerline |

### Operators

| | |
|---|---|
| $\frac{\mathrm{D}}{\mathrm{D}t}$ | material time derivative |
| $\frac{\mathrm{d}}{\mathrm{d}t} = \dot{(\cdot)}$ | total time derivative |
| $\frac{\mathrm{d}}{\mathrm{d}z_{in}} = (\cdot)'$ | total spatial derivative |
| $\frac{\partial}{\partial z}$ | partial spatial derivative |
| $\frac{\partial}{\partial t}$ | partial time derivative |

# CHAPTER 1

# Introduction

Steel is one of the most commonly used materials in industrial production. As the global economy expands, so does the demand for steel. More than three-quarters of the globally processed steel distributes on building and infrastructure (52%), mechanical equipment (16%), and automotive applications (12%) [1]. In all of these applications, safety, durability and thus high quality requirements are crucial. Due to the nature of the process, steel production causes high energy consumption and significant emissions. With about 10%, the steel industry makes a significant contribution to global CO2 emissions. Hence, a large number of research and development activities focus on the improvement of the sustainability of steel. For the production, this also means to minimize scrap and rejects.

This work deals with a heavy plate roughing mill and the quality improvement of the finished products. The quality of the final product is mainly characterized by its geometry in form of the shape of the plate as seen from the top view and the thickness profile of the plate. Maximizing the product quality minimizes rejects, maximizes the usable area of the plate and thus minimizes scrap. The quality of the plate is also essential for safe processing. Imperfections of the product shape and thickness profile are mainly caused by lateral inhomogeneous rolling conditions, e. g., variations of the temperature profile and, the incoming plate thickness, asymmetric mill stretch as well as an off-centered position of the rolled plate. Understanding the roughing process and compensating for various disturbances using active control methods is the content and motivation of the present work.

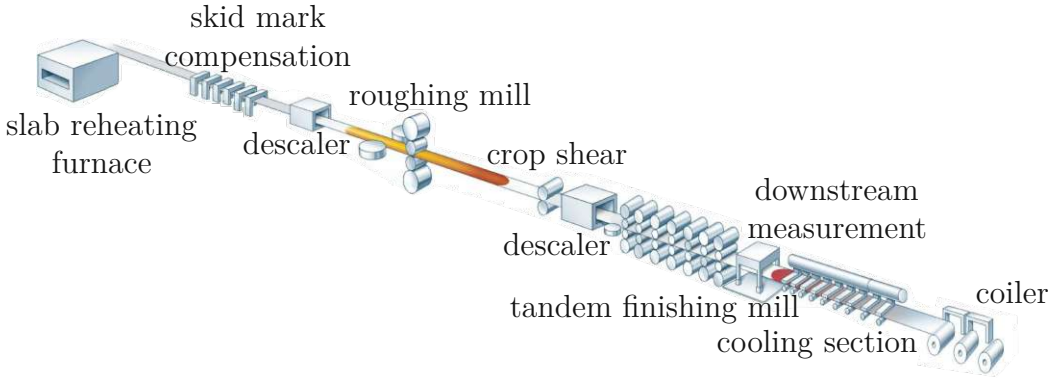


Figure 1.1: Schematic overview of the processing line at voestalpine Stahl GmbH (Linz, Austria).

## 1.1 The roughing process

In this work, the hot strip rolling plant of voestalpine in Linz, Austria is considered. Figure 1.1 shows a schematic overview of this processing line. At the beginning, molten steel is cast into steel slabs. After solidification, these steel slabs are stored so that they cool down to room temperature. Then they are reheated either in a pusher-type furnace or a walking-beam furnace, depending on the particular product. In the pusher-type furnace, slabs are placed on cooled skids, which typically cause longitudinal temperature inhomogeneities (temperature skid marks). An inductive skid mark compensation system counteracts these inhomogeneities. In the walking-beam furnace, the slabs are alternately carried by different skids, which constantly changes the contact area and thus skid marks are less distinct. In the rolling plant, the steel slabs are transported on roller tables. Before the slabs arrive at the roughing mill, they are descaled.

The roughing mill is a single 4-high reversing roughing mill stand where the slabs are reduced in five or seven consecutive reversing rolling passes to their final thickness. In this processing step, slabs are typically reduced from about 200 mm to about 30 mm thickness. This thickness reduction yields an elongation from about 10 m to about 70 m. To counteract spreading and to control the width of the plate, edger rolls are mounted upstream of the work rolls. Those edger rolls are only active in forward rolling passes and ensure a width of typically 1 m to 1.6 m. After the roughing process, the thickness profile, the temperature profile, and the shape of the plate as seen from the top view are accurately measured. After roughing, the product is typically called strip.

Before entering the tandem finishing mill, the strip passes the crop shear, where the head and tail end of the strip are cut off to get a straight edge shape, as well as another descaler. In the tandem finishing mill, seven consecutive 4-high mill stands reduce the thickness of the steel strip to its final thickness of about 0.8 mm to 20 mm. Since the product quality has to be guaranteed, the thickness

Figure 1.2: The considered mill stand at voestalpine Stahl GmbH (Linz, Austria).

and temperature profile as well as the shape of the strip as seen from the top view are measured again. The cooling section cools down the strip in a controlled manner to obtain the desired mechanical properties of the strip material. Finally, the strip has a length of up to 1.5 km, is coiled, and is then ready for sale or further processing, e. g., hot-dip galvanizing.

In this work, the roughing mill of voestalpine Stahl GmbH (Linz, Austria) is considered, see Figure 1.2. Figure 1.3 shows a schematic sketch of such a roughing mill. The mill stand consists of two work rolls and two backup rolls. The plate thickness is reduced between the work rolls. The backup rolls counteract the bending deflection of the work rolls caused by the high rolling forces.

Before every rolling pass, the roll gap height is adjusted to achieve the desired thickness reduction. Self-retaining screws control the roll gap height, meaning that the roll gap cannot be adjusted under load but only between the rolling passes. The resulting roll gap height (nominal height plus elastic deflection) is decisive for the exit thickness profile of the plate. This adjustment of the roll gap height between two rolling passes constitutes a possible control input for the roughing process.

To control the width of the plate, edger rolls are mounted upstream of the roll gap. Their lateral position is hydraulically adjusted. The edger rolls counteract spreading by symmetrically moving the edger rolls together in lateral direction. The lateral movement of the edger rolls represents a control input for the roughing process. This control input can be adjusted also during the rolling passes.

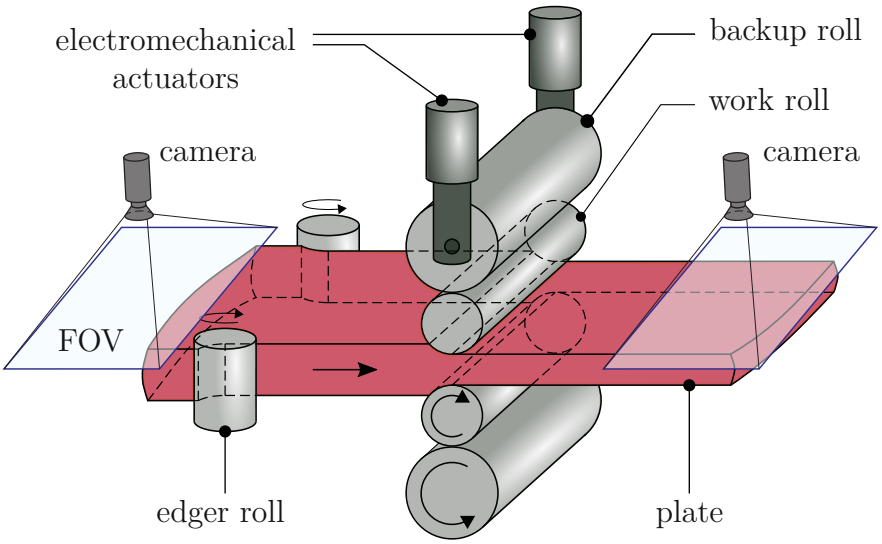


Figure 1.3: Reversing roughing mill: forward pass with active edger rolls.

## 1.2 Problem description and objectives of this work

Steel plates are transported to the roughing mill on a roller table. Before the first forward rolling pass, the steel plate is centered by side guides so that it enters the edger rolls and the roll gap at their lateral center position. During the rolling passes, edger rolls remain laterally centered. The roll gap height is adjusted based on an externally defined schedule and the roll gap tilt is manually defined by experienced operators. Depending on the thickness profile and the shape, measured after the tandem finishing mill, the operator changes the roll gap tilt for upcoming plates. Ideally, the plate centerline coincides with the lateral centerline of the rolling mill and the desired rectangular plate shape is perfectly realized (no wedge, no camber). Because of external asymmetric lateral forces, applied by side guides, edger rolls or the roller table, as well as inhomogeneities in the lateral temperature and/or thickness profile caused by the casting or the reheating process, the plate experiences deformation and tends to rotate in the roll gap with respect to the vertical axis. This further leads to asymmetric rolling conditions, an off-centered position of the plate in the work rolls and the outgoing plate forms a camber (cf. Figure 1.4), a thickness wedge or both. Imperfections of the plate shape not only reduce the product quality. In the worst case, they can cause excessive wear of the side guides or even collisions with the rolling mill or equipment along the roller table. In case of excessive camber at the head end, for safety reasons the plate is not threaded in the subsequent tandem finishing mill but scrapped. Summarizing, high repair costs, unproductive downtime of the plant, and a waste of energy may be the consequences of excessive camber.

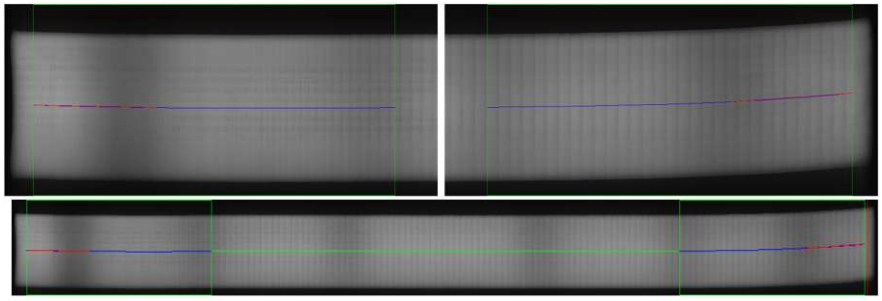

Figure 1.4: Typical shape of the resulting plate in top view, recorded after roughing. The head end of the plate (right side of the image) shows a significant camber.

An important objective of this work is the reduction of the final plates' camber compared to the current roughing process at the considered industrial plant. This should reduce scrap, improve the quality of the final product, and also minimize contact and thus wear of side guides and snaking in the downstream tandem finishing mill. The safety of the industrial plant is always of superior importance.

In most roughing mills, the roll gap tilt is hydraulically adjusted. This is the state-of-the-art control input to control the lateral motion and the camber of the outgoing plate [2, 3]. In the considered roughing mill, the roll gap tilt cannot be adjusted during a rolling pass but only between the rolling passes. This lack of the state-of-the-art control input provokes the following research question for this thesis: *Are edger rolls useful to control the plate motion and the camber in a reversing rolling mill?* A follow-up question can be formulated as follows: *If yes, what are possible control strategies to minimize camber and lateral displacements of the plate?*

To answer these questions, a detailed mathematical model that yields the lateral position of the plate in the roll gap as well as the camber of the outgoing plate is developed, validated based on measurements, and analyzed in simulation studies. Based on this mathematical model, new control concepts are derived, tested in simulations, and compared to the status quo at the industrial plant.

Summarizing, the objectives of this work are threefold:

- Use edger rolls as new control input.
- Safe plate motion: Avoid unwanted contact of the plate with side guides or other parts along the line.
- Correct shape: The final plate should be straight (zero camber) and its thickness should be uniform (zero thickness wedge).

## 1.3 State of the art and contributions of this work

In view of the extensive literature, only a brief overview is given in the following.

The roughing process is often analyzed by the finite element method (FEM) [4–8]. These works focus on the question how camber occurs and how it can be reduced. While [4] suggests to reduce camber by tilting the rolls during the rolling pass, [5–8] propose to influence the camber by exerting lateral forces on the plate while it is clamped in the roll gap. Although the effect of exerting forces on the plate to reduce camber is found to be strong, these works neither consider the lateral plate motion nor do they propose a suitable (feedback) control concept that uses the lateral forces.

An undesirable effect, which is often discussed when edger rolls are used in a roughing mill, is the dog-bone effect. It means that the slab bulges near the edger rolls and thus changes its cross sectional shape from a rectangle to a dog-bone shape. The dog-bone effect is mainly analyzed by FEM studies [9–13].

Other works focus on modeling lateral plate motion [14] and camber evolution [15, 16] by first principles. In [14], a mathematical model of the lateral plate motion in a roughing mill is proposed and used to analyze how the plate motion can be influenced by exerting lateral forces with edger rolls. It is further investigated how forces on the entry or exit side of the roll gap influence the stability of the plate motion. In [15], the contour evolution during the rolling process is modeled with a continuum mechanics approach. A review of models for the evolution of the plate contour is given in [16]. There, it is discussed how different effects like thickness inhomogeneities, roll gap alignment or lateral forces influence the resulting camber.

The works [17–22] focus on detailed mathematical models of a single mill stand. In [17–19], mathematical models of the plastic deformation of the strip in the roll gap and the elastic deformation of the mill stand are derived. These models are used to improve the accuracy and uniformity of the thickness profile by model-based control. The works [20, 21] expand these findings by including disturbances caused by roll gap lubrication in the mathematical model. This extended model serves as a basis for a two-degrees-of-freedom control structure to control the exit strip thickness [22].

The works [23, 24] follow a data-driven approach to predict the camber. The method from [23] combines a model-based and machine-learning approach to predict and control the camber of the outgoing plate. A machine vision method is used for the camber measurement. The combined model is then used to control the roll gap tilt to reduce the camber of the outgoing plate. In [24], a neural network is trained and the sensitivities of the outgoing camber with respect to different plant parameters are analyzed in detail.

The shape of the plate as seen from the top view has to be captured to

measure the camber, which, for instance, is required for feedback control. In the literature, different strategies for camber measurement are documented. In [25], three position measurement devices are employed to obtain a polynomial representation of the product contour. The measured contour is then used for feedback control of the product curvature. More recent works like [26–32] use 2D-CCD or CMOS cameras to capture top views of the plate. Afterwards, image processing techniques like edge detection (e. g., the Canny algorithm [33]) and image stitching are employed to get the product contour. In [34–37], the main focus is the measurement of the lateral strip position in a finishing mill, whereas the contour is of minor importance. In [35] and [36], the measured lateral strip position is used for strip steering control. In addition, [38] focuses on stabilizing the process in longitudinal direction.

Most of the existing solutions concentrate on measuring either the plate contour (heavy plates in roughing mills) or the lateral position (strips in finishing mills). In contrast in [39], both the motion and the contour of the plate are of major interest. In [39], a dynamic model of a heavy-plate roughing mill is reported and both the lateral plate motion and the plate contour are estimated in real time using an optimization-based approach. The measurement system used in the current work is based on [39].

Currently, camber is often manually controlled by experienced operators, meaning that the work rolls are tilted based on the result of previous rolling passes. There are also efforts to improve the skills of these operators [40]. However, the most promising technique to reduce camber is the use of appropriate feedback control methods. In [2, 3] for example, the camber evolution in roughing mills is controlled using hydraulically adjustable work rolls. In fact, the work roll tilt serves as a control input for camber reduction. This control input can also be adjusted while the plate moves through the roll gap.

In contrast, the roll gap tilt is electromechanically adjusted by self-retaining screws in the considered industrial plant. Thus, the roll gap tilt cannot be modified during a rolling pass but only between the passes. However, the plant is equipped with edger rolls that can be moved also during the rolling pass. In this work, the effectiveness of edger rolls as control input is investigated. To this end, two different formulations of a mathematical model, namely the *force-input model* and the *position-input model*, are derived and analyzed in detail. Each of these models is then used to design optimization-based control concepts with the objective to improve the lateral plate motion and the camber of the rolled plate. The advantages and limitations of the respective model and control concept are discussed in detail in the respective section (Section 2.2, Section 2.4, Chapter 4).

Some parts of this research work are already published in the following journal and conference articles.

[41] C. Pietschnig, A. Ettl, U. Knechtelsdorfer, A. Steinboeck, and A. Kugi, “Optimal control of plate motion and camber in a reversing rolling mill”,

*IFAC-PapersOnLine*, vol. 53, no. 2, pp. 11 962–11 967, 2020.

[37] F. Schausberger, C. Pietschnig, A. Ettl, A. Steinboeck, and A. Kugi, "Optimization-based estimator for the lateral strip position in tandem hot rolling", *IFAC-PapersOnLine*, vol. 54, no. 11, pp. 7–12, 2021.

[42] C. Pietschnig, A. Steinboeck, and A. Kugi, "Are edger rolls useful to control the plate motion and camber in a reversing rolling mill?", *Journal of Process Control*, vol. 114, pp. 71–81, 2022.

[43] C. Pietschnig, A. Steinboeck, and A. Kugi, "Optimal control of motion and camber of steel plates in a multi-pass reversing rolling process", *IFAC-PapersOnLine*, vol. 55, no. 21, pp. 180–185, 2022.

## 1.4 Structure of this thesis

The thesis is organized as follows: In Chapter 2, mathematical models of the lateral plate motion during the rolling passes as well as the resulting shape of the plate centerline are developed. In a first step, these models use the lateral forces applied by the edger rolls as inputs. Reformulated versions of these models use the lateral edger position as a control input. Based on these models, a system analysis regarding stability and the limits of the proposed control inputs is performed.

Chapter 3 describes the measurement systems at the considered industrial plant as well as its limitations due to the harsh environmental conditions. This chapter also deals with the estimation of uncertain parameters and with the validation of the mathematical model.

The validated mathematical model then serves as a basis for control design in Chapter 4. First, a control concept using the lateral forces applied by the edger rolls is investigated. Here, an LQR with subordinate admittance controller to limit the lateral position and velocity of the edger rolls is suggested. The second proposed control concept directly uses the lateral position of the edger rolls as control input. Here, a two-degrees-of-freedom control concept containing an optimization-based feedforward controller and a proportional feedback controller with Smith predictor is proposed. In these two concepts, only a single forward rolling pass is considered at a time. In contrast, the third proposed control concept covers the whole rolling process from the first until the last rolling pass and uses the constant roll gap tilts as well as the trajectories of the edger rolls' lateral position as control inputs.

The implementation at the industrial plant and the corresponding results are summarized and discussed in Chapter 5.

Finally, Chapter 6 summarizes the outcomes of the thesis, gives conclusions, and suggests further possible research activities in this field.

# CHAPTER 2

# Mathematical model

In this chapter, two mathematical models are developed. Each of them models the lateral plate motion and the camber of the outgoing plate.

- **Force-input model**: The model considers lateral forces applied to the plate (e. g., by edger rolls) at the entry and exit side of the roll gap, the shape of the incoming plate, an incoming thickness wedge, and the roll gap tilt as model inputs.

- **Position-input model**: To prevent inordinately large lateral edger positions, the force-input model is reformulated so that the lateral forces applied to the plate are replaced by the lateral position of the edger rolls as model input.

Using an elastoplastic modeling approach, it is analyzed how the different model inputs influence the dynamic behavior of the plate in the roll gap and the shape of the outgoing plate. The analysis shows the benefits and limitations of potential control inputs. After a discussion of the general models, they are adapted to the properties of the considered industrial plant. This yields two separate mathematical models for forward rolling passes and backward rolling passes. Moreover, the consequences of the mill stretch and the dog-bone effect, two effects which are often discussed in the context of roughing mills, are investigated.

Large parts of this section are similar to the author's publications [41, 42]. The models built in this chapter will be used for simulation and will be compared to measurement results from the industrial plant in Chapter 3. Moreover, the models will serve as a basis for control design in Chapter 4.

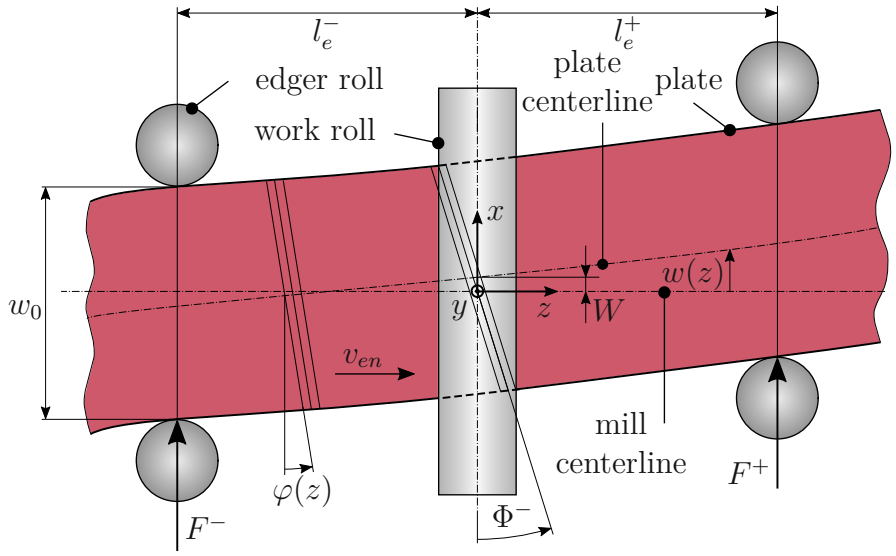


Figure 2.1: Top view of the plate in the rolling mill with edger rolls on the entry and exit side of the roll gap.

## 2.1 Derivation of the force-input model

In this section, the lateral plate motion and the camber of the outgoing plate are modeled. Figure 2.1 shows a top view of the plate and the rolling mill. The global coordinate frame $(x, y, z)$ is located at the center of the mill stand. For quantities at the entry side, the superscript $-$ (e. g., $l_e^-$ for the distance of the edger rolls on the entry side) and on the exit side, the superscript $+$ (e. g., $l_e^+$ for the distance of the edgers rolls on the exit side) will be used. For brevity, the arguments $t$ for the time and $z$ for the longitudinal position are omitted whenever confusion is ruled out.

### 2.1.1 Dynamic model of the lateral plate motion

The mathematical model of the plate motion can be derived using the material derivative

$$\frac{\mathrm{D}}{\mathrm{D}t}(\cdot) = \frac{\partial}{\partial t}(\cdot) + v_{en}\frac{\partial}{\partial z}(\cdot) \tag{2.1}$$

of the angular displacement $\varphi(z)$ of the plate cross section and the lateral position $w(z)$ of the plate centerline. The variable $v_{en}$ denotes the current mean entry

velocity of the plate, which may vary over time. These material derivatives yield

$$\frac{\mathrm{d}}{\mathrm{d}t}\Phi^- = \left.\frac{\partial\varphi}{\partial t}\right|_{z=0^-} = \omega^- - \left.\frac{\partial\varphi(z)}{\partial z}\right|_{z=0^-} v_{en} \tag{2.2a}$$

$$\frac{\mathrm{d}}{\mathrm{d}t}W = \left.\frac{\partial w}{\partial t}\right|_{z=0^-} = -\left.\frac{\partial w(z)}{\partial z}\right|_{z=0^-} v_{en}\ , \tag{2.2b}$$

where $\omega^-$ denotes the upstream ($z<0$) rotational speed of the plate with respect to the axis $y$. In (2.2a), the total rotational speed is

$$\omega^- = \left.\frac{\mathrm{D}\varphi(z)}{\mathrm{d}t}\right|_{z=0^-} \tag{2.3a}$$

and, in (2.2b), zero lateral material flow in the roll gap

$$0 = \left.\frac{\mathrm{D}w(z)}{\mathrm{d}t}\right|_{z=0^-} \tag{2.3b}$$

is assumed [44]. The plate clamped between the edger rolls and the roll gap is modeled as a Timoshenko beam. Thus, the spatial derivatives in (2.2) can be computed from Timoshenko's beam theory [45] in the form

$$\frac{\partial\varphi(z)}{\partial z} = \frac{M^-(z)}{E(z)I_y^-} + \kappa^-(z) \tag{2.4a}$$

$$\frac{\partial w(z)}{\partial z} = \varphi(z) + \frac{Q^-}{G(z)A_s^-}\ . \tag{2.4b}$$

In (2.4), $M^-(z)$ denotes the local bending moment in the beam, $E(z)$ is the local Young's modulus, and $I_y^-$ defines the upstream area moment of inertia of the beam with respect to the axis $y$. The curvature of the beam in the unloaded state before the rolling pass is denoted by $\kappa^-(z)$, $Q^-$ is the upstream shear force, $G(z)$ the local shear modulus and $A_s^-$ is the upstream shear area of the plate. Figure 2.2 shows a free body diagram of upstream and downstream parts of the plate including the lateral forces and torques.

The rotational speed $\omega^-$ in (2.2) is computed in the form

$$\omega^- = \frac{1}{w_0}\left(V^-\left(-\frac{w_0}{2}\right) - V^-\left(\frac{w_0}{2}\right)\right) \tag{2.5}$$

based on the material velocity profile $V^-(X)$ at the entry port of the roll gap and the plate width $w_0$. The coordinate $X$ is the lateral distance measured from the plate centerline as indicated in Figure 2.2. Thus, $\omega^-$ depends on the conditions

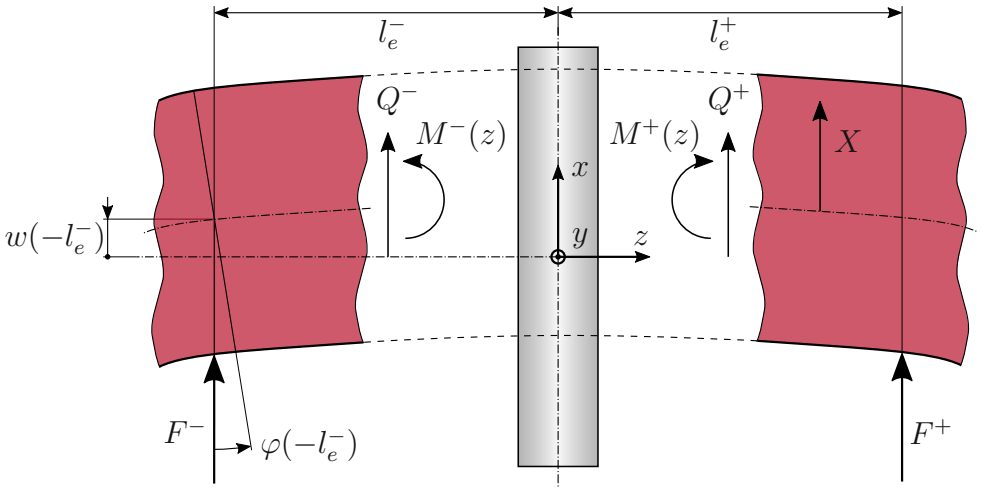


Figure 2.2: Free body diagram of upstream and downstream parts of the plate.

in the roll gap. Therefore, the roll gap model of Sims [46]

$$0 = F_R\Big(q_{roll}, u_r, k_{fm}, h^-, H, \Sigma^-, \Sigma^+\Big) \ , \tag{2.6}$$

with the local roll force $q_{roll}$ per unit width, the circumferential speed $u_r$ of the work rolls, the mean yield stress $k_{fm}$ of the plate material, the entry thickness $h^-$ of the plate, and the roll gap height $H$ (which equals the exit thickness $h^+$ of the plate) is used. It was extended to capture also the influence of tensile stresses $\Sigma^-$ and $\Sigma^+$ in the plate at the entry and exit port of the roll gap [47, 48]. Based on Sims model, the height of the neutral plane $h_n$ is computed in the form

$$h_n = h_n\Big(X, q_{roll}, u_r, k_{fm}, h^-, H, \Sigma^-, \Sigma^+\Big) \ . \tag{2.7}$$

At the neutral plane, the speed of the plate material equals the circumferential speed $u_r$ of the work rolls. Using the continuity equation, the entry velocity profile follows in the form

$$V^-(X) = u_r \frac{h_n(X)}{h^-(0^-, X)} \ . \tag{2.8}$$

Based on (2.7), (2.8), the linear approximation

$$\vartheta(X) = \bar{\vartheta} + \Delta\vartheta \frac{X}{w_0} \tag{2.9}$$

for $\vartheta \in \{\Sigma^-, \Sigma^+, H, h^-\}$, a Taylor series expansion (truncated after the linear

term) yields

$$V^-(X) = v_{en}\left(1 + \left(K^-_{\Sigma^-}\Delta\Sigma^- + K^-_{\Sigma^+}\Delta\Sigma^+ + K^-_H\Delta H + K^-_h\Delta h^-\right)\frac{X}{w_0}\right) . \quad (2.10)$$

The sensitivities in (2.10) are obtained by differentiation of (2.8) in the form

$$K^-_\alpha = \frac{1}{v_{en}}\frac{\partial V^-(X)}{\partial\vartheta}\bigg|_{\vartheta=\bar{\vartheta}} . \quad (2.11)$$

The lateral forces on the upstream part of the plate are denoted by $F^-$, those on the downstream part by $F^+$. The bending moment $M^-(z) = F^-(l^-_e + z)$ in the upstream part of the plate, the bending moment $M^+(z) = F^+(l^+_e - z)$ in the downstream part of the plate, and the corresponding shear forces $Q^- = -F^-$ and $Q^+ = -F^+$ can thus be readily computed. This leads to the expressions $M^-(0) = F^-l^-_e$ and $M^+(0) = F^+l^+_e$, with the distances $l^-_e$ and $l^+_e$ between the edger rolls and the roll gap. Integration of the bending stress over the beam cross section yields

$$\Delta\Sigma^- = -w_0 l^-_e F^-/I^-_y \quad (2.12a)$$

and

$$\Delta\Sigma^+ = -w_0 l^+_e F^+/I^+_y . \quad (2.12b)$$

Using (2.2), (2.4), (2.5), (2.10), and (2.12), the dynamic model can be summarized in the time-free formulation

$$\begin{bmatrix}\Phi^{-\prime}\\ W'\end{bmatrix} = \begin{bmatrix}0 & 0\\ -1 & 0\end{bmatrix}\begin{bmatrix}\Phi^-\\ W\end{bmatrix} + \begin{bmatrix}b^-_1 & b^+_1\\ b^-_2 & 0\end{bmatrix}\begin{bmatrix}F^-\\ F^+\end{bmatrix} + \begin{bmatrix}-1 & -\frac{K^-_h}{w_0} & -\frac{K^-_H}{w_0}\\ 0 & 0 & 0\end{bmatrix}\begin{bmatrix}\kappa^-\\ \Delta h^-\\ \Delta H\end{bmatrix} , \quad (2.13)$$

with the abbreviations

$$b^-_1 = -\frac{l^-_e}{E^-I^-_y} - \frac{l^-_e K^-_{\Sigma^-}}{I^-_y} \qquad b^+_1 = -\frac{l^+_e K^-_{\Sigma^+}}{I^+_y} \quad (2.14a)$$

$$b^-_2 = \frac{1}{G^-A^-_s} , \quad (2.14b)$$

$E^- = E(0^-)$, $G^- = G(0^-)$, and the derivative

$$(\cdot)' = \frac{\mathrm{d}}{\mathrm{d}z_{in}}(\cdot) = \frac{1}{v_{en}}\frac{\mathrm{d}}{\mathrm{d}t}(\cdot) . \quad (2.15)$$

The processed plate length $z_{in} \in \left[0, L^-\right]$, with the total length $L^-$ of the incoming

plate, serves as independent variable instead of the time $t$. Because $v_{en}$ does not appear in the time-free formulation, variations of $v_{en}$ do not affect the dynamic behavior.

### 2.1.2 Mathematical model of the plate shape

The analytical relation for the plate curvature $\kappa^+$ at the exit port of the roll gap is modeled as a linear combination of the angular velocity $\omega^-$ and $\omega^+$ of the plate on the entry side and exit side of the roll gap, respectively, the incoming plate curvature $\kappa^-$, and the upstream elastic deformation, which is rolled in the roll gap (plastic deformation state) [16]. This yields

$$\kappa^+ = \frac{1}{v_{en}\lambda}\left(\omega^+ - \frac{\omega^-}{\lambda}\right) + \frac{\kappa^-}{\lambda^2} + \frac{l_e^- F^-}{I_y^- \lambda^2 E^-} \ . \tag{2.16}$$

Here, $\lambda = \bar{h}^-/\bar{H}$ is the ratio of the mean input and mean output thickness $\bar{h}^-$ and $\bar{H}$, respectively. With (2.5), (2.10), (2.11), (2.12), and analogous relations for $\omega^+$, the algebraic relation

$$\kappa^+ = \begin{bmatrix} d^- & d^+ \end{bmatrix} \begin{bmatrix} F^- \\ F^+ \end{bmatrix} + \begin{bmatrix} \underbrace{\frac{1}{\lambda^2}}_{w_0} & \underbrace{\left(\frac{K_h^-}{\lambda^2} - K_h^+\right)}_{w_0} & \underbrace{\left(\frac{K_H^-}{\lambda^2} - K_H^+\right)}_{w_0} \end{bmatrix} \begin{bmatrix} \kappa^- \\ \Delta h^- \\ \Delta H \end{bmatrix} , \tag{2.17}$$

with the abbreviations

$$d^- = -\frac{l_e^-}{I_y^-}\left(\frac{K_{\Sigma^-}^-}{\lambda^2} - K_{\Sigma^-}^+ - \frac{1}{\lambda^2 E^-}\right) \qquad d^+ = -\frac{l_e^+}{I_y^+}\left(\frac{K_{\Sigma^+}^-}{\lambda^2} - K_{\Sigma^+}^+\right) , \tag{2.18}$$

can be deduced from (2.16). The sensitivities $K_{\Sigma^-}^{\pm}$, $K_{\Sigma^+}^{\pm}$, $K_h^{\pm}$, and $K_H^{\pm}$ determine how the asymmetric tensile stress $\Delta\Sigma^-$ at the entry port of the roll gap, the asymmetric tensile stress $\Delta\Sigma^+$ at the exit port of the roll gap, the thickness wedge $\Delta h^-$ of the incoming plate, and the tilt $\Delta H$ of the roll gap influence the output velocity profile and thus also the resulting camber $\kappa^+$. The sensitivities satisfy [16]

$$K_{\Sigma^-}^- = K_{\Sigma^-}^+ = K_\Sigma \qquad 1 = \bar{h}^-\left(K_h^+ - K_h^-\right) \tag{2.19a}$$

$$K_{\Sigma^+}^- = K_{\Sigma^+}^+ = -K_\Sigma \qquad 1 = \bar{H}\left(K_H^- - K_H^+\right) . \tag{2.19b}$$

Equation (2.17) reveals that lateral forces $F^-$ on the upstream part of the plate influence the camber in two ways:

- The plate is elastically deformed and this deformation is rolled in the roll gap.

- The lateral velocity profile of the plate in the roll gap is non-uniform. Hence, the plate rotates in the roll gap and forms a camber.

Considering (2.18), the relations (2.19), and $I_y^- = I_y^+ \lambda$, the dominant difference between $d^-$ and $d^+$ is the term $\frac{1}{\lambda^2 E^-}$. This term causes an upstream elastic deformation of the plate, which is rolled. This is why upstream lateral forces $F^-$ have usually more influence on the camber $\kappa^+$ of the outgoing plate than downstream forces $F^+$. A typical approximate relation for the fifth rolling pass is $d^- \approx -2.8 d^+$.

The equations (2.13) and (2.17) form the force-input model. It is a linear, time-invariant (LTI) system and the states $\Phi^-$ and $W$ as well as the output $\kappa^+$ are controllable by the control inputs $F^-$ and $F^+$. Moreover, the control inputs $F^-$ and $F^+$ have direct feedthrough on the output $\kappa^+$.

## 2.2 Analysis of the force-input model

In the following, the force input model is analyzed in terms of the model inputs

- lateral forces $F^-$ and/or $F^+$ applied by edger rolls and
- a constant roll gap tilt $\Delta H$

with regard to controlling the outputs

- lateral position $W$ of the plate in the roll gap and
- camber $\kappa^+$ of the outgoing plate.

For this purpose, consider the transfer functions of (2.13)

$$G_{F^-,W}(s) = \frac{b_2^- s - b_1^-}{s^2} \qquad G_{F^+,W}(s) = -\frac{b_1^+}{s^2} \,, \tag{2.20}$$

with the Laplace variable $s$ [49] and the coefficients defined in (2.14). These transfer functions show that both eigenvalues are 0, regardless of whether forces are applied to the plate on the entry or exit side of the roll gap.

Relation (2.17) for the camber of the outgoing plate is independent of the lateral position $W$ of the plate in the roll gap. The camber is directly influenced by the lateral forces $F^-$ and $F^+$ applied to the plate. This shows that both the lateral position and the shape of the plate depend on the lateral forces applied to the plate. Applying lateral forces to correct the shape yields a lateral plate motion and vice versa. There will always be a tradeoff in terms of safe plate motion and correct shape. Thus, minimizing the camber of the outgoing plate irrespective of the lateral plate motion can result in large off-center positions of the plate in the roll gap because of the two zero eigenvalues, see (2.13).

Considering the roll gap tilt $\Delta H$ as model input, the transfer function

$$G_{\Delta H,W}(s) = \frac{K_H^-}{w_0 s^2} \tag{2.21}$$

follows from (2.13). It also has both eigenvalues at 0. According to (2.17), also the roll gap tilt $\Delta H$ directly influences the camber of the outgoing plate. Compared to lateral forces as control inputs, e. g., applied by edger rolls, at first sight, the control input roll gap tilt $\Delta H$ does not show a significant advantage or disadvantage for controlling the lateral plate position $W$ in the roll gap. However, there is a significant difference in the case a constant camber has to be compensated. A constant camber can be eliminated either by a corresponding constant roll gap tilt $\Delta H$ or constant lateral forces $F^-$ or $F^+$. A constant lateral force entails a constant acceleration in lateral direction, which leads to unrealistic off-center positions of the plate in the roll gap. This shows that lateral forces are not suitable to compensate for constant plate camber.

## 2.3 Derivation of the position-input model

The equations of the plate dynamics (2.13) and the camber evolution (2.17) use the lateral edger forces $F^-$ and $F^+$ as control inputs. To prevent inordinately large lateral edger positions, a formulation with the lateral edger positions $w(-l_e^-)$ and $w(l_e^+)$ as alternative control inputs is desirable for feedback control. In the current section, (2.13) and (2.17) are thus reformulated so that the lateral positions $w(-l_e^-)$ and $w(l_e^+)$ replace the lateral forces $F^-$ and $F^+$ as control inputs.

### 2.3.1 Reduced Young's modulus in the roll gap

According to Timoshenko's beam theory a clear relation between the force exerted on a beam and the deflection of the beam can be calculated, whereby only one of these variables can be specified. To reformulate (2.13) and (2.17) this relation is calculated. As outlined in Figure 2.3, a reduced Young's modulus and shear modulus in the roll gap is assumed to capture the reduced deformation resistance in the roll gap (plastic deformation state), i. e.,

$$E(z) = \begin{cases} E_l & \text{if} \quad -L \leq z \leq 0 \\ E_h & \text{else} \end{cases} \tag{2.22a}$$

$$G(z) = \frac{E(z)}{2(1+\nu)} = \begin{cases} G_l & \text{if} \quad -L \leq z \leq 0 \\ G_h & \text{else} \end{cases} \tag{2.22b}$$

with $E_l < E_h$, $G_l < G_h$, and the Poisson's ratio $\nu$. The roll gap has the contact length $L$ [44]. This simplified model does not cover plastic deformation in the roll

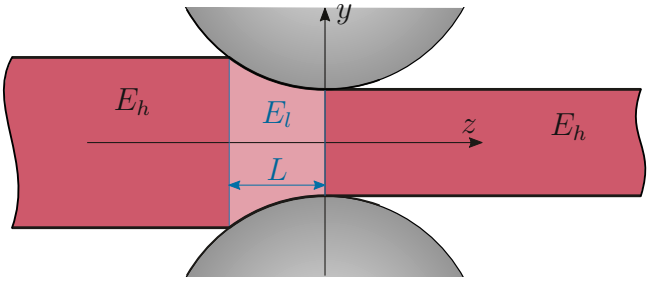


Figure 2.3: Partitioning of the plate into sections with different Young's moduli (side view).

gap in a physically correct way. However, the benefit of the proposed approach is to keep the simple linear system structure (cf., (2.13), (2.17)).

At the entry side of the roll gap, two Timoshenko beams are coupled at $z = -L$ (entry port of the roll gap). Integration of (2.4) with a coupling condition for the continuity of $\varphi(-L)$ and $w(-L)$ yields

$$\varphi\left(0^-\right) l_e^- - w\left(0^-\right) + w\left(-l_e^-\right) - \int_{-l_e^-}^{0} \int_{z}^{0} \kappa^-(\tilde{z}) \mathrm{d}\tilde{z} \mathrm{d}z = F^- k^- \ , \tag{2.23a}$$

with the abbreviation

$$k^- = \frac{(l_e^- - L)^3}{3E_h I_y^-} + \frac{l_e^- - L}{G_h A_s^-} + \frac{L\left(L^2 - 3Ll_e^- + 3(l_e^-)^2\right)}{3E_l I_y^-} + \frac{L}{G_l A_s^-} \ . \tag{2.23b}$$

Similarly, for the downstream part of the plate, Timoshenko's beam theory yields

$$\varphi\left(0^+\right) l_e^+ + w\left(0^+\right) - w\left(l_e^+\right) - \int_{0}^{l_e^+} \int_{0}^{z} \kappa^+(\tilde{z}) \mathrm{d}\tilde{z} \mathrm{d}z = F^+ k^+ \ , \tag{2.24a}$$

with the abbreviation

$$k^+ = \frac{(l_e^+)^3}{3E_h I_y^+} + \frac{l_e^+}{G_h A_s^+} \ . \tag{2.24b}$$

At the point $z = 0$ (end of roll gap), the conditions $\varphi(0^-) = \lambda\varphi(0^+) = \Phi^- = \lambda\Phi^+$ and $w(0^-) = w(0^+) = w(0) = W$ hold [14, 16].

Figure 2.4 shows a typical trajectory of the double integral $\int_{-l_e^-}^{0} \int_{z}^{0} \kappa^-(\tilde{z}) \mathrm{d}\tilde{z} \mathrm{d}z$ from (2.23a) during the fifth rolling pass. The double integral is set to zero at the end of the rolling pass, when edger rolls are not in contact with the plate anymore. The double integral in (2.23a) influences the lateral force $F^-$ in the same way as the lateral position $w(-l_e^-)$ of the edger rolls. However, measured plate centerlines and thus the camber $\kappa^-$ and the integral $\int_{-l_e^-}^{0} \int_{z}^{0} \kappa^-(\tilde{z}) \mathrm{d}\tilde{z} \mathrm{d}z$ suffer from measurement noise and are thus quite uncertain. Furthermore, the double integral is typically in the sub-centimeter range (cf. Figure 2.4). For typical values

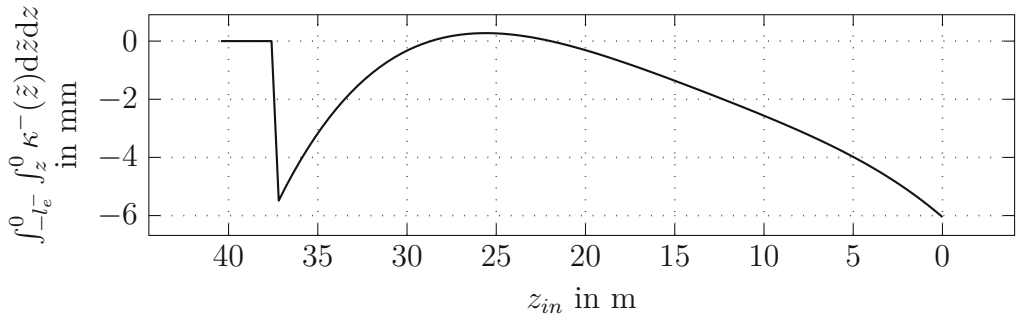


Figure 2.4: Typical double integral $\int_{-l_e^-}^{0}\int_{z}^{0}\kappa^-(\tilde{z})\mathrm{d}\tilde{z}\mathrm{d}z$ over the plate length.

of $\kappa^-$ and $\kappa^+$, the double integrals in (2.23a) and (2.24a) are of minor importance. They can thus be neglected, which gives

$$F^- \approx \frac{1}{k^-}\left(\Phi^- l_e^- - W + w\left(-l_e^-\right)\right) \tag{2.25a}$$

$$F^+ \approx \frac{1}{k^+}\left(\Phi^+ l_e^+ + W - w\left(l_e^+\right)\right) . \tag{2.25b}$$

### 2.3.2 Model assembly

Inserting the lateral forces $F^-$ and $F^+$ from (2.25) into (2.13) and (2.17) yields the mathematical model

$$\begin{aligned}\begin{bmatrix}\Phi^{-\prime}\\ W'\end{bmatrix} =& \begin{bmatrix}\frac{l_e^- b_1^-}{k^-} + \frac{l_e^+ b_1^+}{k^+} & \frac{-b_1^-}{k^-} + \frac{b_1^+}{k^+}\\ -1 + \frac{l_e^- b_2^-}{k^-} & \frac{-b_2^-}{k^-}\end{bmatrix}\begin{bmatrix}\Phi^-\\ W\end{bmatrix} + \begin{bmatrix}\frac{b_1^-}{k^-} & -\frac{b_1^+}{k^+}\\ \frac{b_2^-}{k^-} & 0\end{bmatrix}\begin{bmatrix}w(-l_e^-)\\ w(l_e^+)\end{bmatrix}\\ &+\begin{bmatrix}-1 & -\frac{K_h^-}{w_0} & -\frac{K_H^-}{w_0}\\ 0 & 0 & 0\end{bmatrix}\begin{bmatrix}\kappa^-\\ \Delta h^-\\ \Delta H\end{bmatrix}\end{aligned} \tag{2.26a}$$

$$\begin{aligned}\kappa^+ =& \begin{bmatrix}\frac{l_e^- d^-}{k^-} + \frac{l_e^+ d^+}{k^+} & -\frac{d^-}{k^-} + \frac{d^+}{k^+}\end{bmatrix}\begin{bmatrix}\Phi^-\\ W\end{bmatrix} + \begin{bmatrix}\frac{d^-}{k^-} & -\frac{d^+}{k^+}\end{bmatrix}\begin{bmatrix}w(-l_e^-)\\ w(l_e^+)\end{bmatrix}\\ &+\begin{bmatrix}\frac{1}{\lambda^2} & \frac{\left(\frac{K_h^-}{\lambda^2} - K_h^+\right)}{w_0} & \frac{\left(\frac{K_H^-}{\lambda^2} - K_H^+\right)}{w_0}\end{bmatrix}\begin{bmatrix}\kappa^-\\ \Delta h^-\\ \Delta H\end{bmatrix} .\end{aligned} \tag{2.26b}$$

The lateral positions $w(-l_e^-)$ and $w(l_e^+)$ of the edgers are the new model inputs.

In case of edger rolls being active only on the entry side of the roll gap, the lateral force $F^+$ on the exit side of the roll gap is 0. This can be reflected in the model (2.26) by setting $b_1^+ = 0$ and $d^+ = 0$. Analogously, in case of edger rolls being active only on the exit side of the roll gap, the lateral force $F^-$ on the entry

side of the roll gap is 0, which can be reflected by $b_1^- = 0$, $b_2^- = 0$ and $d^- = 0$.

The equations (2.26) form the position-input model. Similar to the force-input model, it is a linear, time-invariant (LTI) system and the states $\Phi^-$ and $W$ as well as the output $\kappa^+$ are controlled by the control inputs $w(-l_e^-)$ and $w(l_e^+)$. Moreover, the control inputs $w(-l_e^-)$ and $w(l_e^+)$ have direct feedthrough on the output $\kappa^+$.

## 2.4 Analysis of the position-input model

In the following, the position input model is analyzed in terms of the model inputs

- lateral positions $w(-l_e^-)$ and/or $w(l_e^+)$ of the edger rolls and
- a constant roll gap tilt $\Delta H$,

with regard to controlling the outputs

- lateral position $W$ of the plate in the roll gap and
- camber $\kappa^+$ of the outgoing plate.

### 2.4.1 Lateral positions $w(-l_e^-)$ and $w(l_e^+)$ as model inputs

The characteristic equation of the dynamic matrix from (2.26a) is

$$0 = \lambda_{u^\pm}^2 + \lambda_{u^\pm} \underbrace{\left( \frac{b_2^- k^+ - b_1^- k^+ l_e^- - b_1^+ k^- l_e^+}{k^- k^+} \right)}_{k_{u^\pm,1}} + \underbrace{\frac{b_1^+ k^- - b_1^- k^+ - (l_e^- + l_e^+) b_1^+ b_2^-}{k^- k^+}}_{k_{u^\pm,0}} . \tag{2.27}$$

The eigenvalues are typically complex conjugate. For stable system dynamics, the signs of the coefficients $k_{u^\pm,0}$ and $k_{u^\pm,1}$ must be strictly positive. These signs depend on the distances $l_e^-$ and $l_e^+$. Explicit investigation of the terms

$$k_{u^\pm,1} = \frac{b_2^-}{k^-\left((l_e^-)^3\right)} - \frac{b_1^-(l_e^-) l_e^-}{k^-\left((l_e^-)^3\right)} - \frac{b_1^+(l_e^+) l_e^+}{k^+\left((l_e^+)^3\right)} \tag{2.28a}$$

$$k_{u^\pm,0} = \frac{b_1^+(l_e^+)}{k^+\left((l_e^+)^3\right)} - \frac{b_1^-(l_e^-)}{k^-\left((l_e^-)^3\right)} - \frac{(l_e^- + l_e^+) b_1^+(l_e^+) b_2^-}{k^-\left((l_e^-)^3\right) k^+\left((l_e^+)^3\right)} , \tag{2.28b}$$

with the dependencies $b_1^-(l_e^-)$, $b_2^-$, $b_1^+(l_e^+)$ from (2.14), $k^-\left((l_e^-)^3\right)$ from (2.23b), and $k^+\left((l_e^+)^3\right)$ from (2.24b), reveals that disabling the edger rolls on the entry side ($b_1^- = 0$ and $b_2^- = 0$) is equivalent to the transition $l_e^- \to \infty$ and disabling the edger rolls on the exit side ($b_1^+ = 0$) is equivalent to the transition $l_e^+ \to \infty$. The

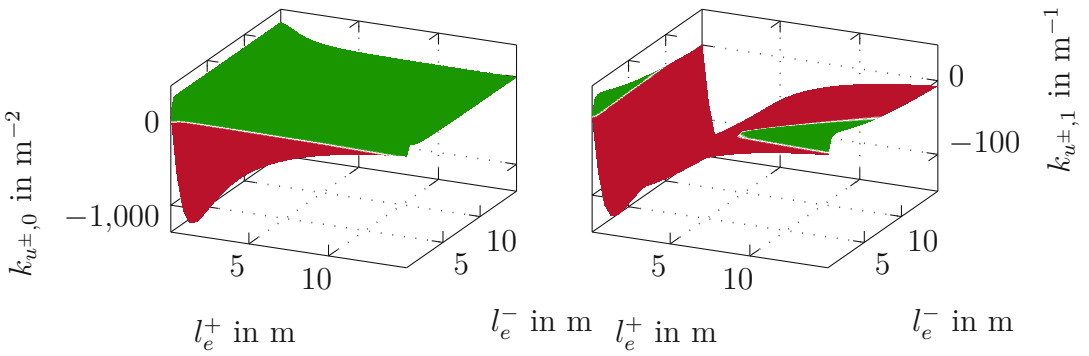


Figure 2.5: Stability depending on the edger rolls' positions $l_e^-$ and $l_e^+$ on the entry and exit side of the roll gap, respectively. Both coefficients $k_{u^\pm,0}$ and $k_{u^\pm,1}$ must be strictly positive for a stable dynamic matrix (2.26a).

terms $k_{u^\pm,0}$ and $k_{u^\pm,1}$ according to (2.28) and the graphical representation of their signs in Figure 2.5 show

- how edger rolls on the entry and exit side have to be located for a stable system dynamics (2.26a),
- that the system (2.26a) is stable for edger rolls being active only on the entry side of the roll gap ($l_e^+ \to \infty$),
- that the system (2.26a) is unstable for edger rolls being active only on the exit side of the roll gap ($l_e^- \to \infty$),
- that both eigenvalues $\lambda_{u^\pm}$ of (2.26a) are 0 in case of all edger rolls being inactive ($l_e^- \to \infty$ and $l_e^+ \to \infty$).

Furthermore, because entry and exit side alter in each rolling pass and because $l_e^- = l_e^+$ is typically in the unstable region (cf. Figure 2.5), it is impossible to design a reversing rolling mill with uncontrolled stable system dynamics where edger rolls are active on both sides of the roll gap for both rolling directions.

### 2.4.2 Roll gap tilt $\Delta H$ as additional control input

The stability analysis from Section 2.4.1 also holds true if the roll gap tilt $\Delta H$ is considered as additional control input. For realistic distances $l_e^-$ and $l_e^+$ (typically a few meters upstream and downstream of the roll gap) which yield a stable system dynamics ($k_{u^\pm,0} > 0$ and $k_{u^\pm,1} > 0$), the steady-state condition of (2.26a)

for $\kappa^- = 0$, $\Delta h^- = 0$ and $w(-l_e^-) = w(l_e^+) = 0$ reads as

$$\begin{bmatrix} \Phi_s^- \\ W_s \end{bmatrix} = -\begin{bmatrix} \frac{l_e^- b_1^-}{k^-} + \frac{l_e^+ b_1^+}{k^+} & \frac{-b_1^-}{k^-} + \frac{b_1^+}{k^+} \\ -1 + \frac{l_e^- b_2^-}{k^-} & \frac{-b_2^-}{k^-} \end{bmatrix}^{-1} \begin{bmatrix} -\frac{K_H^-}{w_0} \\ 0 \end{bmatrix} \Delta H$$
$$= \begin{bmatrix} \frac{b_2^- k^+}{b_1^- k^+ - b_1^+ k^- + b_1^+ b_2^- \left(l_e^- + l_e^+\right)} \\ \frac{k^- k^+ - b_2^- l_e^- k^+}{b_1^- k^+ - b_1^+ k^- + b_1^+ b_2^- \left(l_e^- + l_e^+\right)} \end{bmatrix} \frac{K_H^-}{w_0} \Delta H \ . \tag{2.29}$$

For instance, typical values for $l_e^- = 3.3\,\mathrm{m}$ and $l_e^+ = 10\,\mathrm{m}$ yield $\Phi_s^- \approx -1.65\%\Delta H$ and $W_s \approx -5.56\Delta H$. However, the value of $\Delta H$ is typically in the submillimeter range. Hence, the steady-state influence of the roll gap tilt on the lateral plate position $W$ can be neglected. Very similar considerations apply to the inputs $\kappa^-$ and $\Delta h^-$ in (2.26a). Their steady-state influence on $W$ is even smaller than that of $\Delta H$. These findings justify the neglection of these inputs in (2.26), which yields

$$\begin{bmatrix} \Phi^{-\prime} \\ W' \end{bmatrix} = \begin{bmatrix} \frac{l_e^- b_1^-}{k^-} + \frac{l_e^+ b_1^+}{k^+} & \frac{-b_1^-}{k^-} + \frac{b_1^+}{k^+} \\ -1 + \frac{l_e^- b_2^-}{k^-} & \frac{-b_2^-}{k^-} \end{bmatrix} \begin{bmatrix} \Phi^- \\ W \end{bmatrix} + \begin{bmatrix} \frac{b_1^-}{k^-} & -\frac{b_1^+}{k^+} \\ \frac{b_2^-}{k^-} & 0 \end{bmatrix} \begin{bmatrix} w(-l_e^-) \\ w(l_e^+) \end{bmatrix} \tag{2.30a}$$

$$\kappa^+ = \begin{bmatrix} \frac{l_e^- d^-}{k^-} + \frac{l_e^+ d^+}{k^+} & -\frac{d^-}{k^-} + \frac{d^+}{k^+} \end{bmatrix} \begin{bmatrix} \Phi^- \\ W \end{bmatrix} + \begin{bmatrix} \frac{d^-}{k^-} & -\frac{d^+}{k^+} \end{bmatrix} \begin{bmatrix} w(-l_e^-) \\ w(l_e^+) \end{bmatrix}$$
$$+ \begin{bmatrix} \frac{1}{\lambda^2} & \frac{\left(\frac{K_h^-}{\lambda^2} - K_h^+\right)}{w_0} & \frac{\left(\frac{K_H^-}{\lambda^2} - K_H^+\right)}{w_0} \end{bmatrix} \begin{bmatrix} \kappa^- \\ \Delta h^- \\ \Delta H \end{bmatrix} . \tag{2.30b}$$

Compared to the force-input model, the inputs $F^-$ and $F^+$ (lateral forces applied by edger rolls) are replaced by the lateral positions $w(-l_e^-)$ and $w(l_e^+)$. The model inputs $\kappa^-$, $\Delta h$ and $\Delta H$ directly influence the camber $\kappa^+$ of the outgoing plate in the same way as in the force-input model but can be neglected in the model for the lateral plate motion.

## 2.5 Computation of the outgoing plate centerline

To individually analyze the effects that influence the evolution of the centerline of the plate, (2.30b) is rewritten in the form

$$\kappa^+ = \kappa_{x,u} + \frac{1}{\lambda^2}\kappa^- + \kappa_{\Delta hH} \ , \tag{2.31a}$$

with the abbreviations

$$\kappa_{x,u} = \begin{bmatrix} \frac{l_e^- d^-}{k^-} + \frac{l_e^+ d^+}{k^+} & -\frac{d^-}{k^-} + \frac{d^+}{k^+} \end{bmatrix} \begin{bmatrix} \Phi^- \\ W \end{bmatrix} + \begin{bmatrix} \frac{d^-}{k^-} & -\frac{d^+}{k^+} \end{bmatrix} \begin{bmatrix} w(-l_e^-) \\ w(l_e^+) \end{bmatrix} , \tag{2.31b}$$

and

$$\kappa_{\Delta hH} = \left( \frac{K_h^-}{\lambda^2} - K_h^+ \right) \frac{\Delta h^-}{w_0} + \left( \frac{K_H^-}{\lambda^2} - K_H^+ \right) \frac{\Delta H}{w_0} . \tag{2.31c}$$

Integrating the relation

$$\kappa^+(\zeta) = \frac{\mathrm{d}^2}{\mathrm{d}\zeta^2} cl^+(\zeta) , \tag{2.32}$$

with the independent variable $\zeta \in \left[0, L^+\right]$ and the outgoing plate length $L^+$, yields the centerline of the outgoing plate in the form

$$cl^+ = cl^+(\zeta) = \underbrace{\int_0^\zeta \int_0^{\tilde{\zeta}} \kappa_{x,u} \mathrm{d}\xi \mathrm{d}\tilde{\zeta}}_{cl_{x,u}} + \underbrace{\int_0^\zeta \int_0^{\tilde{\zeta}} \frac{\kappa^-}{\lambda^2} \mathrm{d}\xi \mathrm{d}\tilde{\zeta}}_{cl^-} + \underbrace{\int_0^\zeta \int_0^{\tilde{\zeta}} \kappa_{\Delta hH} \mathrm{d}\xi \mathrm{d}\tilde{\zeta}}_{cl_{\Delta hH}} . \tag{2.33}$$

The terms $cl_{x,u}$, $cl^-$, and $cl_{\Delta hH}$ can be individually calculated. For better comparison, the centerlines $cl^+$ are rotated and shifted (rigid-body motion) according to the procedure described in Appendix A.1 yielding $\tilde{cl}^+$. Because of the linearity in (2.33) and the linearity of the procedure from Appendix A.1, each part of the expression (2.33) can be individually rotated and shifted, yielding $\tilde{(\cdot)}$, which is the rotated and shifted version of $(\cdot)$.

The centerline $cl^-$ of the upstream plate is measured by the camera system before every rolling pass. Thus $\tilde{cl}^-$ can be calculated in advance. Because of the self-retaining behavior of the roll gap adjustment, the roll gap tilt $\Delta H = \Delta h^+$ and also the thickness wedge $\Delta h^-$ are assumed to be constant throughout the rolling pass. This yields a constant value $\kappa_{\Delta hH}$ in (2.31c) and thus the corresponding portion of the centerline

$$cl_{\Delta hH} = \frac{1}{2} \zeta^2 \kappa_{\Delta hH} . \tag{2.34}$$

For numerical efficiency, the relation

$$\kappa_{x,u} = \frac{\mathrm{d}^2}{\mathrm{d}\zeta^2} cl_{x,u}(\zeta) = \frac{1}{\lambda^2} \frac{\mathrm{d}^2}{\mathrm{d}z_{in}^2} cl_{x,u}(\lambda z_{in}) = \frac{cl''_{x,u}}{\lambda^2} \tag{2.35}$$

can be included in the dynamic system (2.30a). This yields the extended linear system

$$\mathbf{x}' = \mathbf{A}\mathbf{x} + \mathbf{B}\mathbf{u}, \qquad \mathbf{x}(0) = \mathbf{x}_0 \tag{2.36a}$$

with

$$\mathbf{A} = \begin{bmatrix} \frac{l_e^- b_1^-}{k^-} + \frac{l_e^+ b_1^+}{k^+} & \frac{-b_1^-}{k^-} + \frac{b_1^+}{k^+} & 0 & 0 \\ -1 + \frac{l_e^- b_2^-}{k^-} & \frac{-b_2^-}{k^-} & 0 & 0 \\ 0 & 0 & 0 & 1 \\ \left(\frac{l_e^- d^-}{k^-} + \frac{l_e^+ d^+}{k^+}\right)\lambda^2 & \left(-\frac{d^-}{k^-} + \frac{d^+}{k^+}\right)\lambda^2 & 0 & 0 \end{bmatrix} \quad \mathbf{B} = \begin{bmatrix} \frac{b_1^-}{k^-} & -\frac{b_1^+}{k^+} \\ \frac{b_2^-}{k^-} & 0 \\ 0 & 0 \\ \frac{d^-}{k^-}\lambda^2 & -\frac{d^+}{k^+}\lambda^2 \end{bmatrix}, \tag{2.36b}$$

the states $\mathbf{x} = \begin{bmatrix} \Phi^- & W & cl_{x,u} & cl'_{x,u} \end{bmatrix}^\mathrm{T}$, and the model inputs $\mathbf{u} = \begin{bmatrix} u^- & u^+ \end{bmatrix}^\mathrm{T} = \begin{bmatrix} w(-l_e^-) & w(l_e^+) \end{bmatrix}^\mathrm{T}$. After integration of (2.36) and the rigid-body motion of $cl_{x,u}$, the centerline of the outgoing plate can be calculated as

$$\tilde{cl}^+ = \tilde{cl}_{x,u} + \tilde{cl}^- + \tilde{cl}_{\Delta hH} \ . \tag{2.37}$$

## 2.6 Specialization of the model for the considered industrial rolling mill

At the considered industrial rolling mill, upstream edger rolls are just active during the rolling passes 1, 3, 5, ... (forward rolling passes). There are no downstream edger rolls. The considerations made in Section 2.4 show that this is quite meaningful as edger rolls on the entry side of the roll gap inherently ensure stable system dynamics. Although the system with edger rolls being active also in backward rolling passes could be stabilized by feedback control, the plant is only operated with edger rolls being active in forward rolling passes for safety reasons.

Thus, backward rolling passes are described by the model from Section 2.1 (specifically (2.13) and (2.17)) with $F^- = 0$ and $F^+ = 0$. This yields the linear mathematical model

$$\mathbf{x}_b' = \mathbf{A}_b \mathbf{x}_b + \mathbf{G}\mathbf{d}, \qquad \mathbf{x}_b(0) = \mathbf{x}_{b,0} \ , \tag{2.38a}$$

with

$$\mathbf{A}_b = \begin{bmatrix} 0 & 0 \\ -1 & 0 \end{bmatrix} \qquad \mathbf{G} = \begin{bmatrix} -1 & -\frac{K_h^-}{w_0} & -\frac{K_H^-}{w_0} \\ 0 & 0 & 0 \end{bmatrix}, \tag{2.38b}$$

the states $\mathbf{x}_b = \begin{bmatrix} \Phi^- & W \end{bmatrix}^\mathrm{T}$, and the model inputs $\mathbf{d} = \begin{bmatrix} \kappa^- & \Delta h^- & \Delta H \end{bmatrix}^\mathrm{T}$.

For forward rolling passes, the model (2.36) with $b_1^+ = 0$ and $d^+ = 0$ (inactive downstream edger rolls) is used. This yields the linear mathematical model

$$\mathbf{x}_f' = \mathbf{A}_f \mathbf{x}_f + \mathbf{B} u^-, \qquad \mathbf{x}_f(0) = \mathbf{x}_{f,0} \tag{2.39a}$$

with

$$\mathbf{A}_f = \begin{bmatrix} \frac{l_e^- b_1^-}{k^-} & \frac{-b_1^-}{k^-} & 0 & 0 \\ -1 + \frac{l_e^- b_2^-}{k^-} & \frac{-b_2^-}{k^-} & 0 & 0 \\ 0 & 0 & 0 & 1 \\ \frac{d^- l_e^- \lambda^2}{k^-} & \frac{-d^- \lambda^2}{k^-} & 0 & 0 \end{bmatrix} \qquad \mathbf{B}_f = \begin{bmatrix} \frac{b_1^-}{k^-} \\ \frac{b_2^-}{k^-} \\ 0 \\ \frac{d^- \lambda^2}{k^-} \end{bmatrix}, \tag{2.39b}$$

the states $\mathbf{x}_f = \begin{bmatrix} \Phi^- & W & cl_{x,u} & cl'_{x,u} \end{bmatrix}^{\mathrm{T}}$, and the model input $u^- = w(-l_e^-)$.

The output

$$\tilde{cl}^+ = \tilde{cl}_{x,u} + \tilde{cl}^- + \tilde{cl}_{\Delta hH} \tag{2.40}$$

applies to both rolling directions. In backward rolling passes, $cl_{x,u} = 0$ holds true because edger rolls are inactive and therefore do not modify the centerline $cl^+$. Moreover, because of the distance between the edger rolls and the roll gap, the last section of the incoming plate (length $l_e^-$) during forward rolling passes is described by (2.38). Hence, the tail end of the incoming plate cannot be influenced by edger rolls in forward rolling passes, i. e., $cl_{x,u} = 0$ for the last few meters of the rolled plate. The models (2.38), (2.39), and (2.40) will henceforth be used for analysis, validation, and control design.

## 2.7 Analysis of the specialized model

In the following, the specialized model is analyzed in terms of the model inputs

- lateral position $u^-$ of the edger rolls and
- initial plate position $W_0$ in the roll gap

and their influence on the outputs

- lateral position $W$ of the plate in the roll gap and
- camber $\kappa_{x,u}$ or centerline $cl_{x,u}$ of the outgoing plate.

### 2.7.1 Lateral position $u^-$ as model input

Consider the eigenvalues $\lambda_{u^\pm}$ according to (2.27) of the dynamic matrix for the case with edger rolls being active only on the entry side of the roll gap ($b_1^+ = 0$,

$d^+ = 0$). Their value is

$$\begin{aligned}
\lambda_{u^\pm,1,2} &= -\frac{b_2^- - b_1^- l_e^-}{2k^-} \pm \sqrt{\frac{\left(b_2^- - b_1^- l_e^-\right)^2}{4(k^-)^2} + \frac{b_1^-}{k^-}} \\
&= -\frac{b_2^- - b_1^- l_e^-}{2k^-} \pm \sqrt{\frac{\left(b_2^- - b_1^- l_e^-\right)^2 + 4b_1^- k^-}{4(k^-)^2}} \\
&= -\frac{b_2^- - b_1^- l_e^-}{2k^-} \pm \sqrt{\frac{\left(b_2^- - b_1^- l_e^- - \frac{2k^-}{l_e^-}\right)^2 + \cancel{k_r}}{4(k^-)^2}} \\
&\approx -\frac{b_2^- - b_1^- l_e^-}{2k^-} \pm \frac{b_2^- - b_1^- l_e^- - \frac{2k^-}{l_e^-}}{2k^-} \,, \qquad (2.41a)
\end{aligned}$$

with the residual term

$$k_r = 4\left(b_2^- - \frac{k^-}{l_e^-}\right)\frac{k^-}{l_e^-} \,. \qquad (2.41b)$$

The absolute value $k_r$ is much smaller than the quadratic term in the radicand of (2.41a). Both eigenvalues in (2.41a) are negative. The eigenvalue with the smaller absolute value determines the slow dynamics of (2.30) and reads as

$$\lambda_{u^\pm,1} \approx -\frac{1}{l_e^-} \,. \qquad (2.42)$$

The distance between the edger rolls and the roll gap is thus most relevant for the system dynamics. The second eigenvalue $\lambda_{u^\pm,2}$ typically satisfies $\lambda_{u^\pm,2} \ll \lambda_{u^\pm,1}$, with $\frac{\lambda_{u^\pm,2}}{\lambda_{u^\pm,1}} \approx 50$. Hence, only the fast dynamics of the lateral plate motion (associated with $\lambda_{u^\pm,2}$) depends on other parameters like the sensitivities $K_\Sigma$, Young's modulus $E(z)$, and thickness $h^-$. The transfer function of the lateral position $u^-$ of the upstream edger rolls to the lateral position $W$ in the roll gap (cf. (2.39)) reads as

$$G_{u^-,W}(s) = \frac{b_2^- s - b_1^-}{s^2 k^- + \left(b_2^- - b_1^- l_e^-\right)s - b_1^-} \,, \qquad (2.43)$$

with the Laplace variable $s$ [49]. The first-order state-space system (2.39) has 4 states. The transfer function (2.43), however, is of order 2. This difference indicates that a subsystem of (2.39) is either uncontrollable with the input $u^-$, unobservable by the output $W$ or both. The rank of the controllability matrix

$$\operatorname{rank}(\mathcal{R}(\mathbf{A}_f, \mathbf{B}_f)) = \operatorname{rank}\left(\begin{bmatrix}\mathbf{B}_f & \mathbf{A}_f\mathbf{B}_f & \mathbf{A}_f^2\mathbf{B}_f & \mathbf{A}_f^3\mathbf{B}_f\end{bmatrix}\right) = 2 \qquad (2.44)$$

and of the observability matrix

$$\operatorname{rank}\Big(\mathcal{O}\Big(\mathbf{c}_{f,W}^{\mathrm{T}}, \mathbf{A}_f\Big)\Big) = \operatorname{rank}\left(\begin{bmatrix} \mathbf{c}_{f,W}^{\mathrm{T}} \\ \mathbf{c}_{f,W}^{\mathrm{T}}\mathbf{A}_f \\ \mathbf{c}_{f,W}^{\mathrm{T}}\mathbf{A}_f^2 \\ \mathbf{c}_{f,W}^{\mathrm{T}}\mathbf{A}_f^3 \end{bmatrix}\right) = 2 \ , \tag{2.45}$$

with $\mathbf{c}_{f,W}^{\mathrm{T}} = \begin{bmatrix} 0 & 1 & 0 & 0 \end{bmatrix}$, are both 2. Hence, the system (2.39) is neither fully controllable with the input $u^-$ nor fully observable with the output $W$.

Because of the dominance of the first eigenvalue (cf. (2.41a)) and because $\left|\frac{b_2^-}{b_1^-}\right| \ll 1$ is typically true,

$$G_{u^-,W}(s) \approx \frac{1}{l_e^- s + 1} \tag{2.46}$$

is a good approximation. The lateral position of the plate in the roll gap thus follows the lateral position $u^-$ of the edger rolls approximately with a first-order low-pass dynamics with the time constant $l_e^-$. The steady-state gain of (2.43) is 1. The lateral position $W$ of the plate in the roll gap is thus not expected to reach extensive values, as long as the lateral position $u^-$ of the edger rolls is restricted.

In the steady state ($\Phi^- = 0$ and $W = u^-$), the camber due to inputs and states (cf. (2.31b)) is

$$\kappa_{x,u,s} = \begin{bmatrix} \frac{d^-}{k^-} l_e^- & -\frac{d^-}{k^-} \end{bmatrix} \begin{bmatrix} 0 \\ 1 \end{bmatrix} u^- + \frac{d^-}{k^-} u^- = 0 \ . \tag{2.47}$$

Hence, a constant input $u^-$ does not cause a camber. If at some point $u^- \neq W$, this is not a steady state which generates a non-zero camber $\kappa_{x,u}$.

The transfer function

$$G_{u^-,cl_{x,u}}(s) = \frac{d^-\lambda^2}{s^2 k^- + \left(b_2^- - b_1^- l_e^-\right)s - b_1^-} \approx \frac{-d^-\lambda^2}{b_1^-} \frac{1}{l_e^- s + 1} \tag{2.48}$$

describes how the lateral position $u^-$ of the edger rolls influences the centerline $cl_{x,u}$. The observability matrix

$$\operatorname{rank}\Big(\mathcal{O}\Big(\mathbf{c}_{f,cl_{x,u}}^{\mathrm{T}}, \mathbf{A}_f\Big)\Big) = \operatorname{rank}\left(\begin{bmatrix} \mathbf{c}_{f,cl_{x,u}}^{\mathrm{T}} \\ \mathbf{c}_{f,cl_{x,u}}^{\mathrm{T}}\mathbf{A}_f \\ \mathbf{c}_{f,cl_{x,u}}^{\mathrm{T}}\mathbf{A}_f^2 \\ \mathbf{c}_{f,cl_{x,u}}^{\mathrm{T}}\mathbf{A}_f^3 \end{bmatrix}\right) = 4 \ , \tag{2.49}$$

with $\mathbf{c}_{f,cl_{x,u}}^{\mathrm{T}} = \begin{bmatrix} 0 & 0 & 1 & 0 \end{bmatrix}$, has rank 4. Thus, the system (2.39) is fully observable with the output $cl_{x,u}$. The difference between the number of states of the system

(2.39) and the order of the transfer function (2.48) is thus attributed to the rank of the controllability matrix (2.44).

A comparison of (2.46) and (2.48) shows that the deformation of the centerline $cl_{x,u}$ induced by the input $u^-$ (lateral position of the edger rolls) is approximately proportional to the lateral plate position $W$ caused by the same input. This means that a desired change of the shape of the centerline $cl_{x,u}$ demands for a proportional change of the lateral position $W$ in the roll gap. Therefore, these two quantities cannot be specified independently.

### 2.7.2 Initial lateral plate position $W_0$ in the roll gap

If the edger rolls on the entry side of the roll gap are active ($u^- = 0$), the influence of the initial value $W_0$ (lateral position of the plate in the roll gap at the roll bite) on the plate centerline $cl_{x,u}$ can be calculated as (cf., (2.39))

$$\hat{cl}_{x,u} = \frac{-d^- \lambda^2}{s^2 k^- + \left(b_2^- - b_1^- l_e\right) s - b_1^-} W_0 \approx \frac{d^- \lambda^2}{b_1^-} \frac{1}{l_e^- s + 1} W_0 \ , \tag{2.50}$$

with $\hat{(\cdot)}(s)$ being the Laplace transform of $(\cdot)(z)$. The steady state of $\hat{cl}_{x,u}$ is, see (2.14) and (2.18)

$$\frac{d^- \lambda^2}{b_1^-} W_0 = \frac{E_l K_\Sigma - \lambda^2 E_l K_\Sigma - 1}{1 + E_l K_\Sigma} W_0 \ . \tag{2.51}$$

Starting at the initial value $cl_{x,u}(0) = 0$, the centerline $cl_{x,u}$ converges to the stationary value (2.51) with the time constant $l_e^-$. An initial lateral position $W_0$ at the roll bite thus causes a deflection of the plate centerline at the head end of the plate with the value (2.51).

### 2.7.3 Analysis of the composition of the outgoing plate centerline

Figure 2.6 shows the influence of the inputs $\tilde{cl}^-$, $\tilde{cl}_{\Delta hH}$, $u^-$, and $W_0$ on a fictitious outgoing plate centerline $\tilde{cl}^+$ (cf. (2.40)) in a forward rolling pass. The linear combination of the constant thickness wedge $\Delta h = 16\,\mu\text{m}$ and the constant roll gap tilt $\Delta H = 16\,\mu\text{m}$ contributes a quadratic function $\tilde{cl}_{\Delta hH}$, according to (2.31c) and (2.34) to the outgoing plate centerline $\tilde{cl}^+$. Because of the linearity of the system, the influence of the initial position $W_0$ of the plate in the roll gap ($u = 0$), which is chosen as $-2.75\,\text{cm}$, and the input $u^-$ ($W_0 = 0$) on the centerline $cl_{x,u}$ can be individually analyzed. The camber due to the initial plate position $W_0$ in the roll gap has the value (2.51). The outgoing plate centerline $\tilde{cl}^+$ is calculated as the sum of these four contributions (cf. (2.40)).

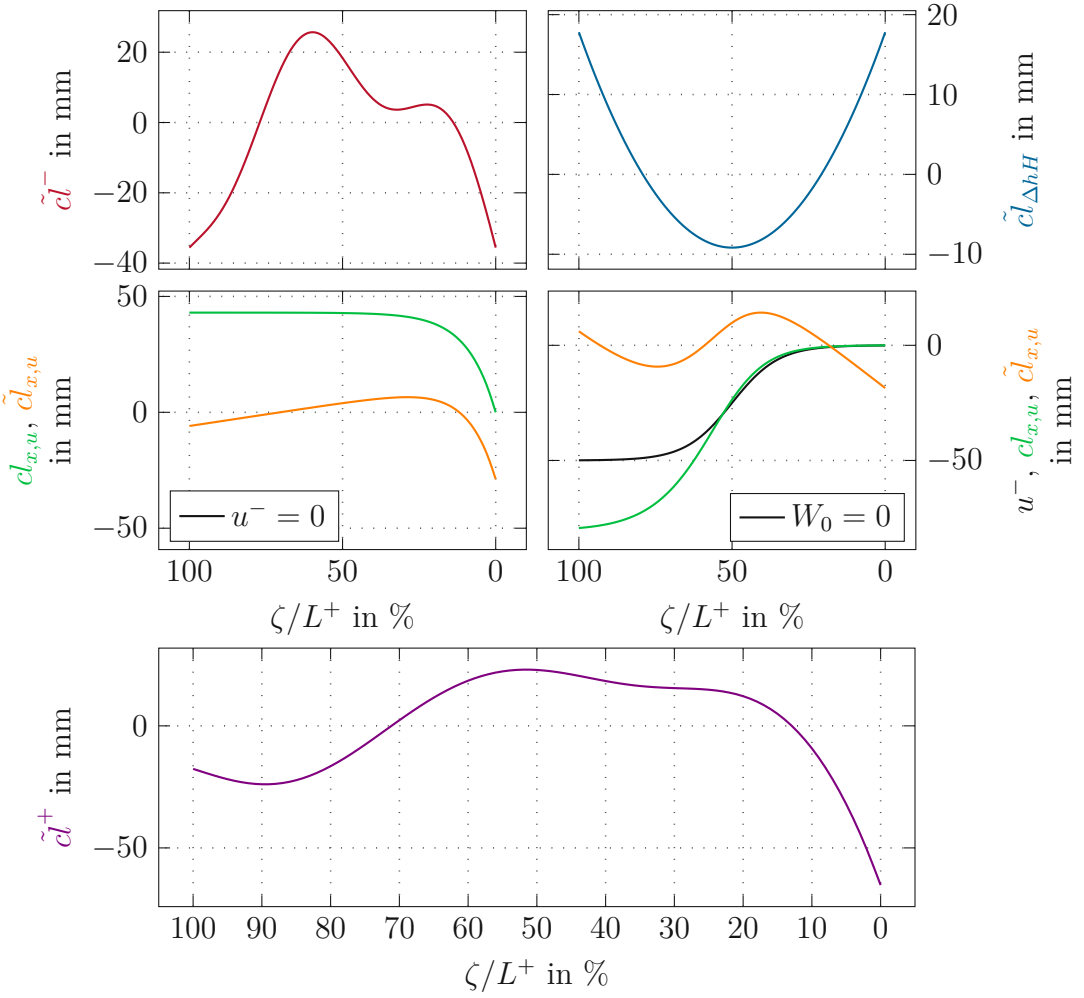


Figure 2.6: Fictitious plate before and after a rolling pass with active upstream edger rolls. The outgoing plate centerline $\tilde{cl}^+$ is the sum of the incoming plate centerline $\tilde{cl}^-$, a contribution $\tilde{cl}_{\Delta hH}$ due to a thickness wedge and a roll gap tilt as well as a contribution $\tilde{cl}_{x,u}$ due to the lateral position $u^-$ of the edger rolls and the initial lateral plate position $W_0$ in the roll gap (cf. (2.40)).

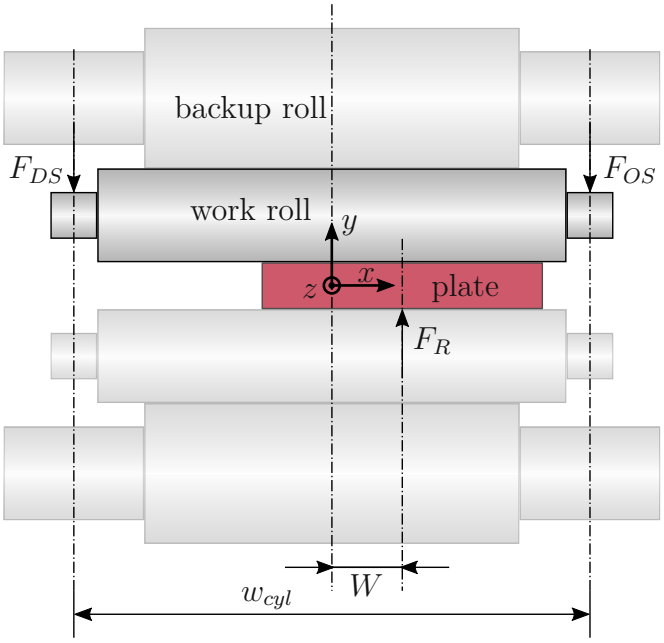


Figure 2.7: Off-centered plate in the roll gap.

## 2.8 Asymmetric mill stretch

The roll gap in the considered roughing mill is adjusted with self-retaining screws. It can only be adjusted when the roll gap is empty but not during the rolling pass. However, the adjusted (nominal) roll gap can differ from the loaded (effective) roll gap because of mill stretch, see, e. g., [18]. Clearly, this influences the thickness profile of the outgoing plate and consequently also the lateral motion of the plate in the roll gap and the outgoing shape of the plate. As described in [18], asymmetric mill stretch typically roots in asymmetric rolling conditions, e. g., lateral temperature and thickness inhomogeneities of the plate or lateral displacement $W$ of the plate in the roll gap. The latter effect is discussed in the following.

Figure 2.7 shows a front view of a mill stand with an off-centered plate and the corresponding resultant rolling and bearing forces. Considering the conservation of momentum

$$F_{DS} + F_{OS} - F_R = 0 \ , \tag{2.52}$$

with the force $F_{DS}$ on the drive side, the force $F_{OS}$ on the operator side, and the total rolling force $F_R$, the relation

$$(F_{DS} - F_{OS})\frac{w_{cyl}}{2} = -(F_{DS} + F_{OS})W = -F_R W \tag{2.53}$$

with the distance $w_{cyl}$ between the cylinders is obtained. This asymmetric bearing

forces $F_{DS} \neq F_{OS}$ generally cause an extra (elastic) roll gap tilt under load. It can be modeled in the form ([18, 50])

$$\Delta H_W = k_W W \ , \tag{2.54a}$$

with

$$k_W = \frac{2F_R}{m_{\Delta,G} - m_{\Delta,M}} \frac{1}{w_{cyl}} \ , \tag{2.54b}$$

the mill modulus $m_{\Delta,G}$, and the material modulus $m_{\Delta,M}$ [44]. The effective roll gap tilt under load is thus

$$\Delta H = \Delta H_{adj} + \Delta H_W \ , \tag{2.55}$$

with the adjusted roll gap tilt $\Delta H_{adj}$ and the additional asymmetric stretch $\Delta H_W$.

Clearly, a lateral off-centered plate position $W \neq 0$ and the associated asymmetric mill stretch $\Delta H_W$ influence the dynamic behavior of the system during the current rolling pass. They also influence the dynamic behavior of the subsequent rolling pass because $\Delta h^+ = \Delta H$ equals $\Delta h^-$ of the next rolling pass. Exploiting this effect would be interesting from a control perspective, in particular for a mill stand with a self-retaining adjustment system. Since at the industrial plant the thickness profile is only measured once at the end of the roughing process and there are no possibilities to measure the plate temperature profile or the roll gap under load, identification of the parameter $k_W$ and its validation are extremely difficult. The effect of asymmetric mill stretch is therefore neglected in the following, i. e., $\Delta H_W = 0$ and $\Delta H = \Delta H_{adj}$.

## 2.9 The dog-bone effect

To control the width of the plate, it is common to use edger rolls (cf. Figure 2.8). They are usually symmetrically adjusted ($F_u^{DS} = F_u^{OS}$). An undesirable consequence of edger rolls is the dog-bone effect [9–13]. It means that the slab bulges near the edger rolls and thus changes its cross sectional shape from a rectangular to a dog-bone shape. Figure 2.9 shows a sketch of the resulting thickness profile. In case of symmetric edge rolling, the deformation is assumed to be symmetric with respect to the $Y$ axis. Hence, it is sufficient to consider one quadrant of the plate cross section.

In case of asymmetric edger forces ($F_u^{DS} \neq F_u^{OS}$), the dog-bone effect is likely to be also asymmetric, which then yields an asymmetric lateral thickness profile along the direction $X$, cf. Figure 2.10. However, the deformation is still assumed to be symmetric with respect to the $X$ axis. Thus it is sufficient to consider two quadrants of the thickness profile.

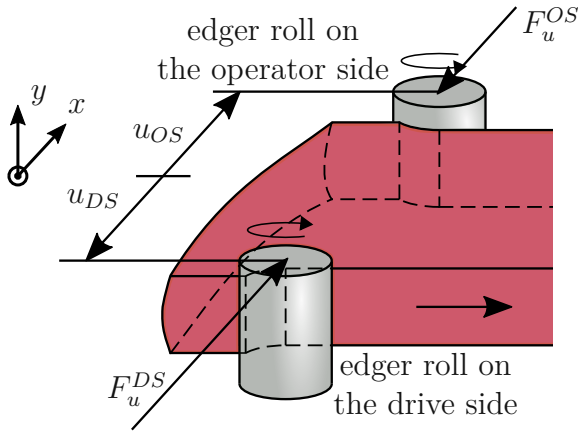


Figure 2.8: Edger rolls and their corresponding positions and forces.

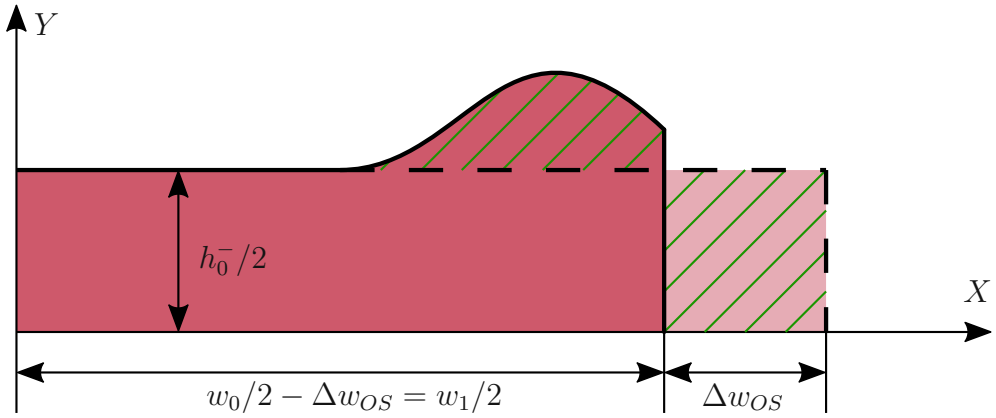


Figure 2.9: Dog-bone effect in case of symmetric edger forces. The dashed lines represent the shape of the plate and the corresponding $Y$-axis before edge rolling.

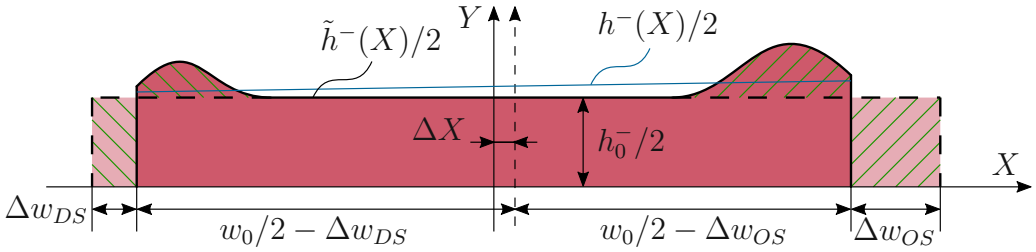


Figure 2.10: Dog-bone effect in case of asymmetric edger forces. The dashed lines represent the shape of the plate and the corresponding $Y$-axis before edge rolling.

Assume that the lateral thickness profile $\tilde{h}^-(X)$ is approximated with a linear function $h^-(X)$, cf. Figure 2.10. To satisfy continuity in both quadrants, the integral relation

$$\int_{-w_1/2}^{0} h^-(X)\,\mathrm{d}X \stackrel{!}{=} \left(\frac{w_0}{2} - \Delta X\right) h_0^- \tag{2.56a}$$

$$\int_{0}^{w_1/2} h^-(X)\,\mathrm{d}X \stackrel{!}{=} \left(\frac{w_0}{2} + \Delta X\right) h_0^- \ , \tag{2.56b}$$

with the initial plate thickness $h_0^-$, the new width of the plate

$$w_1 = w_0 - \Delta w_{DS} - \Delta w_{OS} \tag{2.57}$$

and the displacement

$$\Delta X = \frac{\Delta w_{OS} - \Delta w_{DS}}{2} \tag{2.58}$$

of the centerline (cf. Figure 2.10) must hold true. Here, $\Delta w_{DS}$ and $\Delta w_{OS}$ are the changes of the plate width on the operator and drive side, respectively. The linear thickness profile $h^-(X)$ then follows as

$$h^-(X) = \frac{8h_0^-\Delta X}{w_1^2} X + \frac{w_0}{w_1} h_0^- \ . \tag{2.59}$$

Assuming that asymmetric edger forces $F^- = F_u^{DS} - F_u^{OS} \neq 0$ linearly influence the changes of the widths

$$\Delta w_{DS} = \Delta\bar{w}\left(1 + \frac{F^-}{F_u^\Sigma}\right) \tag{2.60a}$$

$$\Delta w_{OS} = \Delta\bar{w}\left(1 - \frac{F^-}{F_u^\Sigma}\right) \ , \tag{2.60b}$$

with

$$\Delta\bar{w} = \frac{\Delta w_{DS} + \Delta w_{OS}}{2} = \frac{w_0 - w_1}{2} \tag{2.61}$$

and

$$F_u^\Sigma = F_u^{DS} + F_u^{OS} \ , \tag{2.62}$$

the coefficient of the linear term in (2.59) follows as

$$\Delta h^- = h^-\left(\frac{w_1}{2}\right) - h^-\left(-\frac{w_1}{2}\right) = \frac{8h_0^-\Delta X}{w_1} = -\frac{8h_0^-\Delta\bar{w}}{w_1}\frac{F^-}{F_u^\Sigma} \ . \tag{2.63}$$

Because of $\frac{h_0^-}{w_1} \ll 1$ and $\Delta\bar{w} \ll 1$ and because $F^-$ is typically less then 10 % of $F_u^\Sigma$, the estimate (2.63) shows that the contribution of the dog-bone effect to the

lateral thickness profile of the plate can be neglected compared to, e. g., a typical roll gap tilt. The fact $\Delta\bar{w} \ll 1$ also justifies the assumption $w_0 \approx w_1$.

Summarizing, the dog-bone effect gives a nexus of lateral forces $F^-$ applied to the plate and the thickness wedge $\Delta h^-$ of the plate. Similar to the asymmetric mill stretch, exploiting this effect would be very interesting. However, the exact parametrization of the dog-bone effect is extremely difficult without a measurement system for the thickness profile of the plate. Furthermore, the rough estimation of the dog-bone effect shows that this effect is of minor importance. It is thus neglected in the following.

## 2.10 Summary

In this chapter, the force-input model and the position-input model were developed and analyzed. Both models assume edger rolls on the entry and exit side of the roll gap. One of the key findings (see Section 2.2) was that edger rolls are not suitable to compensate for constant plate camber because this would require constant lateral acceleration of the plate in the roll gap. However, the edger rolls can be used to eliminate (offset-free) deviations from the ideal straight centerline of the plate. Furthermore, it was shown that edger rolls on the entry side of the roll gap

- have potentially more influence on the camber of the outgoing plate than edger rolls on the exit side of the roll gap (cf. Section 2.1.2) and
- inherently ensure a stable system dynamics if edger rolls on the exit side are inactive (cf. Section 2.4.1).

At the considered industrial plant, edger rolls are only active in forward rolling passes. This represents a special case of the force-input model in backward rolling passes and the position-input model in forward rolling passes. Thus, a specialized model capturing the conditions at the industrial plant was derived based on the already discussed models.

The two effects mill stretch and dog-bone shape, which are often discussed in the context of roughing mills, were analyzed in the Sections 2.8 and 2.9. Exploiting these effects would be interesting from a control perspective. However, because of the lack of suitable measurements (temperature, thickness profile, ...), parametrization and validation of these effects is difficult. A rough estimate justifies to neglect these effects in the mathematical model.

The specialized model built in this chapter will be used in simulations and will be compared to measurement results from the industrial plant in Chapter 3. Moreover, the model will serve as a basis for control design in Chapter 4.

# CHAPTER 3

## Model parametrization and validation

In this chapter, the mathematical models (2.38), (2.39) and (2.40) are parameterized and validated based on measurements from the industrial plant at voestalpine Stahl GmbH. To this end, the measurement system, which is based on [39], is discussed first. For the purpose of model validation, experiments were conducted where edger rolls move in a lateral direction while the plate is rolled. During these experiments, the edger rolls were active in the third (17 plates) and the fifth rolling pass (38 plates). The model is parameterized based on these experiments.

For the velocity profile (2.10) in the roll gap, the roll gap model of Sims [46] is used and extended to capture the influence of tensile stress. Although the original roll gap model of Sims [46] was not intended to capture asymmetric stress in the roll gap, it turns out that this approach is meaningful [48]. This approximation is also one reason why the resulting sensitivities $K_\Sigma$ are uncertain. Another reason is that the temperature profile is not measured before or during the rolling process in the roughing mill. Thus, only a nominal value of the mean temperature of the strip is known. Typically, the temperature profile is considered in the mean yield stress $k_{fm}$ according to the Hensel-Spittel approach [51, 52]. In the current work, only the nominal mean yield stress $k_{fm}$ according to the nominal mean temperature can be considered. This uncertainty is inherited by the sensitivities $K_\Sigma$, which thus have to be identified based on the experiments.

The assumption of two coupled Timoshenko beams (cf. Section 2.3.1) yields a simple linear system. However, it adds the uncertain variable $E_l$.

Summarizing, the parameters $K_\Sigma$ and $E_l$ are uncertain in the model (2.39) (cf. (2.14), (2.18) and (2.19)). In (2.31c) and thus (2.34), the parameters $K_h^-$, $K_h^+$, $K_H^-$, and $K_H^+$ as well as the thickness and temperature wedge, and the roll gap tilt (mill stretch, offset) are uncertain. Therefore, the curvature $\kappa_{\Delta hH}$ is assumed as one uncertain parameter.

In the following, the parameters $E_l$ and $K_\Sigma$ and $\kappa_{\Delta hH}$ are estimated based on measurement data from the industrial plant. In backward rolling passes, only the parameter $\kappa_{\Delta hH}$ can be estimated. For an overview of known parameters and parameters to be estimated, see Tab. 3.1. Note that the shear modulus $G_l$ is also an uncertain variable. Even though, there is no need to separately identify it because it is coupled with the Young's modulus $E_l$ by Poisson's ratio $\nu$ (cf., (2.22)).

Table 3.1: Overview of known parameters and parameters to be estimated.

| known parameters | | | | |
|---|---|---|---|---|
| $E_h$ | $G_h$ | $I_y^-$ | $A_s^-$ | $w_0$ |
| $l_e^-$ | $\lambda$ | $\nu$ | $L$ | $L^+$ |
| parameters to be estimated | | | | |
| $E_l$ | $K_\Sigma$ | $\kappa_{\Delta hH}$ | | |

Large parts of this section are similar to the author's publication [42].

## 3.1 Measurement system at the industrial plant

At the considered industrial plant, two CMOS cameras are installed above the roller table at the entry and exit side of the mill stand. Figure 1.3 illustrates the setup. With the algorithm discussed in [39], it is possible to capture both the lateral position in the field of view (FOV) and the shape of the plate. After the roughing process, the shape of the plate is accurately measured again in a downstream measurement unit. This measurement is mainly utilized for quality control of the plate before entering the tandem finishing mill. The setup and the algorithm used for the final measurement are discussed in [27, 28].

As usual in the roughing process, the work rolls are cooled with water sprays. This causes water and steam at the upstream plate surface and thus reduces the contrast between the hot edge and the environment. Because of this problem, neither the upstream lateral position nor the upstream shape of the plate can be accurately measured with the entry-side camera. The exit-side camera image is usually not deteriorated by cooling water and thus provides reliable measurement data. Figure 3.1 shows a comparison of two measurements, one with good image quality and one where the measurement is disturbed by steam and water.

While the plate passes the FOV of the exit-side camera, the lateral position and shape of the plate between the roll gap and the FOV is not directly measured and thus unknown. For an accurate calculation of the lateral position $W$ in the roll gap, the camber $\kappa^+$ of the outgoing plate centerline is necessary (cf. (2.24)). This information is only available after the rolling pass is finished. Thus, a reliable calculation of the lateral position $W$ of the plate in the roll gap is only possible after the rolling pass, but not in real time. This considerable measurement delay

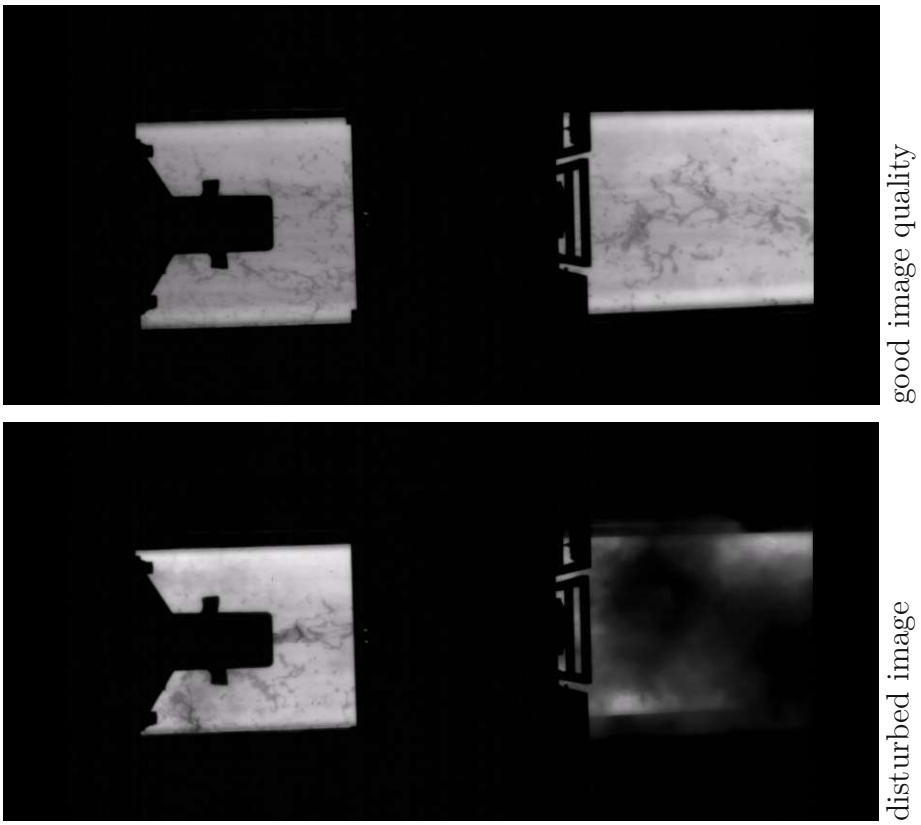


Figure 3.1: Comparison of a measurement with good image quality (upper image) and a measurement disturbed by steam and water (lower image).

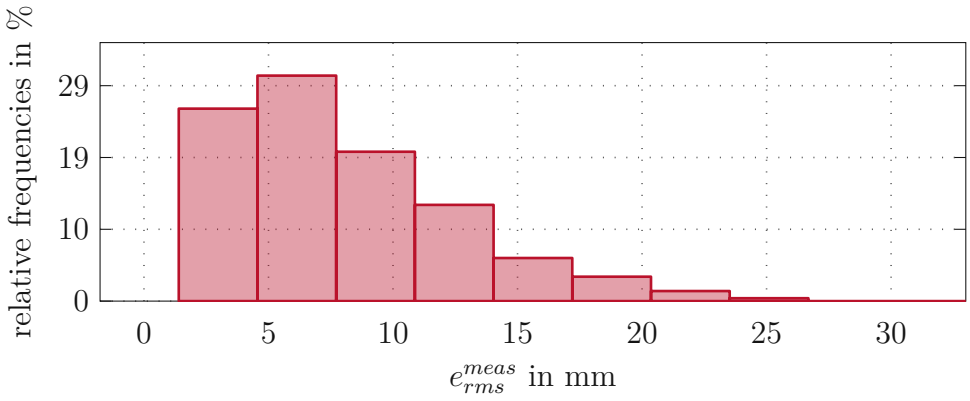


Figure 3.2: Histogram of the mean square error $e_{rms}^{meas}$ between two measurement systems of the plate centerline, mean value 8.0 mm (518 plates).

does not matter for validation purposes but is a significant limitation for feedback control.

The measurement of the plate centerline $cl^+$ at the measurement house is usually not disturbed by cooling water or steam. This measurement thus serves as ground truth. A comparison of the measurement $\tilde{cl}_{cam}^+$ obtained by the camera system after the last rolling pass and the measurement $\tilde{cl}_{MH}^+$ obtained by the downstream measurement unit is shown in Figure 3.2. Here, the error

$$e_{rms}^{meas} = \sqrt{\frac{1}{L^+}\int_0^{L^+}\left(\tilde{cl}_{MH}^+ - \tilde{cl}_{cam}^+\right)^2 \mathrm{d}z} \tag{3.1}$$

is used. The mean square error of 518 plates is about 8.0 mm.

The calculation of the outgoing plate centerline $\tilde{cl}^+$, e. g., according to (2.40), is based on the measurement of the incoming plate centerline $\tilde{cl}^-$. Because the camera on the entry side of the roll gap is usually disturbed by cooling water and steam, the outgoing plate centerline measured in the previous rolling pass (which is the incoming plate centerline of the actual rolling pass) is used as $\tilde{cl}^-$. This incoming plate centerline $\tilde{cl}^-$ is assumed to have the same accuracy as the outgoing plate centerline $\tilde{cl}^+$ of the last rolling pass (cf. Figure 3.2). The accuracy of the measurement system thus limits the accuracy of the centerline $cl^+$ obtained by the mathematical model. Considering the error (3.1), a model-plant mismatch of less than 8.0 mm is thus not expected.

## 3.2 Identification of uncertain parameters

According to (2.40), all uncertain parameters $E_l$, $K_\Sigma$ and $\kappa_{\Delta hH}$ influence the outgoing plate centerline $\tilde{cl}^+$ ($E_l$, $K_\Sigma$ in $\tilde{cl}_{x,u}$ with (2.39), (2.14) and $\kappa_{\Delta hH}$ in

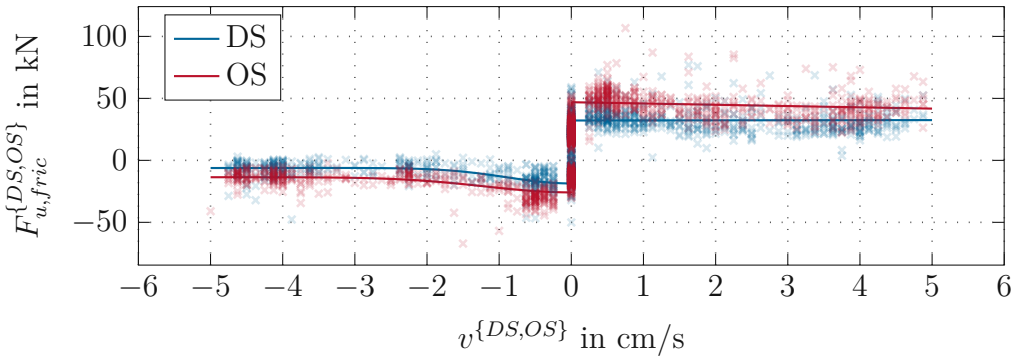


Figure 3.3: Measured (points x) and identified (solid line) friction curves for the drive side (DS, blue) and operator side (OS, red).

$\tilde{cl}_{\Delta hH}$ with (2.34)). Since the parameters $E_l$ and $K_\Sigma$ have nearly the same influence on $cl_{x,u}$, they cannot be independently identified without considering a further measurement signal. Therefore, the lateral force $F^-$, applied by the edger rolls, is used as a further measurement signal. According to (2.25a), $F^-$ depends on $E_l$. Summarizing, to independently identify the uncertain parameters $E_l$, $K_\Sigma$ and $\kappa_{\Delta hH}$, measurements of the incoming plate centerline $\tilde{cl}^-$, the outgoing plate centerline $\tilde{cl}^+$, and the force $F^-$ are required.

### 3.2.1 Friction forces during lateral adjustment of the edger rolls

When measuring the lateral edger force $F^-$, friction forces in the adjustment system of the edgers have to be considered. To investigate these friction forces, force measurements were conducted with laterally moving edger rolls while no plate was clamped between them. Results of such a measurement are shown in Figure 3.3. Because there are no other loads in this scenario and because inertia forces are negligibly small, the measured forces are attributed to the friction forces $F_{u,fric}^{DS}$ and $F_{u,fric}^{OS}$ at the drive side and operator side, respectively. Based on these measurements, friction is modeled by the Stribeck curve [53]

$$F_{u,fric} = r_v v + r_C \operatorname{sgn}(v) + (r_H - r_C) \exp\left(-\left(\frac{v}{v_0}\right)^2\right) \operatorname{sgn}(v) + r_{off} \ , \tag{3.2}$$

with the lateral velocity $v$ of the edger rolls and the unknown model parameters $r_v$, $r_C$, $r_H$, $v_0$, and $r_{off}$. They are identified by minimizing the cost function

$$\min_{r_v, r_C, r_H, v_0, r_{off}} \int_0^{L^-} \left(F_{u,fric} - F_{u,fric}^{meas}\right)^2 \mathrm{d}z_{in} \tag{3.3}$$
$$\text{s.t. } (3.2) \ .$$

The optimization problem (3.3) is individually solved for positive and negative velocities $v$ and for the drive and operator side. This leads to four parameter sets for $r_v$, $r_C$, $r_H$, $v_0$ and $r_{off}$. The resulting curves are also depicted in Figure 3.3. They are subtracted from the measured force to obtain the net force $F^-$ exerted by the edger rolls on the plate.

### 3.2.2 Initial position $W_0$ of the plate in the roll gap

In Section 3.1, it is explained that cooling water and steam usually deteriorate the upstream measurement of the lateral plate position and shape. Nevertheless, adequate filtering methods (like a Savitzky-Golay filter [54], cf. Figure 3.4) and ignoring plates which are strongly affected (i. e., plates where no measurement is available around $t = 0$) would allow to compute the initial lateral plate position $W_0^{cam}$ in the roll gap (i. e., the position upon roll bite). To this end, consider (2.25a) with $F^- = 0$, which gives

$$0 \approx \Phi_0^- l_e^- - W_0^{cam} + w\left(-l_e^-\right) . \tag{3.4a}$$

Similar considerations for the FOV yield

$$0 \approx \Phi_0^- l_{FOV}^- - W_0^{cam} + w\left(-l_{FOV}^-\right) , \tag{3.4b}$$

where $l_{FOV}^-$ describes the distance between the upstream FOV and the roll gap. Elimination of $\Phi_0^-$ in (3.4) gives

$$W_0^{cam} \approx \frac{l_e^-}{l_{FOV}^- - l_e^-}\left(\frac{l_{FOV}^-}{l_e^-} w\left(-l_e^-\right) - w\left(l_{FOV}^-\right)\right) . \tag{3.5}$$

Using this approach, the initial lateral position $W_0 = W_0^{cam}$ is obtained only at the moment of the roll bite. This would suffice for feedback control but not for feedforward control or upfront calculations that require the initial lateral position $W_0$ of the plate. To circumvent this drawback, the initial position $W_0$ has to be estimated by a different approach.

Before the rolling pass, plates are centered and aligned by side guides. It is thus assumed that the position and rotation of the incoming plate matches the definition of $\tilde{cl}^-$ (zero mean, zero mean slope). Furthermore, the lateral position $u^-$ of the edger rolls is typically zero. With this, the lateral position $W_0^{cl}$ can be calculated in advance as

$$W_0^{cl} \approx \tilde{cl}^-(0) - \tilde{cl}^-\left(l_e^-\right) . \tag{3.6}$$

Figure 3.5 shows the estimation of $W_0^{cl}$. To validate this approach, the initial lateral plate position $W_0$ is compared based on the two described methods. The results are shown in Figure 3.6. The fact that $W_0^{cam} = 0$ does not necessarily

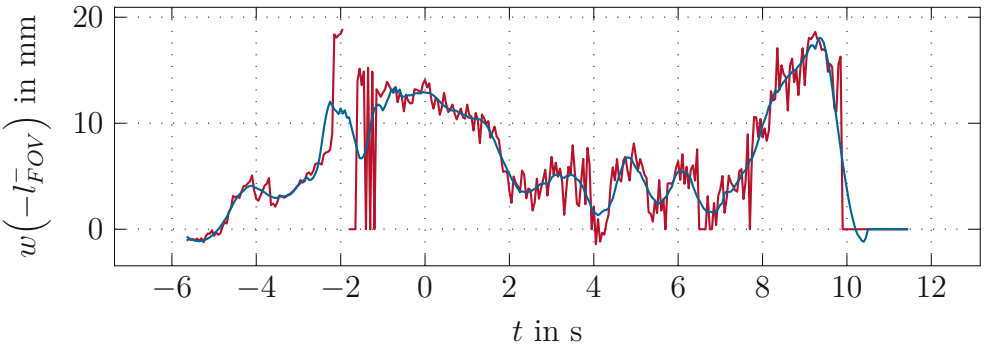


Figure 3.4: Measured (red) and filtered (blue) lateral position $w\left(-l_{FOV}^{-}\right)$ at the entry side's field of view.

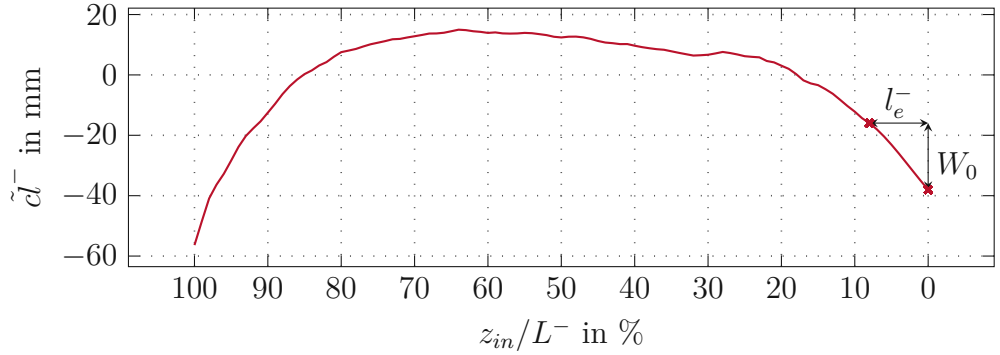


Figure 3.5: The initial lateral position $W_0$ of the plate is estimated based on the shape $\tilde{cl}^{-}$ of the plate centerline before the rolling pass.

imply $W_0^{cl} = 0$ indicates a possible lateral offset of the camera position or a deterministic rotation of the incoming plate, e. g., caused by an asymmetry of plant components. Nevertheless, the strong correlation observed in Figure 3.6 justifies the (real-time feasible) estimation $W_0 = W_0^{cl}$, which is used in all further considerations.

### 3.2.3 Parameter estimation

The estimation of the uncertain parameters $E_l$, $K_\Sigma$ and $\kappa_{\Delta hH}$ is done in forward rolling passes. The estimated parameters are normalized with respect to their nominal values in the form

$$\breve{E}_l = f_{E_l} E_l \tag{3.7a}$$

$$\breve{K}_\Sigma = f_{K_\Sigma} K_\Sigma \tag{3.7b}$$

$$\breve{\kappa}_{\Delta hH} = f_{\Delta hH} \kappa_{\Delta hH} \ . \tag{3.7c}$$

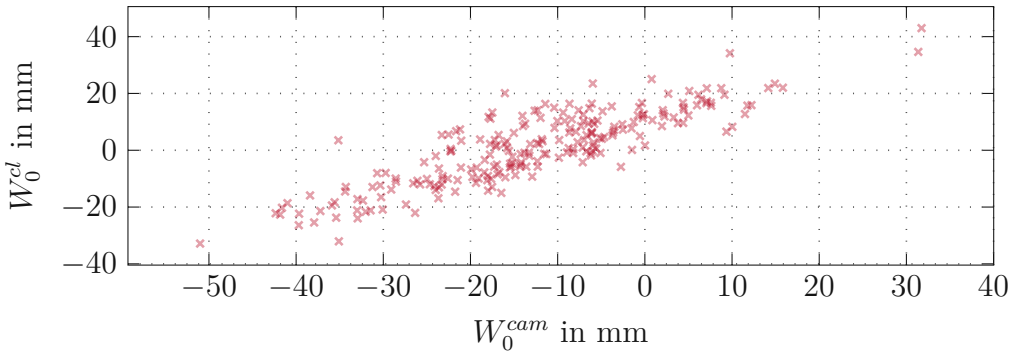


Figure 3.6: Correlation of $W_0$, estimated based on the lateral position $w\left(-l_{FOV}^{-}\right)$ measured by the upstream camera and based on the centerline $\tilde{cl}^{-}$.

Here, $\breve{(\cdot)}$ refers to the estimation of the corresponding parameter $(\cdot)$. The initial lateral position $W_0$ of the plate is extended by an offset

$$\breve{W}_0 = W_0 + W_{0,offset} \tag{3.8}$$

to systematically cover asymmetries of the plant, e. g., asymmetrically adjusted side guides during thread in, imperfections in the alignment of the edger rolls and the roll gap.

The optimization problem to estimate the uncertain parameters reads as

$$\min_{f_{E_l}, f_{K_\Sigma}, f_{\Delta hH}, W_{0,offset}} \int_0^{L^-} \chi_F \left(F^- - F_{meas}^-\right)^2 + \chi_{cl}\left(\tilde{cl}^+ - \tilde{cl}_{meas}^+\right)^2 \mathrm{d}z_{in} \tag{3.9}$$
$$\text{s.t. (2.25a), (2.40)} ,$$

with the scalar weights $\chi_F > 0$ and $\chi_{cl} > 0$. It covers a single plate in one forward rolling pass. A reliable identification of the parameters $f_{E_l}$ and $f_{K_\Sigma}$ requires a sufficiently high excitation (lateral motion of the edger rolls and thus $cl_{x,u}$). Similar, the parameter $f_{\Delta hH}$ can only be identified if the contribution $\kappa_{\Delta hH}$ (cf. (2.31c)) is sufficiently large.

Figure 3.7 shows the relative frequency distributions of the identified parameters. The first row shows the optimized parameters $f_{E_l}$ and $f_{K_\Sigma}$ for 27 plates where edgers were moved during the fifth rolling pass. The peaks in these distributions are quite distinct. Based on their locations, the constant empirical choices of $f_{E_l} = 1\,\%$ and $f_{K_\Sigma} = 10\,\%$ were made and proved reasonable. Thus, all further investigations are performed with these values.

The frequency distribution of the parameter $f_{\Delta hH}$ shown in Figure 3.7 was obtained for 325 plates where measurement data are available in the fifth rolling pass (irrespective of a lateral motion of the edger rolls). Because of uncertainties like temperature gradient, offset, and mill stretch, the parameter $f_{\Delta hH}$ is subject

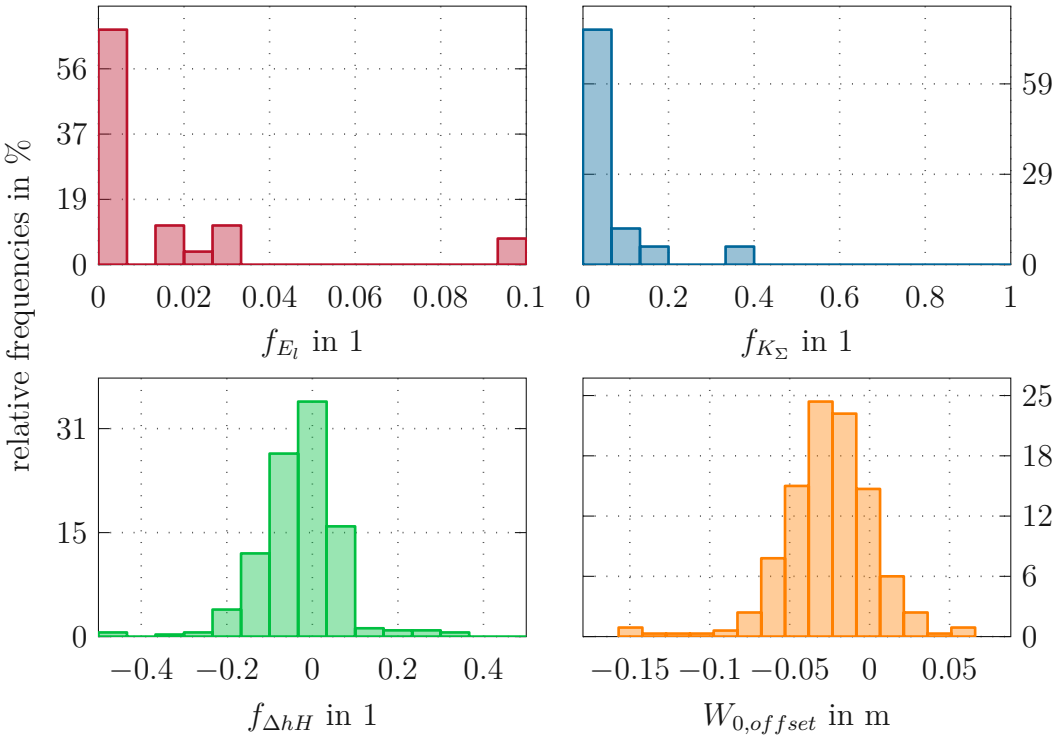


Figure 3.7: Relative frequency distribution of the identified parameters $f_{E_l}$ (27 plates, red), $f_{K_\Sigma}$ (27 plates, blue), $f_{\Delta hH}$ (325 plates, green), and $W_{0,offset}$ (325 plates, orange).

to considerable fluctuations. Figure 3.7 also shows the frequency distribution of the identified parameter $W_{0,offset}$. This distribution is approximately normally distributed and the mean value is clearly negative. This mean value is used for further calculations.

In backward rolling passes, the optimization problem reads as

$$\min_{f_{\Delta hH}} \int_0^{L^-} \left(\tilde{cl}^+ - \tilde{cl}^+_{meas}\right)^2 \mathrm{d}z_{in} \qquad (3.10)$$
$$\text{s.t. } (2.40) \ .$$

Here, only the parameter $f_{\Delta hH}$ can be estimated. It turned out that the factor $f^{(4)}_{\Delta hH}$ estimated in the fourth rolling pass correlates with the factor $f^{(5)}_{\Delta hH}$ determined in the fifth rolling pass (cf. Figure 3.8). This allows to predict $f^{(5)}_{\Delta hH}$ based on the value $f^{(4)}_{\Delta hH}$ identified in the fourth rolling pass. This gives

$$f^{(5)}_{\Delta hH} = f_{f\Delta hH} f^{(4)}_{\Delta hH} \ , \qquad (3.11)$$

i. e., $f^{(5)}_{\Delta hH}$ is not identified by optimization. The factor $f_{f\Delta hH}$ in (3.11) represents

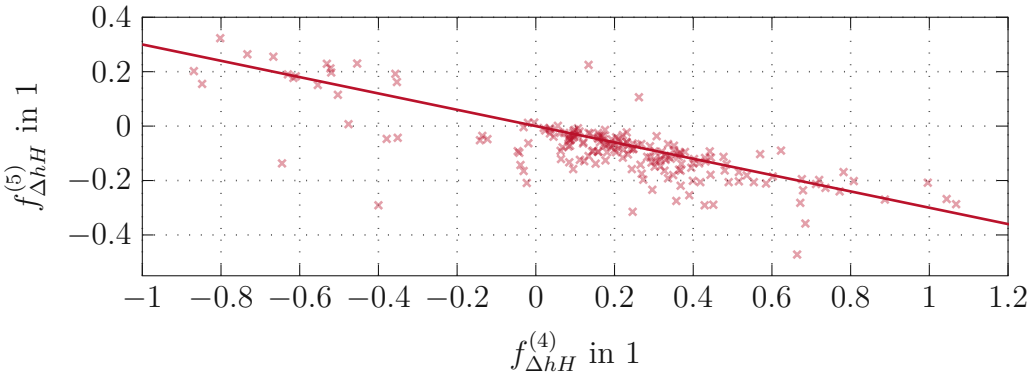


Figure 3.8: Correlation of $f_{\Delta hH}$ determined in the fourth and fifth rolling pass, indicated by the upper index (4) and (5).

the slope of the regression line in Figure 3.8. This approach has the advantage that minor changes of the industrial plant, like a change of work rolls, are implicitly captured in the estimation of the factor $f^{(4)}_{\Delta hH}$ in the fourth rolling pass. Furthermore, this approach is real-time feasible because the factor $f^{(5)}_{\Delta hH}$ can be calculated in advance.

Generally, the parameters $f_{E_l}$ and $f_{K_\Sigma}$ have to be individually identified for every rolling pass and every product class. Moreover, the parameter $f_{\Delta hH}$ is likely to change if plant components are maintained or changed (e. g., work rolls). The parameters $f_{f\Delta hH}$ and $W_{0,offset}$ may change if major modifications are implemented at the industrial plant (e. g., if the positioning system of the side guides or the frame are damaged, maintained or renewed). Thus, for permanent use of the mathematical model or model-based control concepts at the industrial plant, a recurring adaptation of the parameters is recommended. A possible approach is given in Appendix A.2.

During the production process, the adjusted roll gap tilt $\Delta H$ is only rarely changed and constant for many plates. Furthermore, the thickness profile is only measured once, after the final rolling pass. Thus, the influence of $\Delta h^-$ and $\Delta H$ on $cl^+$ (cf. (2.31c)) cannot be easily separated and validated. This would be desirable to use $\Delta H$ as control input. However, this is not possible at the considered plant. This is why $\Delta H$ is considered as an (rather uncertain) externally defined system input not available for control purposes.

## 3.3 Validation of the lateral plate motion

In this section, the computed lateral plate position $W$ is compared to the measurement data from the considered industrial plant. This comparison is only made for forward passes where the edger rolls were active. In cases where edger rolls are active, but remain in their center ($u^- = 0$), the lateral plate position $W$ in the

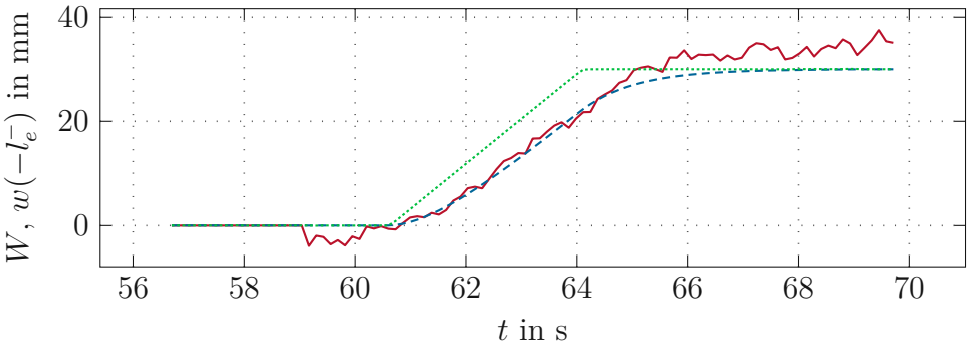


Figure 3.9: Measured (red) and calculated (blue) lateral position $W$ of the plate in the roll gap and lateral position $u^-$ of the edger rolls (green) for a typical plate during the fifth rolling pass.

roll gap is only subject to small fluctuations and is thus not considered in this section. The lateral plate motion in backward rolling passes cannot be influenced at the considered industrial plant. Its validation is thus of minor importance. For rolling passes with inactive edgers ($F^- = 0$), refer to [16].

Figure 3.9 shows the lateral position obtained by the camera system and the calculated lateral position in the roll gap in the fifth rolling pass. The edger rolls were moved in lateral direction (green) and the model of the lateral position of the plate (blue) fits the measurement (red) with satisfying accuracy. The lateral position of the plate in the roll gap follows the lateral position of the edger rolls approximately with first-order low-pass dynamics (eigenvalue $\lambda_{u^\pm,1} = -\frac{1}{l_e^-}$), see Section 2.7.1. Figure 3.9 indicates that the computed lateral position of the plate in the roll gap is limited by the lateral position of the edger rolls. This only approximately holds true for the measured lateral plate position because of measurement noise and camera offset as well as the influence of the inputs $\kappa^-$, $\Delta h^-$ and $\Delta H$, which were neglected in the mathematical model.

## 3.4 Validation of the shape of the plate centerline

This section is dedicated to the validation of the outgoing centerline shape $\tilde{cl}^+$ of the plate according to (2.40). A reliable measurement of this shape is available after the plate has passed the FOV of the downstream camera [39]. After the final rolling pass, the shape of the plate is additionally measured with high accuracy for the purpose of quality control [27, 28].

Figure 3.11 shows a representative measured (red camera [39] / orange measurement house [27, 28]) and calculated (blue) centerline after the fifth rolling pass. The lateral position of the edger rolls (green) is horizontally shifted so

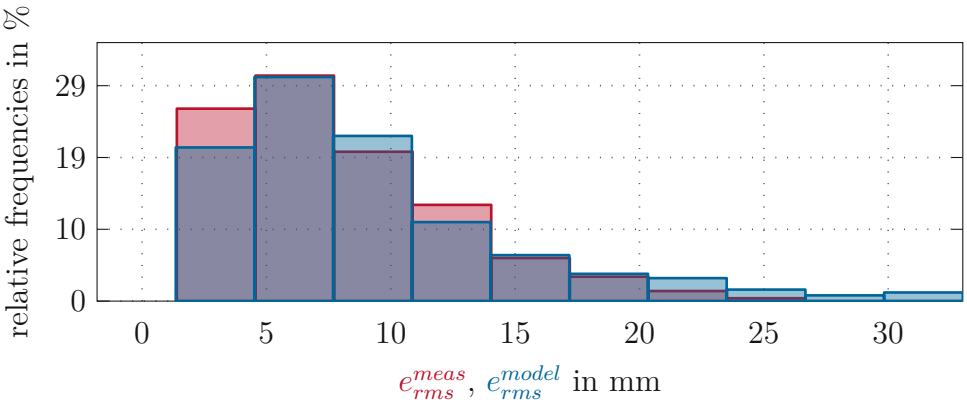


Figure 3.10: Histogram of the mean square errors $e^{meas}_{rms}$ and $e^{model}_{rms}$, mean values 8.0 mm and 9.1 mm (518 plates).

that the figure shows which part of the plate experiences which lateral position of the edger rolls. The measured and calculated centerlines show a significant deformation, which demonstrates the suitability of the edger rolls to control the shape of the outgoing plate centerline. Furthermore, the measured and calculated centerlines match quite well. A histogram of the error (cf. (3.1))

$$e^{model}_{rms} = \sqrt{\frac{1}{L^+}\int_0^{L^+}\left(\tilde{cl}^+_{MH} - \tilde{cl}^+_{model}\right)^2 \mathrm{d}z} \tag{3.12}$$

is depicted in Figure 3.10. The mean square error of 518 plates is 9.1 mm. Thus, the accuracy of the mathematical model is close to the accuracy of the measurement system.

Figure 3.11 shows that a significant deformation appears when the edger rolls start or stop moving. This behavior can be explained based on the force $F^-$ calculated for the same plate, which is shown in Figure 3.12. The force peaks cause changes of the camber of the plate according to (2.17).

## 3.5 Summary

In this chapter, the model of the lateral position $W$ of the plate in the roll gap and the centerline $cl^+$ of the outgoing plate was parameterized and compared to measurement data recorded at the industrial plant. For this purpose, dedicated experiments were conducted where the edger rolls moved in lateral direction.

The lateral plate position $W$ of the plate in the roll gap is almost independent of the uncertain model parameters. Its dynamic behavior depends mainly on the (well known) distance $l^-_e$ between the edger rolls and the roll gap (cf., Section 2.7.1). It was found that the lateral position $W$ of the plate in the roll gap follows the

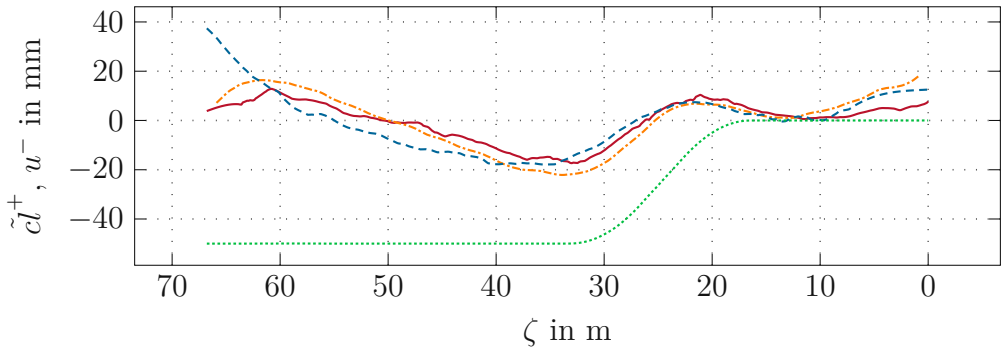


Figure 3.11: Measured (red camera [39] / orange measurement house [27, 28]) and calculated (blue) plate centerlines and lateral position of (horizontally shifted) the edger rolls (green) for a typical plate after the fifth rolling pass.

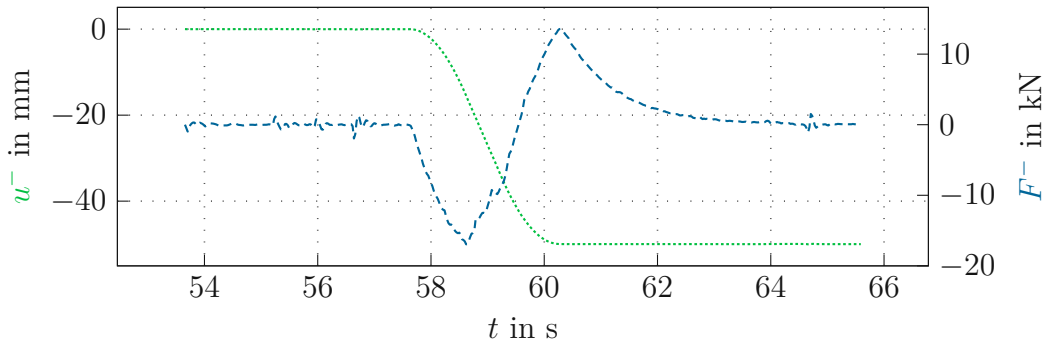


Figure 3.12: Calculated edger force (blue) and position of the edger rolls (green) for the same plate as shown in Figure 3.11.

lateral position $u^-$ of the edger rolls approximately with a first-order low-pass dynamics. The assumption to neglect the model inputs $\kappa^-$, $\Delta h^-$, and $\Delta H$ proved to be justified, especially because the focus in this thesis is on safe plate motion and not precise modeling of the lateral plate position in the roll gap. A safe lateral plate motion can thus be ensured by limiting the lateral position $u^-$ of the edger rolls.

The experiments conducted at the industrial plant show that moving the edger rolls in lateral direction changes the centerline $\tilde{cl}^+$ of the outgoing plate. Furthermore, the mathematical model is able to calculate the deformation of the plate centerline.

The model from Chapter 2 is thus parameterized and validated. It is a suitable basis for subsequent controller designs.

# CHAPTER 4

# Control design

This chapter is dedicated to the control design. The mathematical model from Chapter 2 and the measurement system discussed in Chapter 3 are used in different control approaches. All control approaches proposed in this chapter pursue the following control objectives:

- Safe plate motion: The lateral position of the plate in the roll gap should not exceed a given maximum.
- Correct shape: The final plate should be as straight as possible (small camber).

The following three sections describe three different control approaches.

The first control concept, presented in Section 4.1, uses lateral forces, e. g. applied by edger rolls, on the entry and exit side of the roll gap as control inputs (force-input model, cf., Section 2.2). To control the plate motion and the shape of the plate, a linear quadratic regulator (LQR) is designed. To observe constraints of the maximal lateral position and velocity of the edger rolls, a subordinate admittance controller with nonlinear stiffness and damping coefficients is used.

The second control concept uses the lateral position of the edger rolls as control input (position-input model, cf., Section 2.4) and is presented in Section 4.2. In this concept, only single forward rolling passes with edger rolls on the entry side of the roll gap are considered. Because camber essentially occurs in the roll gap and the camera is a few meters apart from the roll gap, an optimization-based feedforward controller (does not require feedback) is designed. Furthermore, a proportional feedback controller with Smith predictor is proposed. The controllers are then assembled in a two-degrees-of-freedom control structure.

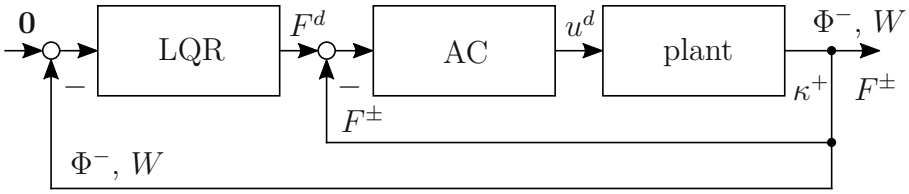


Figure 4.1: Cascade control structure, inner loop: admittance control (AC); outer loop: LQR.

The third control concept, presented in Section 4.3, addresses the task of considering all upcoming rolling passes in a joint optimization problem. It simultaneously calculates the trajectories for the edger roll position in forward rolling passes and the constant roll gap tilts in forward and backward rolling passes. An update is performed after every rolling pass, which gives the proposed control concept its model predictive control (MPC) character.

The three different control strategies are analyzed in simulation studies based on the validated model of Chapter 2 and 3.

Large parts of this section are similar to the author's publications [41–43].

## 4.1 Optimal control of the lateral plate motion and shape by applying lateral forces with edger rolls

A control concept based on the force-input model (cf. Section 2.2) is proposed. In the force-input model, all eigenvalues are 0 independent of the case if edger rolls are active on the entry side, exit side or on both sides of the roll gap. All of these three scenarios are analyzed in simulation studies. Thus, in this section, it is considered that the inputs $F^-$ and $F^+$ (defined by edger positions) can be chosen and actively modified during the rolling pass. A cascade control structure as outlined in Figure 4.1 is proposed. In an outer loop, an LQR controls the plate motion and camber. An admittance controller (AC) in the inner loop ensures that the lateral position and velocity of the edger rolls do not violate given safety limits.

### 4.1.1 Admittance control (inner loop)

The following considerations apply equally to edger rolls on the entry and exit side of the roll gap. Thus, lateral forces applied by edger rolls are described by the variable $F$ and lateral positions of edger rolls are denoted by $u$ for simplicity throughout this section.

In the considered rolling mill, the edger rolls are positioned with an underlying position controller. In this way, the desired plate width $w_0 = u_{OS} + u_{DS} - 2R_e$, where $u_{OS}$ and $u_{DS}$ are the lateral positions of the edger rolls and $R_e$ is their radius (cf. Figure 2.8), can be reliably maintained. Their mean position $u = \frac{u_{OS}-u_{DS}}{2}$, which is relevant for $F$, can also be easily adjusted. To exert the desired forces, but also satisfy given constraints for $u$ and $\dot{u}$, an admittance controller with nonlinear gains is designed. Assume that $F^d$ is the desired lateral force of the edger rolls. The desired values are denoted by the superscript $d$. The admittance control law [55]

$$m^d \ddot{u}^d + d^d \dot{u}^d + k^d u^d = \underbrace{k^P e + k^I \int e \mathrm{d}\tau}_{\tilde{F}} \ , \tag{4.1}$$

with the desired mass $m^d$, the damping coefficient $d^d$, the stiffness $k^d$, the control parameters $k^P$ and $k^I$, and the force control error $e = F^d - F$, is used. The integral term on the right-hand side of (4.1) ensures a zero steady-state error. This controller requires the lateral force $F$ to be measured. This was already assumed in Section 3.2.

In the steady state, (4.1) reduces to

$$k^d u^d = \tilde{F} \ . \tag{4.2}$$

The stiffness coefficient $k^d$ is chosen in the form

$$k^d = k_1^d + k_2^d \, , \qquad k_1^d = \frac{k_0}{e^{\frac{|\tilde{F}|}{k_0 u_{max}^d}}} \, , \qquad k_2^d = \frac{\left|\tilde{F}\right|}{u_{max}^d} \tag{4.3}$$

to avoid at least in the steady-state case that the absolute lateral displacement $|u^d|$ exceeds the bound $u_{max}^d$. In (4.3), $k_0$ is a constant tuning parameter. Figure 4.2 shows the chosen stiffness and the resulting desired displacement $u^d$.

In an analogous manner, a nonlinear damping coefficient

$$d^d = \frac{d_0}{e^{\frac{|\tilde{F}-k^d u^d|}{d_0 \dot{u}_{max}^d}}} + \frac{\left|\tilde{F} - k^d u^d\right|}{\dot{u}_{max}^d} \ , \tag{4.4}$$

with a constant $d_0 > 0$, is used to avoid an absolute velocity $|\dot{u}^d|$ larger than $\dot{u}_{max}^d$. Note that (4.3) and (4.4) cannot strictly guarantee satisfaction of the constraints of $u^d$. For instance, small values of $d^d$ can lead to $u^d > u_{max}^d$ during transient

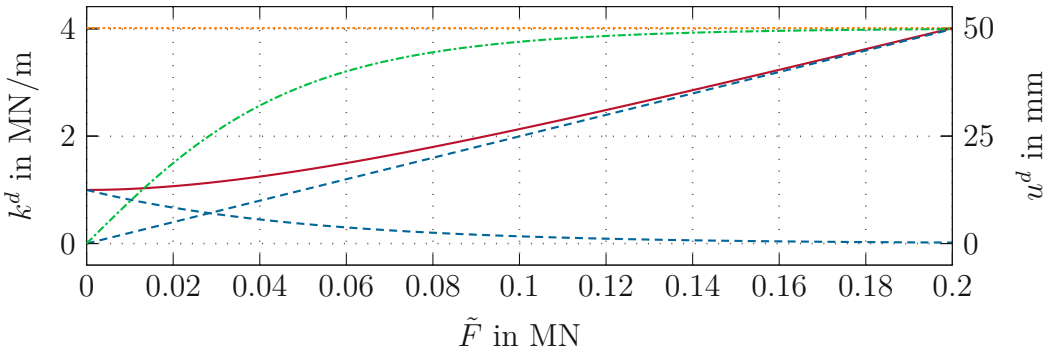


Figure 4.2: Desired stiffness $k^d$ (solid red), components of the stiffness $k_1^d$ and $k_2^d$ (dashed blue) and displacement $u^d$ (dashdotted green) depending on $\tilde{F}$ for $u_{max}^d = 50\,\text{mm}$ (dotted orange) and $k_0 = 1\,\text{MN/m}$.

phases. The desired mass is chosen as a constant $m^d = m_0$.

Because of the nonlinear stiffness (4.3), the steady-state value of the error $e$ is not necessarily zero and thus the integral term on the right hand side of (4.1) would grow without bounds. To avoid this undesirable behavior, an anti-wind-up (AWP) strategy is considered in the control design. Simple box constraints for the value of the integral yield a satisfactory result. Moreover, this value is reset to zero if the error $e$ changes its sign.

### 4.1.2 LQR (outer loop)

In this section, an LQR for the lateral motion and the camber of the outgoing plate is designed. It is assumed that the underlying admittance controller works sufficiently fast and accurate. Thus, the following control concept is developed for the model (2.13) and (2.17) with the control inputs $F^-$ and $F^+$.

Because the shape of the plate is measured with cameras directly before and after the mill stand, the curvature $\kappa^-$ is known [39, 56]. The roll gap height $\Delta H$ is defined by self-retaining electromechanical actuators. This implies that $\Delta H$ can only be adjusted between the rolling passes. During a pass, $\Delta H$ remains essentially constant, apart from the load-induced mill stretch which is neglected (cf. Section 2.8). It is assumed that the thickness profile of the outgoing plate equals the roll gap height ($\Delta h^+ = \Delta H$). Therefore, $\Delta h^-$ is known for the subsequent rolling pass. Furthermore, the process variables $\Delta H$ and $\Delta h^-$ can be treated as known exogenous inputs for the controller design.

Assume that the design model (2.13) and (2.17) is discretized in the form

$$\mathbf{x}_{F,k+1} = \mathbf{\Phi}_F \mathbf{x}_{F,k} + \mathbf{\Gamma}_{F,\alpha} \mathbf{F}_k + \mathbf{\Gamma}_d \mathbf{d}_k\,, \qquad \mathbf{x}_{F,0} = \mathbf{x}_F(0) \tag{4.5a}$$

$$\kappa_k^+ = \mathbf{D}_\alpha \mathbf{F}_k + \mathbf{H}\mathbf{d}_k\,, \qquad \alpha \in \{b, i, o\}\,. \tag{4.5b}$$

The index $k = 0, \ldots, N-1$ refers to the equidistant nodes of a grid on the incoming plate, i. e. $\mathbf{x}_{F,k} = \mathbf{x}_F(k\Delta z^-)$. The spatial (independent) variable is $z_{in}$ and the grid step size is $\Delta z^-$. Thus, the length $L^-$ of the incoming plate satisfies the relation $L^- = (N-1)\Delta z^-$. Moreover, $\Phi^-$ and $W$ are summarized in the vector $\mathbf{x}_F = \begin{bmatrix} \Phi^- & W \end{bmatrix}^{\mathrm{T}}$, $F^-$ and $F^+$ are assembled in $\mathbf{F} = \begin{bmatrix} F^- & F^+ \end{bmatrix}^{\mathrm{T}}$, and $\mathbf{d} = \begin{bmatrix} \kappa^- & \Delta h^- & \Delta H \end{bmatrix}^{\mathrm{T}}$ combines the known inputs $\kappa^-$, $\Delta h^-$ and $\Delta H$. Because the camber of the outgoing plate (2.17) does not depend on the lateral position of the plate in the roll gap (2.13), (4.5b) does not depend on $\mathbf{x}_{F,k}$ either. In (4.5), three operational situations for a rolling mill with edger rolls on the entry and exit side are distinguished:

- Edger rolls are active on both sides of the roll gap, $\alpha = b$.
- Edger rolls are active only on the entry side of the roll gap, $\alpha = i$.
- Edger rolls are active only on the exit side of the roll gap, $\alpha = o$.

During a rolling pass, the system switches between these three situations. Situation $\alpha = i$ is relevant for the thread-in phase, when the plate has not yet reached the edger rolls on the exit side of the roll gap. Then, situation $\alpha = b$ follows where both edger rolls on the entry and exit side of the roll gap touch the plate. Finally, situation $\alpha = o$ describes the thread-out phase when the plate has left the edger rolls on the entry side of the roll gap. By analogy, model formulations for rolling mills that have edger rolls only at the entry or only at the exit side can be found. In these cases, however, there are also situations where the plate is clamped in the roll gap but not in contact with any edger rolls (thread-in or thread-out phase). During these phases, the motion and the camber of the plate cannot be controlled. Therefore, three different controllers have to be designed for the situations $\alpha \in \{b, i, o\}$.

The control objective is to regulate both the lateral plate motion $W$ and the camber $\kappa^+$ of the outgoing plate to zero. The relative importance of these two objectives should be adjustable based on user-defined weighting parameters. Inspired by the classical stationary LQR design problem, the optimization problem

$$\begin{aligned} \min_{\mathbf{F}} \sum_{k=0}^{\infty} & \begin{bmatrix} \mathbf{x}_{F,k}^{\mathrm{T}} & \mathbf{F}_k^{\mathrm{T}} & \kappa_k^+ \end{bmatrix} \begin{bmatrix} \mathbf{Q} & \mathbf{0} & \mathbf{0} \\ \mathbf{0} & \mathbf{R}_\alpha & \mathbf{0} \\ \mathbf{0} & \mathbf{0} & T \end{bmatrix} \begin{bmatrix} \mathbf{x}_{F,k} \\ \mathbf{F}_k \\ \kappa_k^+ \end{bmatrix} \\ \text{s.t. } & (4.5) \end{aligned} \tag{4.6}$$

has to be solved. In (4.6), $\mathbf{Q}$, $\mathbf{R}_\alpha$ denote positive definite weighting matrices, and $T > 0$ is a scalar weighting factor. The optimization problem (4.6) directly leads to the optimal control input

$$\mathbf{F}_k^* = \mathbf{K}_{x,\alpha}\mathbf{x}_{F,k} + \mathbf{K}_{d,\alpha}\mathbf{d}_k\,, \qquad k = 0, \ldots, N-1 \tag{4.7}$$

with

$$\mathbf{K}_{x,\alpha} = -\left(\mathbf{R}_\alpha + \mathbf{D}_\alpha^{\mathrm{T}} T \mathbf{D}_\alpha + \mathbf{\Gamma}_{F,\alpha}^{\mathrm{T}} \mathbf{P}_{s,\alpha} \mathbf{\Gamma}_{F,\alpha}\right)^{-1} \mathbf{\Gamma}_{F,\alpha}^{\mathrm{T}} \mathbf{P}_{s,\alpha} \mathbf{\Phi}_F \tag{4.8a}$$

$$\mathbf{K}_{d,\alpha} = -\left(\mathbf{R}_\alpha + \mathbf{D}_\alpha^{\mathrm{T}} T \mathbf{D}_\alpha + \mathbf{\Gamma}_{F,\alpha}^{\mathrm{T}} \mathbf{P}_{s,\alpha} \mathbf{\Gamma}_{F,\alpha}\right)^{-1} \left(\mathbf{D}_\alpha^{\mathrm{T}} T \mathbf{H} + \mathbf{\Gamma}_{F,\alpha}^{\mathrm{T}} \mathbf{P}_{s,\alpha} \mathbf{\Gamma}_d\right) . \tag{4.8b}$$

Moreover, $\mathbf{P}_{s,\alpha}$ is found by solving the discrete algebraic Riccati equation

$$\begin{aligned} \mathbf{P}_{s,\alpha} =& \mathbf{Q} + \mathbf{\Phi}_F^{\mathrm{T}} \mathbf{P}_{s,\alpha} \mathbf{\Phi}_F - \mathbf{\Phi}_F^{\mathrm{T}} \mathbf{P}_{s,\alpha}^{\mathrm{T}} \mathbf{\Gamma}_{F,\alpha} \\ & \left(\mathbf{R}_\alpha + \mathbf{D}_\alpha^{\mathrm{T}} T \mathbf{D}_\alpha + \mathbf{\Gamma}_{F,\alpha}^{\mathrm{T}} \mathbf{P}_{s,\alpha} \mathbf{\Gamma}_{F,\alpha}\right)^{-\mathrm{T}} \mathbf{\Gamma}_{F,\alpha}^{\mathrm{T}} \mathbf{P}_{s,\alpha} \mathbf{\Phi}_F . \end{aligned} \tag{4.9}$$

During the rolling pass, the control law (4.7), (4.8) switches from $\mathbf{K}_{x,i}$ and $\mathbf{K}_{d,i}$ to $\mathbf{K}_{x,b}$ and $\mathbf{K}_{d,b}$ and further to $\mathbf{K}_{x,o}$ and $\mathbf{K}_{d,o}$. Because the switching points depend only on $z_{in}$ and each controller is used just once, the asymptotic stability of the individual control laws implies the stability of the switched control law.

### 4.1.3 Simulation results

As indicated in Figure 4.1, the plant input used by the admittance controller is the desired lateral edger position $u^d$. For the mathematical model (2.13) and (2.17), however, the forces $F^-$ and $F^+$ serve as control inputs. Thus, a simulation model is required that links $u^d$ with $F^-$ and $F^+$, respectively. Considering the Timoshenko beam models with different Young's moduli according to Figure 2.3, the forces $F^-$ and $F^+$ can be calculated as functions of $u^- = w(-l_e^-)$ and $u^+ = w(l_e^+)$ based on (2.25).

The following simulations were conducted with the grid spacing $\Delta z^-$ of the independent coordinate $z_{in}$ which satisfies the relation $\Delta z_k^- = v_{en,k} T_s$ with the sampling time $T_s = 1\,\mathrm{ms}$.

### 4.1.4 Results of the admittance control

In this section, the admittance controller is investigated based on the force-input model (2.13), (2.17) and the relation (2.25). Consider a scenario where the plate is clamped by the edgers on the entry side and by the work rolls in the roll gap. Assume that the plate does not move forward, i. e., $v_{en} = 0$. In this situation, a step of the desired asymmetric edger force is requested. The simulated response of the inner admittance control loop is shown in Figure 4.3. The desired force level is not reached because of the constraint $u^d \leq u^d_{max}$. Figure 4.3 also shows that neither $u^d$ and $\dot{u}^d$ nor $u$ and $\dot{u}$ violate their constraints.

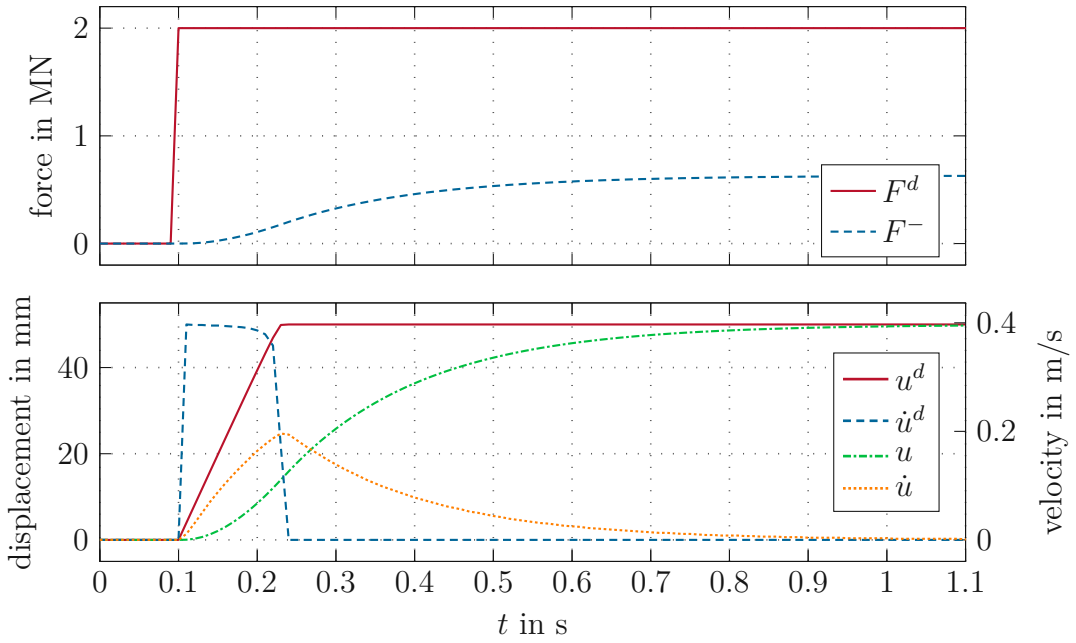


Figure 4.3: Desired and actual force (upper graph) caused by a lateral displacement of the edger rolls (lower graph).

### 4.1.5 Results of the LQR for the plate motion and camber

A simulation study of the whole cascade control structure according to Figure 4.1 is performed. Figure 4.4 shows the corresponding simulation results. The system behavior significantly changes at the switching points (between 2.8 m and 6.7 m both edgers are active). Because the control law is only switched at the respective points and changes are not considered in advance, the method with edger rolls active on both sides of the roll gap causes a camber at the switching points. Moreover, the figure shows that the desired values $\Phi^- = 0°$, $W = 0\,\mathrm{m}$ and $\kappa^+ = 0\,\mathrm{m}^{-1}$ are asymptotically reached if the controller is active.

From Figure 4.4, it can be inferred that the control performance of a rolling mill with edgers at the entry and at the exit side is not significantly better compared to a rolling mill with edger rolls solely on one side. The only advantage is the fact that the head end as well as the tail end of the plate can be straightened with the edger rolls on both sides of the roll gap.

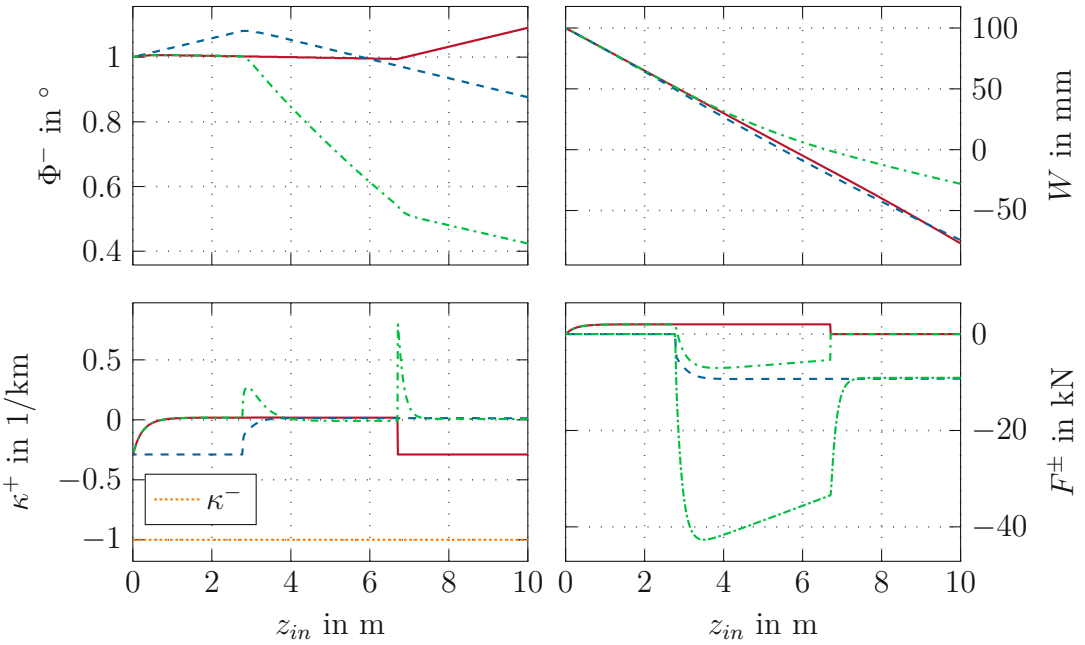


Figure 4.4: Angular deflection (upper left graph), lateral displacement (upper right graph), camber of the outgoing plate (lower left graph), and control input (lower right graph) for the first rolling pass depicted for the case of edger rolls on the entry (solid red), exit (dashed blue) and both sides (dashdotted green) of the roll gap.

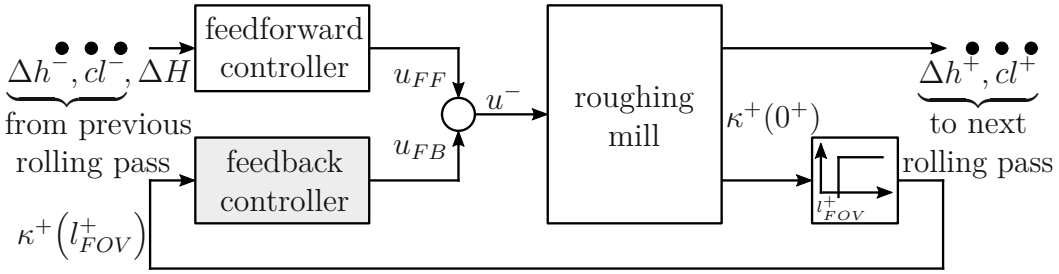


Figure 4.5: Block diagram of the 2-DOF control structure.

## 4.2 Optimal control of the lateral plate motion and shape using the lateral position of edger rolls

The mathematical model from Section 2.6, which was validated in Chapter 3, serves as a basis for the controller design in this section. Here, only a single forward rolling pass (fifth rolling pass) is considered.

The measurement of the outgoing shape $cl^+$ with the measurement system described in Section 3.1 starts as soon as the head end of the plate reaches the FOV of the exit-side camera system. Because camber essentially develops in the roll gap but can only be measured in the FOV of the downstream camera system, the measurement exhibits a delay. This lack of real-time measurement is also the reason why the head end of the plate cannot be straightened by simple feedback control. Therefore, to achieve the stated control objectives, an optimal feedforward controller is designed in a first step. It is then supplemented by a feedback controller to further reduce the remaining camber. Hence, a two-degrees-of-freedom (2-DOF) control concept is proposed (cf. Figure 4.5). Note that the feedforward controller uses the centerline $cl^+$ and the feedback controller the camber $\kappa^+$ of the outgoing plate as controlled variable.

### 4.2.1 Optimal feedforward control

In the following, an optimal feedforward control law for the lateral edger position $u^- = u_{FF}$ is derived based on the model (2.39) and (2.40). The theoretical foundations can be found, e. g., in [57]. In contrast to [57], where the input $u^-$ and the states $\mathbf{x}$ are used with an embedded integrator, in this work only the input variable $u^-$ is used with an embedded integrator (i. e., input increments are used as optimization variables). Furthermore, the predictive control is extended by a term to compensate for the incoming centerline $cl^-$ and for the contribution $cl_{\Delta hH}$ to the outgoing centerline $cl^+$.

Using the spatial discretization $\Delta z^-$ and the zero-order-hold method, (2.39)

and (2.40) can be written in discretized form

$$\mathbf{x}_{k+1} = \mathbf{\Phi}\mathbf{x}_k + \mathbf{\Gamma}u_k^- \,, \qquad \mathbf{x}_0 = \mathbf{x}(0) \tag{4.10a}$$

$$\mathbf{y}_k = \mathbf{C}\mathbf{x}_k + \mathbf{D}\Big(cl_k^- + cl_{\Delta hH,k}\Big) \,, \tag{4.10b}$$

with the matrices

$$\mathbf{\Phi} = e^{\mathbf{A}_f \Delta z^-} \,, \qquad \mathbf{\Gamma} = \int_0^{\Delta z^-} e^{\mathbf{A}_f \tilde{z}} \mathrm{d}\tilde{z}\mathbf{B} \,, \tag{4.11}$$

$$\mathbf{C} = \begin{bmatrix} 0 & 1 & 0 & 0 \\ 0 & 0 & 1 & 0 \end{bmatrix} \,, \qquad \mathbf{D} = \begin{bmatrix} 0 \\ 1 \end{bmatrix} \tag{4.12}$$

and the output $\mathbf{y} = \begin{bmatrix} W & cl^+ \end{bmatrix}^\mathrm{T}$. The solution of $\mathbf{x}_{k+l}$ and $\mathbf{y}_{k+l}$ at an arbitrary spatial point $k+l$ directly follows as

$$\mathbf{x}_{k+l} = \mathbf{\Phi}^l \mathbf{x}_k + \sum_{j=k}^{k+l-1} \mathbf{\Phi}^{k+l-j-1} \mathbf{\Gamma} \underbrace{\left( u_{k-1}^- + \sum_{m=k}^{j} \Delta u_m^- \right)}_{u_j^-} \tag{4.13a}$$

$$\mathbf{y}_{k+l} = \mathbf{C}\mathbf{x}_{k+l} + \mathbf{D}\Big(cl_{k+l}^- + cl_{\Delta hH,k+l}\Big) \,, \tag{4.13b}$$

with

$$\Delta u_k^- = u_k^- - u_{k-1}^- \tag{4.13c}$$

$$u_{k+l}^- = u_{k-1}^- + \sum_{m=k}^{k+l} \Delta u_m^- \,. \tag{4.13d}$$

With this formulation, the predicted future solution (solution in the prediction horizon) can be written as

$$\mathbf{Y} = \mathbf{F}_x \mathbf{x}_k + \mathbf{F}_u u_{k-1}^- + \mathbf{F}_{\Delta u} \Delta\mathbf{U} + \mathbf{F}_{cl}\Big(\mathbf{CL}^- + \mathbf{CL}_{\Delta hH}\Big) \,, \tag{4.14}$$

with

$$\mathbf{Y} = \begin{bmatrix} \mathbf{y}_k^\mathrm{T} & \mathbf{y}_{k+1}^\mathrm{T} & \dots & \mathbf{y}_{k+l}^\mathrm{T} \end{bmatrix}^\mathrm{T} \tag{4.15a}$$

$$\Delta\mathbf{U} = \begin{bmatrix} \Delta u_k^- & \Delta u_{k+1}^- & \dots & \Delta u_{k+l}^- \end{bmatrix}^\mathrm{T} \tag{4.15b}$$

$$\mathbf{CL}^- = \begin{bmatrix} cl_k^- & \dots & cl_{k+l}^- \end{bmatrix}^\mathrm{T} \tag{4.15c}$$

$$\mathbf{CL}_{\Delta hH} = \begin{bmatrix} cl_{\Delta hH,k} & \dots & cl_{\Delta hH,k+l} \end{bmatrix}^\mathrm{T} \tag{4.15d}$$

and

$$\mathbf{F}_x = \begin{bmatrix} \mathbf{C}^{\mathrm{T}} & (\mathbf{C}\mathbf{\Phi})^{\mathrm{T}} & \dots & \left(\mathbf{C}\mathbf{\Phi}^l\right)^{\mathrm{T}} \end{bmatrix}^{\mathrm{T}} \tag{4.16a}$$

$$\mathbf{F}_u = \begin{bmatrix} \mathbf{0} & \mathbf{F}_{\Delta u,1,1}^{\mathrm{T}} & \dots & \mathbf{F}_{\Delta u,l,1}^{\mathrm{T}} \end{bmatrix}^{\mathrm{T}} \tag{4.16b}$$

$$\mathbf{F}_{\Delta u} = \begin{bmatrix} \mathbf{0} & \mathbf{0} & \dots & \mathbf{0} \\ \mathbf{F}_{\Delta u,1,1} & \mathbf{0} & \dots & \mathbf{0} \\ \vdots & \vdots & \ddots & \vdots \\ \mathbf{F}_{\Delta u,l,1} & \mathbf{F}_{\Delta u,l,2} & \dots & \mathbf{0} \end{bmatrix} \tag{4.16c}$$

$$\mathbf{F}_{cl} = \mathrm{diag}(\mathbf{D}, \dots, \mathbf{D}) \tag{4.16d}$$

and

$$\mathbf{F}_{\Delta u,n,m} = \mathbf{C} \sum_{j=k+m-1}^{k+n-1} \mathbf{\Phi}^{k+n-j-1}\mathbf{\Gamma} \; . \tag{4.16e}$$

To rotate and shift the plate centerline $cl^+$, the output vector $\mathbf{Y}$ is transformed with the rotation matrix (cf. Appendix A.1)

$$\tilde{\mathbf{S}} = \begin{bmatrix} 1 & 0 & 0 & 0 & \dots & 0 \\ 0 & S_{1,1} & 0 & S_{1,2} & & S_{1,l} \\ 0 & 0 & 1 & 0 & & 0 \\ 0 & S_{2,1} & 0 & S_{2,2} & & S_{2,l} \\ \vdots & & & & \ddots & \\ 0 & S_{l,1} & 0 & S_{l,2} & \dots & S_{l,l} \end{bmatrix} \tag{4.17}$$

to get

$$\tilde{\mathbf{Y}} = \tilde{\mathbf{S}}\mathbf{Y} \; . \tag{4.18}$$

Note that $S_{i,j}$ denotes the entry of the matrix $\mathbf{S}$ in the $i^{th}$ row and $j^{th}$ column.

For safety reasons, the edger rolls are subject to the following restrictions:

- The lateral position of the edger rolls is restricted to the interval $u^- \in \begin{bmatrix} -u_{max}^- & u_{max}^- \end{bmatrix}$.
- The lateral velocity of the edger rolls is restricted to the interval $v^- \in \begin{bmatrix} -v_{max}^- & v_{max}^- \end{bmatrix}$.
- The lateral acceleration of the edger rolls is restricted to the interval $a^- \in \begin{bmatrix} -a_{max}^- & a_{max}^- \end{bmatrix}$.

The mathematical implementation of these restrictions as linear inequalities in terms of $\Delta\mathbf{U}$ is outlined in Appendix A.3.

In forward rolling passes, it is considered that the initial position $W_0$ of the plate in the roll gap can be influenced by the position $u_{-1}^-$ of the edger rolls at the beginning of the rolling pass [58]

$$W_0 = u_{-1}^- + W_0^{cl} \ . \tag{4.19}$$

Apart from constraints on $u_{-1}^-$, $W_0$ can thus be freely chosen. Solving the optimization problem

$$\begin{aligned} &\min_{u_{-1}^-, \Delta\mathbf{U}} \ \tilde{\mathbf{Y}}^{\mathrm{T}} \boldsymbol{\chi}_Y \tilde{\mathbf{Y}} + \Delta\mathbf{U}^{\mathrm{T}} \boldsymbol{\chi}_{\Delta u} \Delta\mathbf{U} \\ &\text{s.t. (4.14), (4.18) and (A.6), (A.7), (A.8) ,} \end{aligned} \tag{4.20}$$

with the user-defined positive definite weighting matrices $\boldsymbol{\chi}_Y$ and $\boldsymbol{\chi}_{\Delta u}$, yields the optimal input trajectory and the optimal initial lateral position of the edger rolls. Optimizing also the initial lateral edger position is reasonable because

- it facilitates a larger stroke of the lateral position $u^-$ of the edger rolls at the head end of the plate, which allows to better compensate for the camber, and

- it generates an additional control input $W_0$ at the beginning of the rolling pass. Note that a specific lateral initial position $W_0$ at the roll bite especially helps to compensate for the camber at the head end of the plate (cf. Section 2.7.2 and Section 2.7.3).

The dimension of the problem (4.20) depends on the user-defined length $l$ of the prediction horizon. The length $(k+l)\Delta z^-$ is restricted by the incoming plate length $L^-$, i. e., $(k+l)\Delta z^- \leq L^-$. In practice, the choice $k = 0$ and $l = N_P < N$, with $N_P \Delta z^- = (L^- - l_e^-)$ being the plate length where the edger rolls are active proved useful.

Finally, it is emphasized that (4.10), (4.14) and (4.20) are only applicable while the plate is clamped both in the roll gap and between the edger rolls. After this period, i. e., when the plate has left the edger rolls, the model changes to (2.38). To ensure safe plate motion also during the tail-out phase, it is recommended that the lateral position $W$ of the plate in the roll gap is small when the tail end of the plate leaves the edger rolls. This can easily be realized by increasing the corresponding factor in the weighting matrix $\boldsymbol{\chi}_Y$.

For the sake of completeness, a time-varying formulation of the matrices (4.16) is outlined in Appendix A.4. This formulation allows to consider that edger rolls do not have an effect at the end of the rolling pass. However, it turned out that this consideration does not yield a significant improvement of the concept and is thus not further used in the feedforward control concept outlined in this section.

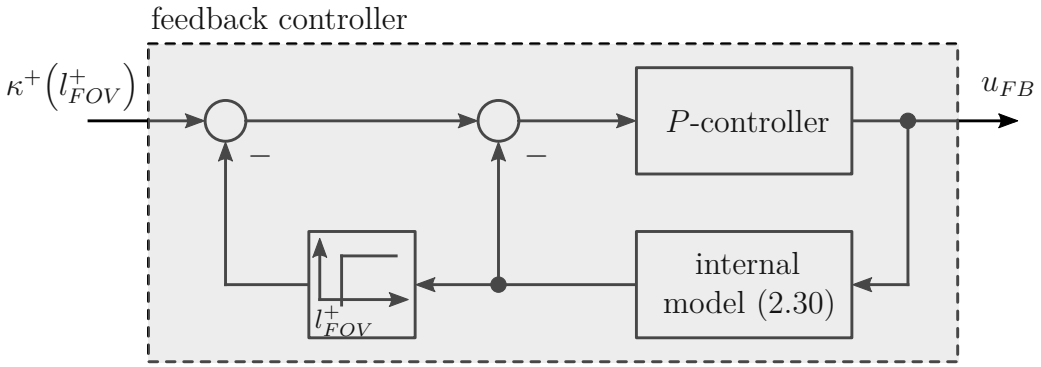


Figure 4.6: Classical Smith predictor controller for the feedback controller in Figure 4.5.

### 4.2.2 Feedback control

In the previous section, a feedforward controller was designed to calculate the optimal trajectory $u_{FF}$ of the edger rolls' lateral position during the rolling pass. In the following, a feedback controller for the lateral edger position $u^- = u_{FB}$ is proposed to further reduce the curvature of the plate centerline. Using only the feedforward controller, a camber may remain due to a model-plant mismatch or uncertain parameters (e. g., $\kappa_{\Delta hH}$). The controller uses the camber measured in the FOV of the exit-side camera as feedback.

The camber of the outgoing plate $\kappa^+$ is only measured after a transport delay associated with the distance $l^+_{FOV}$ between the roll gap and the camera FOV. A proven controller for plants with delay is the Smith predictor [59, 60]. A block diagram of the classical Smith predictor controller is depicted in Figure 4.6.

The first step of the Smith predictor design concerns a controller for the plant without delay. For this purpose, consider the transfer function (cf. (2.30), Section 2.7.1)

$$G_{u^-,\kappa^+}(s) = \frac{\hat{\kappa}^+}{\hat{u}^-} = \frac{V_1 s^2}{\left(1+\frac{s}{s_1}\right)\left(1+\frac{s}{s_2}\right)} , \tag{4.21}$$

with the Laplace variable $s$ [49], $\hat{(\cdot)}$ being the Laplace transform of $(\cdot)$ and $s_{1,2}$ are the negative real eigenvalues $s_{1,2} = -\lambda_{u^\pm,1,2}$ of $\mathbf{A}$ (cf. Section 2.7.1). The camera system features a sampling rate of 20 frames/s, which is generally too low for the fast eigenvalue $\lambda_{u^\pm,2}$. Therefore, the fast dynamics will be neglected in (4.21). To cancel the double differentiating term ($s^2$ in the numerator) in the transfer function (4.21), the lateral acceleration $u^{-\prime\prime}$ of the edger serves as a new control input yielding

$$G_{u^{-\prime\prime},\kappa^+}(s) = \frac{\hat{\kappa}^+}{\hat{u}^{-\prime\prime}} \approx \frac{V_1}{\left(1+\frac{s}{s_1}\right)} . \tag{4.22}$$

To prevent a non-zero steady-state control error of the camber $\kappa^+$, an integrating controller has to be employed. In general, such a controller will demand a non-zero steady-state lateral acceleration of the edger rolls. This means that the elimination of a constant camber would require a constant acceleration of the edger rolls. This is practically unfeasible. A non-zero constant roll gap tilt would therefore be a better solution to eliminate a constant camber, see, e. g., [2, 3], which was already pointed out in Section 2.2. This demonstrates that edger rolls are not the right actuators to compensate for a constant camber. However, edger rolls can be advantageously used to eliminate zero-mean deviations from the desired straight plate centerline. In the following, a simple proportional controller with gain $P$ is designed for (4.22). For the closed-loop system $(\frac{PG_{u^-\prime\prime,\kappa^+}}{1+PG_{u^-\prime\prime,\kappa^+}})$ to be stable, the condition $P > -1/V_1$ must be satisfied.

In the next design step, the spatial distance $l^+_{FOV}$ between the roll gap and the exit-side camera is considered. To do so (cf. [59, 60]), a discretized version of the model (2.30) is simulated as an internal model (cf. Figure 4.6) with the step size $\Delta z^-$. The exogenous inputs $\kappa^-$, $\Delta h^-$ and $\Delta H$ are compensated by the feedforward controller and thus set to zero in the internal model of the Smith predictor. Hence, both the internal model and the spatial delay $l^+_{FOV}$ are independent of the potentially varying entry velocity $v_{en}$. Because $v_{en}$ is well known and $l^+_{FOV}$ is constant and well known, stability issues are not expected in this formulation [3, 59, 60].

### 4.2.3 Simulation results

In the following, the performance of the developed control concept is analyzed in simulations. Figure 4.7 shows the performance of the feedforward control without any constraints on the lateral position, velocity, or acceleration of the the edger rolls. The simulation shows that the feedforward control can straighten the plate in the area where the edger rolls are in contact with the plate. The tail end cannot be straightened. However, this version of the feedforward controller requires inordinately large edger roll positions, which are unfeasible for the industrial plant.

In Figure 4.8, the following three scenarios are compared:

- Edger rolls are not moved during the rolling pass (simulation, $u^- = 0$, black, measurement from the industrial plant, red [39], blue [27, 28]).
- Edger rolls are moved according to the feedforward controller with constraints (simulation, $u^- = u_{FF}$, orange).
- Edger rolls are moved according to both feedforward controller with constraints and feedback controller (simulation, $u^- = u_{FF} + u_{FB}$, green).

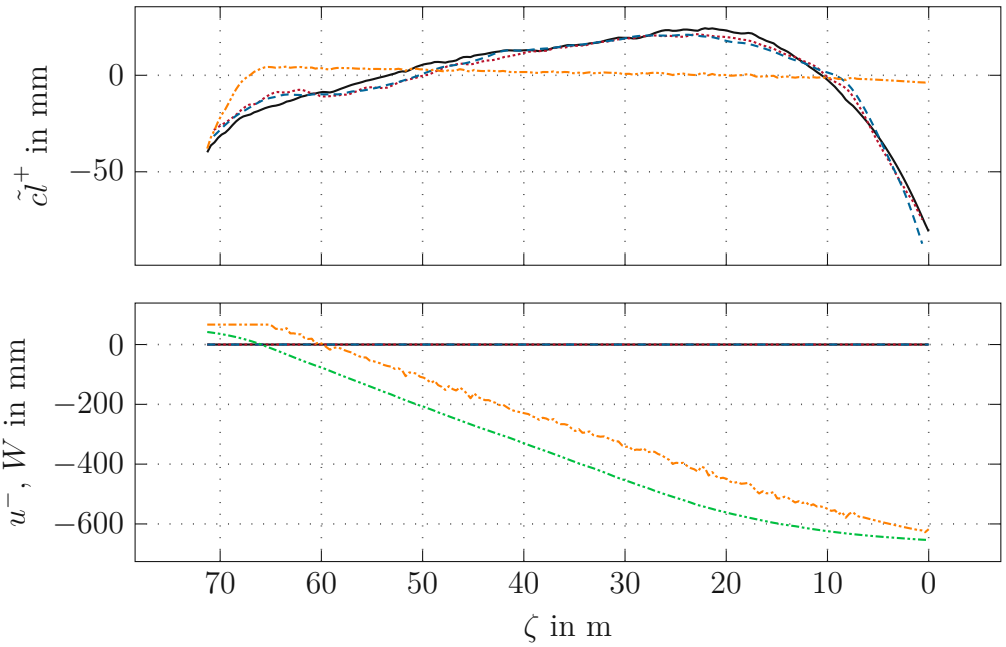


Figure 4.7: Comparison of plate centerlines without control (simulated black (2.39) / measured red [39] / measured blue [27, 28]) and simulated with the feedforward controller without constraints (orange). The corresponding lateral edger position $u^-$ (orange) and the lateral position $W$ (green) of the plate in the roll gap are shown in the bottom plot.

The simulations show that if the feedforward controller or the two-degrees-of-freedom control structure is used, the centerline of the outgoing plate is significantly improved. The constraint (A.6) on the lateral position of the edger rolls is hit but not violated with the feedforward controller only. Thanks to the predicting behavior of the feedforward controller, an acceptable lateral shift of the edger rolls and thus an acceptable lateral position of the plate in the roll gap can be achieved. This is also true for the constraints (A.7) and (A.8), which concern the velocity and acceleration of the edger rolls, respectively. Moreover, the lateral position $W$ of the plate in the roll gap is zero when the plate leaves the edger rolls. This is not necessarily the case if additional feedback control is used. Even though, the overall lateral position, velocity, and acceleration of the edger rolls could be limited by simple box constraints, a possible rapid change of the edger roll velocity and acceleration would cause an undesired camber (cf. (4.22)). Such box constraints are thus not recommended. However, the simulation results indicate that camber can be compensated by the proposed control concepts. In this case, local variations of the camber are mainly compensated by feedforward control whereas camber due to uncertainties of $\kappa_{\Delta hH}$ (which cause a constant camber) is mainly reduced by feedback control.

Figure 4.8 also shows the corresponding input trajectories. As discussed in Section 2.7.1, the lateral position of the plate in the roll gap is more or less limited by the lateral edger roll position. The term $cl_{\Delta hH}$ due to a thickness wedge and a roll gap tilt mainly causes a constant camber. As discussed in Section 4.2.2, constant camber requires edger rolls to accelerate throughout the rolling pass (cf. bottom part of Figure 4.8). In view of these findings, the best control strategy would be to compensate a constant camber by tilting the roll gap and to reduce the local variations of the camber by a lateral motion of the edger rolls. Using the roll gap tilt as a control input is unfeasible in the considered industrial plant and thus not part of this section.

In the following, the measurement results of 331 plates (some of them have also been used for parameter identification in Section 3.2.3) where the edger rolls were not moved during the production process, i. e. $\tilde{cl}_{x,u}^{meas} = 0$, are superposed with $\tilde{cl}_{x,u}$ resulting from the feedforward ($u^- = u_{FF}$) or the two-degrees-of-freedom control law ($u^- = u_{FF} + u_{FB}$) (cf. (2.39)).

$$\underbrace{\tilde{cl}^{+}}_{\substack{\text{simulated, considering}\\ \text{model-plant mismatch}}} = \tilde{cl}^{+}_{meas}\Big|_{\tilde{cl}_{x,u}^{meas}=0} + \tilde{cl}_{x,u} \tag{4.23}$$

This superposition is reasonable because the influence of the control input $u^-$ on the final shape of the plate $cl^+$ is reproduced quite well in simulation (cf. Section 3.4). In this way, the model-plant mismatch, e. g., caused by deviations in $\kappa_{\Delta hH}$, is considered in the simulation studies.

Figure 4.9 depicts the relative frequency distribution of the simulated (root

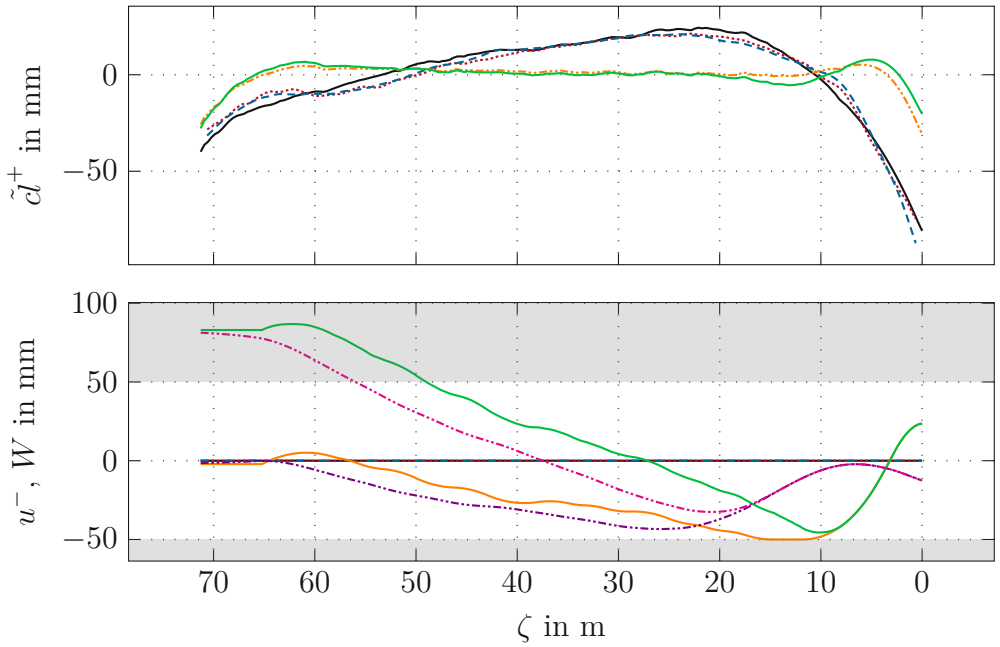


Figure 4.8: Comparison of plate centerlines without control (simulated black (2.39) / measured red [39] / measured blue [27, 28]), simulated with the feedforward controller with constraints (orange) and simulated with both feedforward and feedback controller (green). The corresponding lateral edger position $u^-$ (orange / green) and the lateral position $W$ (violet / magenta) of the plate in the roll gap are shown in the bottom plot. Prohibited values of the lateral positions of the edger rolls are indicated in gray.

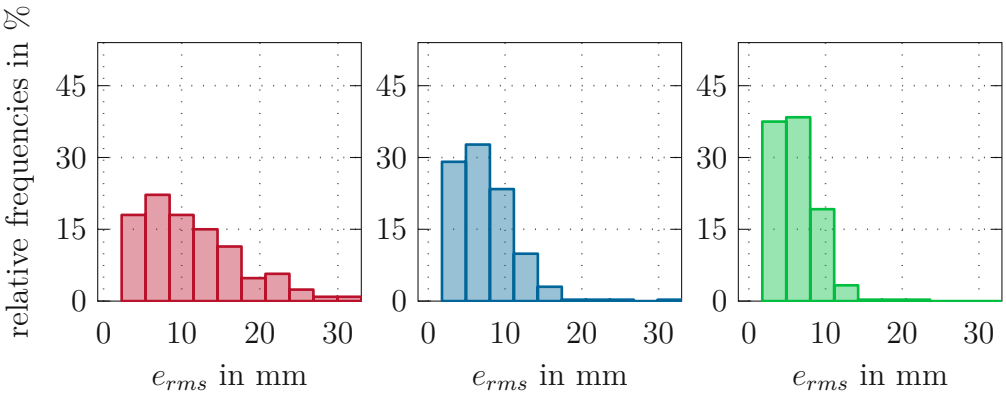


Figure 4.9: Simulated relative frequency distribution of $e_{rms}$ of 331 plates without control (red), with feedforward control (blue), and with feedforward and feedback control (green).

mean square) shape error

$$e_{rms} = \sqrt{\frac{1}{L^+} \int_0^{L^+} \left(\tilde{cl}^+\right)^2 \mathrm{d}z} \tag{4.24}$$

for these 331 plates. The simulation results in Figure 4.9 indicate that the centerlines of the plates can be improved with the proposed control concept. The average value of $e_{rms}$ is reduced from approximately 11.2 mm to approximately 7.4 mm (reduction of $\approx 33.9\,\%$) with feedforward control only and to approximately 6.1 mm (reduction of $\approx 45.5\,\%$) using the two-degrees-of-freedom control structure.

The optimization-based feedforward control theoretically has the potential to completely compensate for the camber of the incoming plate centerline $cl^-$ and the contribution $cl_{\Delta hH}$ to the outgoing plate centerline. However, there are three reasons why a perfectly straight shape of the outgoing plate centerline is not realized with the proposed feedforward controller.

- The tail end of the plate cannot be straightened because edger rolls do not touch the plate at the end of forward rolling passes.
- There are model-plant mismatches, e. g., due to various simplifications (soft beam in the roll gap, ...), parameter uncertainties ($f_{E_l}$, $f_{K_\Sigma}$, $f_{f\Delta hH}$ and $W_{0,offset}$), and uncertainties in the measurement of the incoming plate.
- The perfect shape cannot be realized because of constraints on the movement of the edger rolls (A.6), (A.7) and (A.8) (cf. Appendix A.3).

In the subsequent simulation, the feedforward controller is used without the constraints (A.6), (A.7) and (A.8). The results are shown in Figure 4.10. With

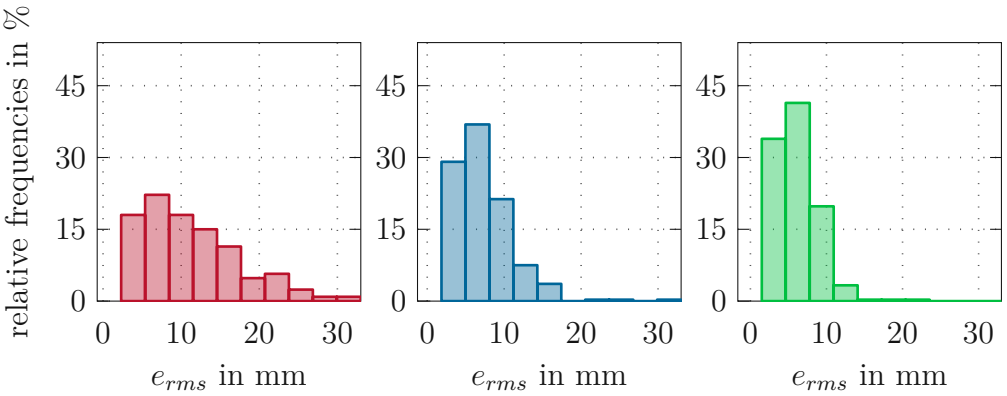


Figure 4.10: Simulated relative frequency distribution of $e_{rms}$ of 331 plates without control (red), with feedforward control (blue), and with feedforward and feedback control (green). The feedforward controller is used without constraints in the lateral position, velocity, and acceleration of the edger rolls.

this feedforward controller, the average value of $e_{rms}$ is reduced from approximately 11.2 mm to approximately 7.3 mm (reduction of $\approx 34.8\,\%$) with feedforward control only and to approximately 6.1 mm (reduction of $\approx 45.5\,\%$) using the two-degrees-of-freedom control structure. A comparison with the previous simulation results in Figure 4.9 shows that the unconstrained feedforward controller does not bring a significant improvement compared to the constrained feedforward controller. The remaining curvature in the plate centerline is thus mainly attributed to the model-plant mismatch. As stated in Section 3.1, the model-plant mismatch is limited by the accuracy of the measurement system of the incoming plate centerline $cl^-$. Because the performance of the feedforward controller is inherently limited by the model-plant mismatch, the accuracy of the feedforward controller is in the best case in the order of the measurement system. The simulation study above shows that this case is reached by the proposed control strategy.

## 4.3 Optimal multi-pass control of the lateral plate motion and shape

This section is dedicated to the control design based on the mathematical model from Section 2.6. In this section, forward and backward rolling passes are considered. In addition to the already stated control objectives

- safe plate motion: In each rolling pass, the lateral position of the plate in the roll gap should not exceed a given maximum,
- correct shape: The final plate should be as straight as possible (small camber),

this section further tackles the objective

- correct thickness profile: The final thickness profile should be uniform (zero thickness wedge),

in a multi-pass approach. The current section assumes that both static adjustment of the roll gap tilt and dynamic adjustment of the lateral position of the edger rolls can be used as control inputs and proposes an optimal control concept considering all remaining rolling passes at the reversing roughing mill.

### 4.3.1 Optimal multi-pass control

In the following, an optimal control law for the roll gap tilt value $\Delta H$ and for the trajectory of the lateral edger position $u^-$ is derived based on (2.39) (forward rolling passes), (2.38) (backward rolling passes), and (2.40). The developed solution routine of the optimization problem is inspired by [57].

Using a spatial discretization with the step size $\Delta z^-$ and the zero-order-hold method, (2.39), (2.38), and (2.40) can be written in discretized form

$$\mathbf{x}_{f,k+1} = \mathbf{\Phi}_f \mathbf{x}_{f,k} + \mathbf{\Gamma}_f u_k^- \,, \qquad \mathbf{x}_{f,0} = \mathbf{x}_f(0) \tag{4.25a}$$

$$\mathbf{y}_{f,k} = \mathbf{C}_f \mathbf{x}_{f,k} + \mathbf{D}\Big(cl_k^- + \tilde{cl}_{\Delta h,k} + \tilde{cl}_{\Delta H,k}\Big) \,, \tag{4.25b}$$

and

$$\mathbf{x}_{b,k+1} = \mathbf{\Phi}_b \mathbf{x}_{b,k} + \mathbf{\Gamma}_b \mathbf{d}_k \,, \qquad \mathbf{x}_{b,0} = \mathbf{x}_b(0) \tag{4.26a}$$

$$\mathbf{y}_{b,k} = \mathbf{C}_b \mathbf{x}_{b,k} + \mathbf{D}\Big(cl_k^- + \tilde{cl}_{\Delta h,k} + \tilde{cl}_{\Delta H,k}\Big) \,, \tag{4.26b}$$

with the matrices

$$\mathbf{\Phi}_{\{f,b\}} = e^{\mathbf{A}_{\{f,b\}}\Delta z^-} \,, \tag{4.27}$$

$$\mathbf{\Gamma}_f = \int_0^{\Delta z^-} e^{\mathbf{A}_f \tilde{\zeta}} \mathrm{d}\tilde{\zeta} \mathbf{B} \,, \qquad \mathbf{\Gamma}_b = \int_0^{\Delta z^-} e^{\mathbf{A}_b \tilde{\zeta}} \mathrm{d}\tilde{\zeta} \mathbf{G} \,, \tag{4.28}$$

$$\mathbf{C}_f = \begin{bmatrix} 0 & 1 & 0 & 0 \\ 0 & 0 & 1 & 0 \end{bmatrix} \,, \qquad \mathbf{C}_b = \begin{bmatrix} 0 & 1 \\ 0 & 0 \end{bmatrix} \,, \qquad \mathbf{D} = \begin{bmatrix} 0 \\ 1 \end{bmatrix} \,, \tag{4.29}$$

the input $\mathbf{d} = \begin{bmatrix} \kappa^- & \Delta h^- & \Delta H \end{bmatrix}^\mathrm{T}$ and the output $\mathbf{y}_{\{f,b\}} = \begin{bmatrix} W & cl^+ \end{bmatrix}^\mathrm{T}$. In contrast to (4.10), the contributions, see (2.34) with (2.31c),

$$cl_{\Delta h} = \frac{1}{2w_0}\left(\zeta - \frac{L^+}{2}\right)^2 \left(\frac{K_h^-}{\lambda^2} - K_h^+\right) = F_{\Delta h} \Delta h^- \tag{4.30a}$$

and

$$cl_{\Delta H} = \frac{1}{2w_0}\left(\zeta - \frac{L^+}{2}\right)^2\left(\frac{K_H^-}{\lambda^2} - K_H^+\right) = F_{\Delta H}\Delta H \tag{4.30b}$$

to the outgoing plate centerline $\tilde{cl}^+$ are written separately, replacing $cl_{\Delta hH}$. The initial conditions of forward rolling passes are chosen as $\mathbf{x}_{f,0} = \begin{bmatrix}0 & W_0 & 0 & 0\end{bmatrix}^{\mathrm{T}}$, where $W_0$ can be freely chosen. In backward rolling passes, they are chosen as $\mathbf{x}_{b,0} = \mathbf{0}$ because they are usually unknown and their influence is assumed to be small ($\tilde{cl}_{x,u} = 0$ in backward rolling passes). The solution of $\mathbf{x}_{f,k+l}$ and $\mathbf{y}_{f,k+l}$ at an arbitrary spatial point $k+l$ directly follows as

$$\mathbf{x}_{f,k+l} = \mathbf{\Phi}_f^l\mathbf{x}_{f,k} + \sum_{j=k}^{k+l-1}\mathbf{\Phi}_f^{k+l-j-1}\mathbf{\Gamma}_f\underbrace{\left(u_{k-1}^- + \sum_{m=k}^{j}\Delta u_m^-\right)}_{u_j^-} \tag{4.31a}$$

$$\mathbf{y}_{f,k+l} = \mathbf{C}_f\mathbf{x}_{f,k+l} + \mathbf{D}\left(cl_{k+l}^- + \tilde{cl}_{\Delta h,k+l} + \tilde{cl}_{\Delta H,k+l}\right), \tag{4.31b}$$

with $\Delta u_k^- = u_k^- - u_{k-1}^-$. For backward rolling passes, the solution of $\mathbf{x}_{b,k+l}$ and $\mathbf{y}_{b,k+l}$ is calculated analogously. With this formulation, the series of future output values can be predicted in the form

$$\mathbf{Y}_f = \mathbf{F}_x\mathbf{x}_{f,k} + \mathbf{F}_u u_{k-1}^- + \mathbf{F}_{\Delta u}\Delta\mathbf{U} + \mathbf{F}_{f,cl}\mathbf{CL}^- + \mathbf{F}_{f,\Delta h}\Delta h^- + \mathbf{F}_{f,\Delta H}\Delta H \tag{4.32a}$$

$$\mathbf{Y}_b = \mathbf{F}_{b,cl}\mathbf{CL}^- + \mathbf{F}_{b,\Delta h}\Delta h^- + \mathbf{F}_{b,\Delta H}\Delta H \tag{4.32b}$$

with

$$\mathbf{Y}_{\{f,b\}} = \begin{bmatrix}\mathbf{y}_{\{f,b\},k}^{\mathrm{T}} & \mathbf{y}_{\{f,b\},k+1}^{\mathrm{T}} & \cdots & \mathbf{y}_{\{f,b\},k+l}^{\mathrm{T}}\end{bmatrix}^{\mathrm{T}} \tag{4.33a}$$

$$\Delta\mathbf{U} = \begin{bmatrix}\Delta u_k^- & \Delta u_{k+1}^- & \dots & \Delta u_{k+l}^-\end{bmatrix}^{\mathrm{T}} \tag{4.33b}$$

$$\mathbf{CL}^- = \begin{bmatrix}cl_k^- & \dots & cl_{k+l}^-\end{bmatrix}^{\mathrm{T}}. \tag{4.33c}$$

The matrices follow as

$$\mathbf{F}_x = \begin{bmatrix}\mathbf{C}_f^{\mathrm{T}} & (\mathbf{C}_f\mathbf{\Phi}_f)^{\mathrm{T}} & \dots & \left(\mathbf{C}_f\mathbf{\Phi}_f^l\right)^{\mathrm{T}}\end{bmatrix}^{\mathrm{T}} \tag{4.34a}$$

$$\mathbf{F}_u = \begin{bmatrix}\mathbf{0} & \mathbf{F}_{\Delta u,1,1}^{\mathrm{T}} & \dots & \mathbf{F}_{\Delta u,l,1}^{\mathrm{T}}\end{bmatrix}^{\mathrm{T}} \tag{4.34b}$$

$$\mathbf{F}_{\Delta u} = \begin{bmatrix}\mathbf{0} & \mathbf{0} & \dots & \mathbf{0}\\ \mathbf{F}_{\Delta u,1,1} & \mathbf{0} & \dots & \mathbf{0}\\ \vdots & \vdots & \ddots & \vdots\\ \mathbf{F}_{\Delta u,l,1} & \mathbf{F}_{\Delta u,l,2} & \dots & \mathbf{0}\end{bmatrix} \tag{4.34c}$$

$$\mathbf{F}_{f,cl} = \operatorname{diag}(\mathbf{D}, \ldots, \mathbf{D}) \tag{4.34d}$$

$$\mathbf{F}_{f,\epsilon} = \begin{bmatrix} 0 & F_{\epsilon,k} & 0 & \ldots & F_{\epsilon,k+l} \end{bmatrix}^{\mathrm{T}}, \quad \epsilon \in \{\Delta h, \Delta H\} \tag{4.34e}$$

$$\mathbf{F}_{b,cl} = \begin{bmatrix} \mathbf{0} & \mathbf{0} & \ldots & \mathbf{0} \\ \mathbf{F}_{\kappa,1,1} & \mathbf{0} & \ddots & \mathbf{0} \\ \vdots & \ddots & \ddots & \vdots \\ \mathbf{F}_{\kappa,l,1} & \mathbf{F}_{\kappa,l,2} & \ldots & \mathbf{0} \end{bmatrix} \frac{1}{\Delta\zeta^2}\mathbf{D}\mathbf{D} + \begin{bmatrix} \mathbf{D} & \mathbf{0} & \ldots & \mathbf{0} \\ \mathbf{0} & \mathbf{D} & \ddots & \mathbf{0} \\ \vdots & \ddots & \ddots & \vdots \\ \mathbf{0} & \mathbf{0} & \ldots & \mathbf{D} \end{bmatrix} \tag{4.34f}$$

$$\mathbf{F}_{b,\epsilon} = \begin{bmatrix} \mathbf{D}F_{\epsilon,k} \\ \mathbf{C}_b\boldsymbol{\Gamma}_{b,\epsilon} + \mathbf{D}F_{\epsilon,k+1} \\ \vdots \\ \mathbf{C}_b \sum_{j=k}^{k+l-1} \boldsymbol{\Phi}_b^{k+l-j-1}\boldsymbol{\Gamma}_{b,\epsilon} + \mathbf{D}F_{\epsilon,k+l} \end{bmatrix}, \quad \epsilon \in \{\Delta h, \Delta H\}\ , \tag{4.34g}$$

with

$$\mathbf{F}_{\Delta u,n,m} = \mathbf{C}_f \sum_{j=k+m-1}^{k+n-1} \boldsymbol{\Phi}_f^{k+n-j-1}\boldsymbol{\Gamma}_f \tag{4.34h}$$

$$\mathbf{F}_{\kappa,n,m} = \mathbf{C}_b \sum_{j=k+m-1}^{k+n-1} \boldsymbol{\Phi}_b^{k+n-j-1}\boldsymbol{\Gamma}_{b,\kappa}\ , \tag{4.34i}$$

and $\boldsymbol{\Gamma}_{b,\kappa}$, $\boldsymbol{\Gamma}_{b,\Delta h}$ and $\boldsymbol{\Gamma}_{b,\Delta H}$ are the first, second and third column of $\boldsymbol{\Gamma}_b$ according to their inputs $\kappa^-$, $\Delta h$ and $\Delta H$

$$\boldsymbol{\Gamma}_b = \begin{bmatrix} \boldsymbol{\Gamma}_{b,\kappa} & \boldsymbol{\Gamma}_{b,\Delta h} & \boldsymbol{\Gamma}_{b,\Delta H} \end{bmatrix}\ . \tag{4.34j}$$

Furthermore, the matrix with $\mathbf{D}\mathbf{D}$ yielding the numerical approximation of the second derivative according to Appendix A.5 is used.

To rotate and shift the plate centerline $cl^+$, the output vector $\mathbf{Y}_{\{f,b\}}$ is transformed according to the procedure of Appendix A.1 yielding $\tilde{\mathbf{Y}}_{\{f,b\}}$.

Equation (4.32) shows how inputs influence the lateral plate position in the roll gap as well as the centerline of the outgoing plate during a single forward or backward rolling pass. In the following, all quantities are assigned an extra superscript $(\cdot)^{(j)}$ indicating the corresponding rolling pass. To consider all rolling passes in a consolidated model, a few assumptions have to be made:

- The incoming thickness wedge of the first rolling pass is neither measured nor known and is thus set to zero ($\Delta h^{-(1)} = 0$).
- The roll gap tilt of the rolling pass $j$ defines the incoming thickness wedge of the subsequent pass $j+1$ and is constant along the whole plate ($\Delta H^{(j)} = \Delta h^{-(j+1)}$).
- The outgoing centerline of a rolling pass is equal to the incoming centerline of the subsequent rolling pass ($\mathbf{CL}^{+(j)} = \mathbf{CL}^{-(j+1)}$).

Considering (4.32) for all $RP$ rolling passes thus yields

$$\begin{aligned}
\begin{bmatrix} \mathbf{Y}^{(1)} \\ \mathbf{Y}^{(2)} \\ \vdots \\ \mathbf{Y}^{(RP)} \end{bmatrix} = &\begin{bmatrix} \mathbf{F}_x^{(1)} & \mathbf{0} & \dots & \mathbf{0} \\ \mathbf{0} & \mathbf{0} & \ddots & \mathbf{0} \\ \vdots & \ddots & \ddots & \vdots \\ \mathbf{0} & \mathbf{0} & \dots & \mathbf{F}_x^{(RP)} \end{bmatrix} \begin{bmatrix} \mathbf{x}_{f,0}^{(1)} \\ \mathbf{x}_{f,0}^{(3)} \\ \vdots \\ \mathbf{x}_{f,0}^{(RP)} \end{bmatrix} + \begin{bmatrix} \mathbf{F}_u^{(1)} & \mathbf{0} & \dots & \mathbf{0} \\ \mathbf{0} & \mathbf{0} & \ddots & \mathbf{0} \\ \vdots & \ddots & \ddots & \vdots \\ \mathbf{0} & \mathbf{0} & \dots & \mathbf{F}_u^{(RP)} \end{bmatrix} \begin{bmatrix} u_{-1}^{(1)} \\ u_{-1}^{(3)} \\ \vdots \\ u_{-1}^{(RP)} \end{bmatrix} + \\
&\begin{bmatrix} \mathbf{F}_{\Delta u}^{(1)} & \mathbf{0} & \dots & \mathbf{0} \\ \mathbf{0} & \mathbf{0} & \ddots & \mathbf{0} \\ \vdots & \ddots & \ddots & \vdots \\ \mathbf{0} & \mathbf{0} & \dots & \mathbf{F}_{\Delta u}^{(RP)} \end{bmatrix} \begin{bmatrix} \Delta\mathbf{U}^{(1)} \\ \Delta\mathbf{U}^{(3)} \\ \vdots \\ \Delta\mathbf{U}^{(RP)} \end{bmatrix} + \\
&\begin{bmatrix} \mathbf{F}_{f,\Delta H}^{(1)} & \mathbf{0} & \dots & \mathbf{0} \\ \mathbf{F}_{b,\Delta h}^{(2)} & \mathbf{F}_{b,\Delta H}^{(2)} & \ddots & \mathbf{0} \\ \vdots & \ddots & \ddots & \vdots \\ \mathbf{0} & \mathbf{0} & \dots & \mathbf{F}_{f,\Delta H}^{(RP)} \end{bmatrix} \begin{bmatrix} \Delta H^{(1)} \\ \Delta H^{(2)} \\ \vdots \\ \Delta H^{(RP)} \end{bmatrix} + \\
&\begin{bmatrix} \mathbf{F}_{f,cl}^{(1)} & \mathbf{0} & \dots & \mathbf{0} \\ \mathbf{0} & \mathbf{F}_{b,cl}^{(2)} & \ddots & \mathbf{0} \\ \vdots & \ddots & \ddots & \vdots \\ \mathbf{0} & \mathbf{0} & \dots & \mathbf{0} \end{bmatrix} \begin{bmatrix} \mathbf{I} & \mathbf{0} & \dots & \mathbf{0} \\ \mathbf{0} & \mathbf{c}_{b,W}^{\mathrm{T}} & \dots & \mathbf{0} \\ \vdots & \vdots & \ddots & \vdots \\ \mathbf{0} & \mathbf{0} & \dots & \mathbf{c}_{b,W}^{\mathrm{T}} \end{bmatrix} \begin{bmatrix} \left(\mathbf{C}\mathbf{L}^{-}\right)^{(1)} \\ \mathbf{Y}^{(1)} \\ \vdots \\ \mathbf{Y}^{(RP)} \end{bmatrix},
\end{aligned} \tag{4.35}$$

with the identity matrix $\mathbf{I}$, $\mathbf{c}_{b,W}^{\mathrm{T}} = \begin{bmatrix} 0 & 1 \end{bmatrix}$, and an odd number $RP$. For safety reasons, the edger position is limited to the range $\left[-u_{max}^{-}, u_{max}^{-}\right]$. The implementation of these constraints is discussed in Appendix A.3.

In forward rolling passes, it is considered that the initial position $W_0$ of the plate in the roll gap can be influenced by the position $u_{-1}^{-}$ of the edger rolls at the beginning of the rolling pass

$$W_0 = u_{-1}^{-} + W_0^{cl} \,, \tag{4.36}$$

and can be (almost freely) chosen. The optimization problem

$$\begin{aligned}
&\min_{u_{-1}^{-}, \mathcal{U}} \mathcal{Y}^{\mathrm{T}} \boldsymbol{\chi}_{\mathcal{Y}} \mathcal{Y} + \mathcal{U}^{\mathrm{T}} \boldsymbol{\chi}_{\mathcal{U}} \mathcal{U} \\
&\text{s.t. (4.35) and (A.6)} \,,
\end{aligned} \tag{4.37}$$

with the positive definite weighting matrices $\boldsymbol{\chi}_{\mathcal{Y}}$ and $\boldsymbol{\chi}_{\mathcal{U}}$ and the optimization

variables

$$\mathcal{Y} = \left[ \left(\mathbf{Y}^{(1)}\right)^{\mathrm{T}} \quad \left(\mathbf{Y}^{(2)}\right)^{\mathrm{T}} \quad \dots \quad \left(\mathbf{Y}^{(RP)}\right)^{\mathrm{T}} \right]^{\mathrm{T}} \tag{4.38a}$$

$$\mathcal{U} = \left[ \left(\Delta\mathbf{U}^{(1)}\right)^{\mathrm{T}} \quad \left(\Delta\mathbf{U}^{(3)}\right)^{\mathrm{T}} \quad \dots \quad \left(\Delta\mathbf{U}^{(RP)}\right)^{\mathrm{T}} \quad \Delta H^{(1)} \quad \Delta H^{(2)} \quad \dots \quad \Delta H^{(RP)} \right]^{\mathrm{T}} \tag{4.38b}$$

constitutes a quadratic program (QP), which can be solved by standard QP solvers (e. g. the *quadprog* command of MATLAB). The optimization problem (4.37) is formulated for the whole rolling process (first to last rolling pass) and can be solved successively for subsequent rolling passes. For the optimum solution of (4.37) in different rolling passes, Bellman's principle of optimality applies. However, due to model-plant mismatches and measurement noise, a recalculation of (4.37), considering the latest measurement of the plate centerline, before every rolling pass is recommendable. This update between the rolling passes is the only feedback and gives the proposed concept its model predictive control character. The prediction horizon becomes shorter with each rolling pass because the calculation always ends with the last rolling pass $RP$.

The optimization problem (4.37) yields the optimal edger trajectories for all odd rolling passes and the optimal roll gap tilt values for all rolling passes. Additionally, it provides the optimum initial position of the edger rolls (defines the lateral position of the plate in the roll gap at the beginning of the rolling pass according to (4.36)). This optimum initial position is not necessarily zero and helps to keep the mean lateral plate position during the rolling pass small in absolute terms.

Finally, it is emphasized that (2.39), (4.25), (4.32a) and (4.37) are only applicable while the plate is clamped both in the roll gap and between the edger rolls. After this period, i. e., when the plate has left the edger rolls, the model changes to (2.38), which is not explicitly shown in the equations to keep the notation compact. For details on the time-varying formulation of the forward rolling passes, see Section A.4.

### 4.3.2 Simulation results

In this section, the optimal multi-pass control concept is applied and analyzed in simulations. Five rolling passes are considered. Before every rolling pass, the roll gap tilts and the trajectories of the lateral edger roll position are calculated and updated for all remaining rolling passes. After each rolling pass, the computed centerline is superposed with random measurement noise (uniformly distributed in the range $\left[-0.5\,\mathrm{mm}, 0.5\,\mathrm{mm}\right]$). For a representative scenario, the simulation results are shown in Figure 4.11. The initial centerline of the plate changes in every rolling pass and even if the camber is quite significant in some intermediate

passes, the plate shape after the final pass is straight. The reason for temporarily high camber is that the lateral position of the plate in the roll gap is forced to be small also in backward rolling passes where this can only be influenced by the constant roll gap tilt. In forward rolling passes, the lateral plate position in the roll gap is limited by the lateral position of the edger rolls anyway (cf., Section 2.7.1). The limits of the lateral edger roll position ($u^-_{max} = 100\,\mathrm{mm}$) are also respected. Due to the two control inputs (roll gap tilt $\Delta H$ and lateral position $u^-$ of the edger rolls) and the predictive behavior of the proposed algorithm, even the tail end, where edger rolls do not have a direct influence on the shape of the plate, can be straightened. In the last rolling pass, the roll gap tilt is forced to be small by an increased value of the corresponding entry in $\boldsymbol{\chi}_U$. This minimizes the thickness wedge of the final plate.

Compared to the status quo at the considered industrial plant (edger rolls remain centered, roll gap tilt is manually adjusted), the root mean square shape error

$$e_{rms} = \sqrt{\frac{1}{L^+}\int_0^{L^+} \left(\tilde{cl}^+\right)^2 \mathrm{d}z} \tag{4.39}$$

reduces from about 11.2 mm to about 0.4 mm, which is in the range of the assumed measurement noise. The final thickness wedge reduces from about 270 µm to almost zero.

The simulation study is done in MATLAB for five rolling passes. The plate is partitioned into $N = 101$ pieces yielding a step size $\Delta z^-$ of 120 mm in the first rolling pass to 401 mm in the last rolling pass. Here, the preparation of the matrices of (4.35) for five rolling passes lasts about 129 ms. Solving the constrained optimization problem (4.37) from the first to the last rolling pass takes about 376 ms, in the last rolling pass it takes about 46 ms. The proposed concept is thus real-time feasible.

## 4.4 Summary

In this chapter, three different control designs and their specific advantages, disadvantages and limitations were discussed. The first concept uses lateral forces applied by edger rolls as control input. The lateral plate position in the roll gap and the camber of the outgoing plate are controlled with a linear quadratic regulator (LQR). Nonlinear stiffness and damping coefficients in a subordinate admittance controller ensure safe plant operation.

The second concept directly uses the lateral position of the edger rolls as control input during forward rolling passes. This ensures a safe plant operation as long as the lateral position of the edger rolls is kept within certain bounds. These bounds can easily be incorporated in an optimization-based feedforward controller. However, the feedback control part of the two-degrees-of-freedom control concept does not guarantee a limited lateral position of the edger rolls. The overall lateral

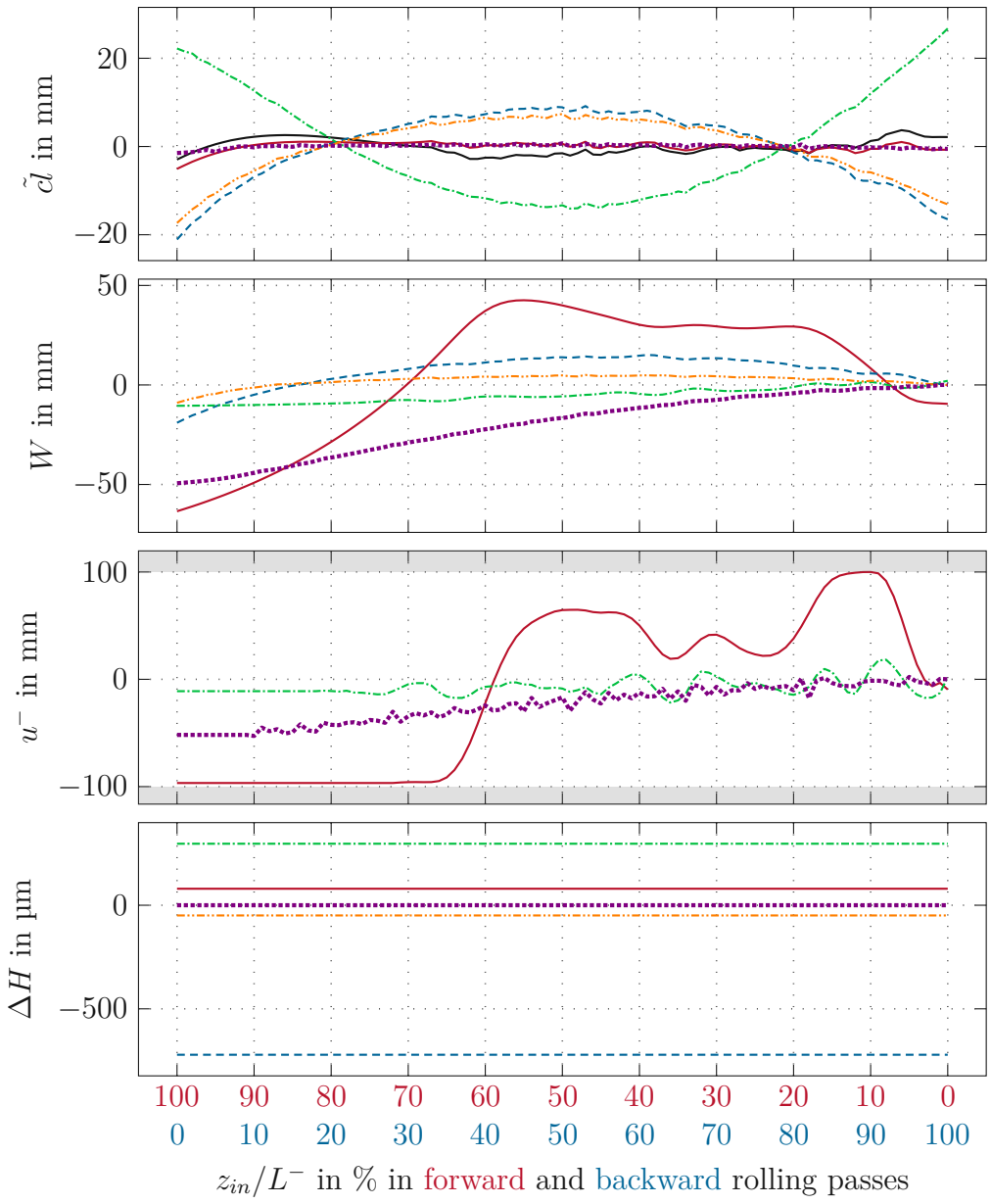


Figure 4.11: Incoming plate centerline (black) and resulting simulated plate centerlines after the first, second, third, fourth and fifth rolling pass. The lateral plate position in the roll gap $W$, the lateral position $u^-$ of the edger rolls and the roll gap tilt $\Delta H$ are shown with corresponding colors. Prohibited values of the lateral positions of the edger rolls are indicated in gray.

position of the edger rolls could be limited using box constraints but the rapid change of the edger velocity and acceleration would cause the plate to form an undesired camber. This strategy is thus not recommended. Generally, the use of the optimization-based feedforward controller and the two-degrees-of-freedom control structure both show significant reductions of the shape error.

The third control concept supposes that in addition to the lateral position of the edger rolls the roll gap tilt is also used as control input. Considering future rolling passes in this way proved to be a versatile and powerful control concept. It is not possible to distinguish between the model inputs thickness wedge and roll gap tilt due to the lack of suitable measurement systems at the industrial plant. Consequently, the feedforward controller from Section 4.2 seems most suitable for the industrial plant. The following chapter is thus dedicated to the implementation and results of this feedforward controller.

# CHAPTER 5

# Results

In the previous chapters, a mathematical model, its validation based on measurement data recorded at the industrial plant, and suitable control concepts were developed and discussed in detail. The presented mathematical models contain a number of simplifications and assumptions and despite an elaborate parametrization based on measurements, unknown disturbances and model-plant mismatches may occur. Hence a pilot installation of the control concept on the industrial plant is required. This chapter is dedicated to the implementation, commissioning, and performance evaluation of the proposed feedforward control concept at the considered industrial plant. Safe plate motion and improvement of the shape of the outgoing plate are the main objectives of the proposed concept.

Section 5.1 describes the implementation of the feedforward controller at the considered industrial plant. Numerical results are then discussed in Section 5.2.

## 5.1 Implementation at the industrial plant

In Section 4.2, a two-degrees-of-freedom control concept was proposed. It consists of an optimization-based feedforward controller and a feedback controller including a Smith predictor. In Section 4.2.3, it was shown in simulations that the optimization-based feedforward part of the control concept satisfies constraints of the lateral position, velocity, and acceleration of the edger rolls. However, the feedback part of the control concept does not consider these restrictions. Because these restrictions are essential for a safe plant operation, only the optimal feedforward controller is implemented on the industrial plant.

Between the end of the fourth and the beginning of the fifth rolling pass, the plate is typically descaled, transported, and aligned for the next rolling pass.

Within this time slot (usually a few seconds), the actual measurements (e. g., incoming plate centerline $cl^-$) and the parameters (e. g., roll gap tilt $\Delta H$, plate velocity $v_{en}$) are loaded and the feedforward controller is calculated. The plate is partitioned into $N = 201$ parts, which allows to solve the constrained optimization problem (4.20) in real time with a calculation time of about 150 ms. The input trajectories of the feedforward controller are then applied to the plant starting with the roll bite at the work rolls.

## 5.2 Performance of the proposed control concept at the industrial plant

In the daily operation of the industrial plant, the work roll tilt $\Delta H$ is adjusted by operators such that the camber and the thickness wedge of the final plate are small (typically a few centimeters camber at the head end and a few hundred micrometers thickness wedge). Thus, the optimal work roll tilt is a tradeoff in terms of safe plant operation (small camber) and product quality (small thickness wedge).

For safe commissioning of the proposed feedforward controller, the limit $u^-_{max}$ of the lateral edger position is successively increased from 1 cm to the final value 5 cm. Furthermore, the work roll tilt $\Delta H$ is successively changed so that the final thickness wedge is decreased (better product quality). The camber which results from the roll gap tilt is reduced and the safe plant operation has to be guaranteed by the feedforward controller. In rare cases, it is impossible to calculate an edger trajectory with the feedforward controller, e. g., because of bad image quality before the fifth rolling pass. Since safe plant operation must also be guaranteed in these cases, the work roll tilt $\Delta H$ cannot be chosen completely free.

Figures 5.1 and 5.2 show the measured resulting plate centerlines of two consecutively rolled plates (red). For these two plates, the environmental conditions (material class, temperature profile, roll gap tilt, ...) are known to be very similar. Therefore, these two plates facilitate an assessment of how the final plate centerline will look like if the feedforward controller is active (Figure 5.1, $u^- = u_{FF}$) and if the feedforward controller is not active (Figure 5.2, $u^- = 0$).

In the first case (Figure 5.1), the feedforward controller is active (red, $u^- = u_{FF}$). The resulting plate centerline has only a small curvature. The shape error (4.24) is 7.9 mm. A simulation shows how the plate centerline would look like if the feedforward controller were inactive (blue, $u^- = 0$). Without control, the plate has more camber. The shape error (4.24) is 13.5 mm (41.5 % better with feedforward control).

In the second case (Figure 5.2), the feedforward controller is inactive (red, $u^- = 0$). The resulting plate has a significant camber at the head end. The shape error (4.24) is 15.4 mm. A simulation study shows the calculated trajectory of

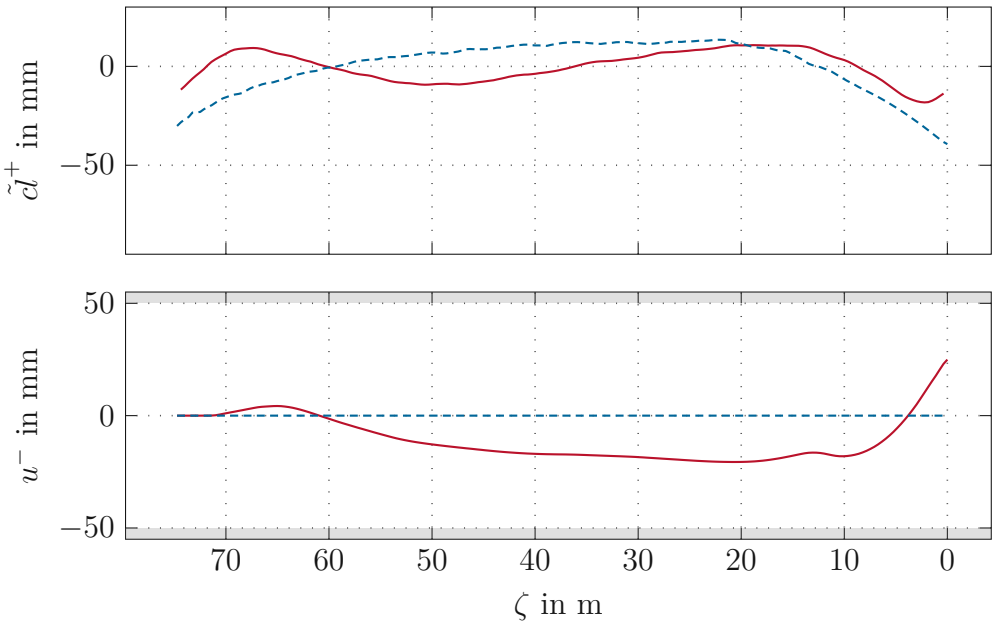


Figure 5.1: Comparison of plate centerlines with the feedforward controller with constraints (measured red [27, 28]) and without control (simulated blue (2.39)). The corresponding lateral edger positions $u^-$ are shown in the bottom plot. Prohibited values of the lateral positions of the edger rolls are indicated in gray.

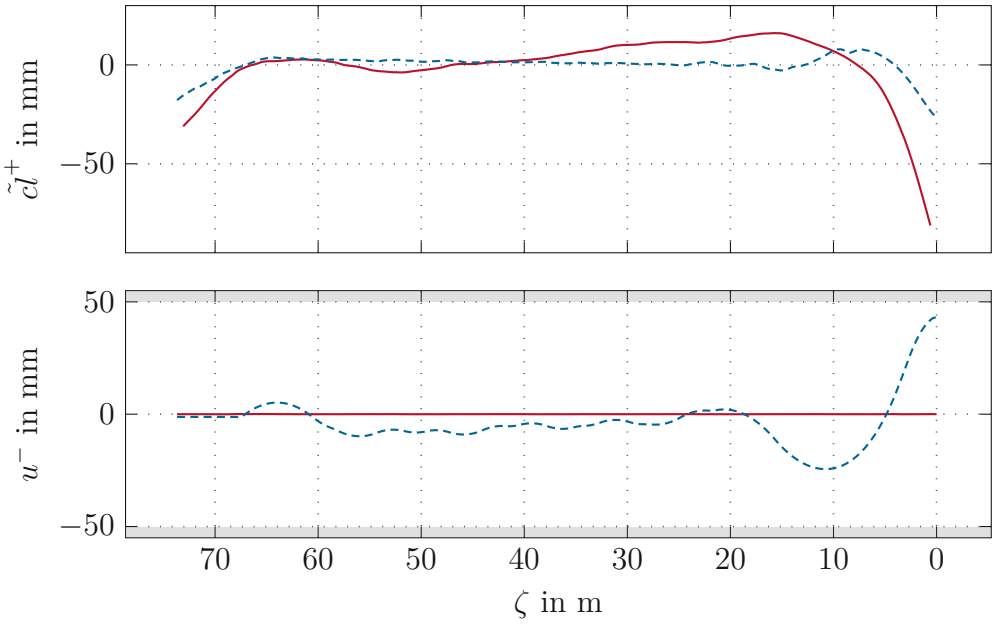


Figure 5.2: Comparison of plate centerlines without control (measured red [27, 28]) and with the feedforward controller with constraints (simulated blue (2.39)). The corresponding lateral edger positions $u^-$ are shown in the bottom plot. Prohibited values of the lateral positions of the edger rolls are indicated in gray.

the edger rolls and how the resulting shape of the plate would look like if the feedforward control were active (blue, $u^- = u_{FF}$). Then, camber (especially at the head end) would be much smaller. The shape error (4.24) would be 5.4 mm (64.9 % better with feedforward).

Figure 5.3 shows some resulting plate centerlines from the same measurement campaign. The considered plates are rolled with active feedforward controller (left column, $u^- = u_{FF}$) and inactive feedforward controller (right column, $u^- = 0$). Considering these representative measurements validates the above discussion.

The benefit of the proposed feedforward control is clearly shown based on these examples. Both, the experiments at the industrial plant and the simulation studies show that the straightness of the plate centerline (especially at the head end) is improved with feedforward control.

## 5.3 Summary

In this chapter, the implementation and the performance of the proposed feedforward controller of Section 4.2.1 at the industrial plant were discussed. For safe commissioning of the controller, the lateral limits $u^-_{max}$ of the edger rolls were successively increased and the roll gap tilt $\Delta H$ was successively changed so that the final thickness wedge is decreased.

The comparison of two consecutively rolled plates (one where the feedforward controller was active and one where it was inactive) clearly shows that the plate centerline is improved with the feedforward controller. Long-term data of resulting centerlines with active and inactive feedforward control should further confirm these results before switching to fully automatic permanent use of the feedforward controller at the industrial plant.

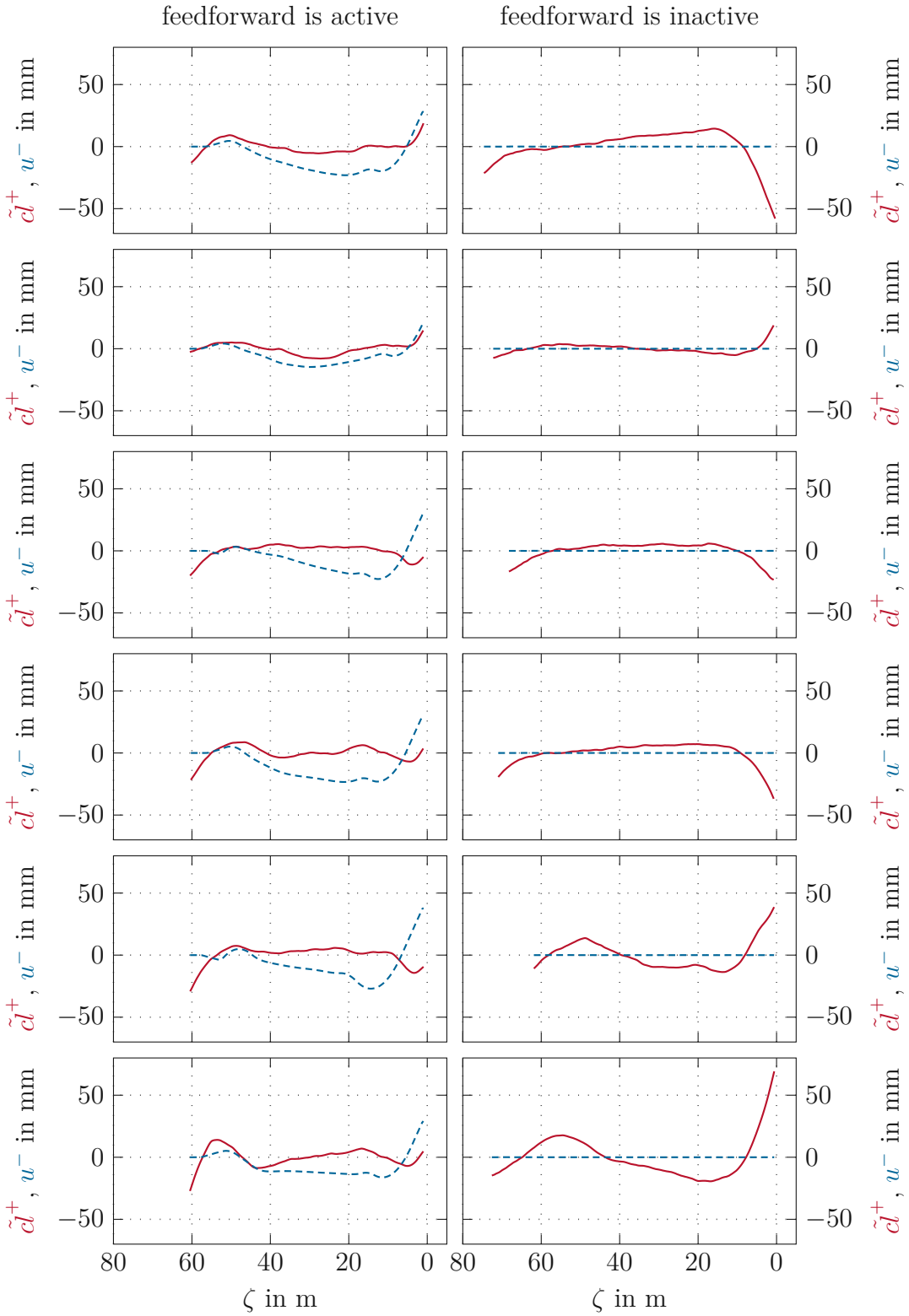


Figure 5.3: Comparison of plate centerlines with active (left column) and inactive (right column) feedforward controller with constraints (measured red [27, 28]). The corresponding lateral edger positions $u^-$ are shown in blue.

# CHAPTER 6

# Conclusions

The entire work as well as its challenges and results are summarized in Section 6.1. Section 6.2 provides suggestions for future research in this field and research questions that are still open.

## 6.1 Summary

In this work, a reversing rolling mill with edger rolls is considered. From the multiple objectives of the rolling process, the following are relevant for the current work.

- Safe plate motion: The plate should not touch any side guides or other parts along the line.
- Correct shape: The final shape of the plate centerline should be as straight as possible.

Lateral inhomogeneities, e. g., of the thickness or the temperature profile, make it difficult to meet these control objectives. Because the work rolls of the considered roughing mills are electromechanically adjusted with self-retaining screws, the frequently used control input *roll gap tilt* cannot be changed during rolling passes. The absence of this control input induces the central research question of this thesis: *Are edger rolls useful to control the plate motion and camber in a reversing rolling mill?*.

To answer this question, a first-principles model was presented and discussed. For system analysis, the mathematical model was presented in different forms:

- The force-input model covers lateral forces applied to the plate, upstream and downstream of the roll gap, as model input.
- The position-input model directly uses the lateral position of the edger rolls as control input.

Both models were analyzed in detail in terms of stability and effectiveness of the particular control input on the upstream side, downstream side, and on both sides of the roll gap. A key finding was that edger rolls on the entry side of the roll gap are stabilizing the rolling process and are a more effective control input than edger rolls on the exit side of the roll gap. A roughing mill with edger rolls active on both sides of the roll gap just yields a stable system dynamics if the distances from the roll gap to the edger rolls on the entry side and on the exit side satisfy certain relations. The mathematical model of the considered industrial plant is a special case of the position-input model, where edger rolls are active only on the entry side of the roll gap.

Another finding was that edger rolls are an adequate input to control the lateral plate motion and camber in a reversing roughing mill. However, this control input suffers a noteworthy disadvantage, compared to the more common control input roll gap tilt. A constant camber can only be compensated by a constant lateral force which requires a constant lateral acceleration of the edger rolls. In contrast, a constant camber can be compensated by a constant roll gap tilt. Insofar, edger rolls are not suitable to compensate for constant camber, but may be employed to eliminate (offset-free) deviations from the ideal straight centerline of the plate.

The mathematical model was validated based on measurement data recorded at the industrial plant. Uncertain model parameters were identified based on experiments conducted at the industrial plant. Harsh environmental conditions and the presence of only a few measurements were the main challenges in terms of model validation. The thickness profile is only measured once, at the end of the roughing process, which is why the influence of the thickness profile and the roll gap tilt cannot be clearly separated in the mathematical model and the constant roll gap tilt, which could be adjusted between the rolling passes, cannot be used as a second control input. However, the mathematical model and the measurement data showed good agreement. This applies to both the lateral position of the plate in the roll gap and the shape of the outgoing plate centerline.

The validated models served as a basis for control design. Three different control strategies were proposed and discussed. A challenge in this context was that the camber of the outgoing plate is only measured a few meters downstream of the roll gap but it is generated essentially in the roll gap. With the current measurement system, camber at the head end can thus not be straightened with simple feedback control. This problem does not occur with the optimization-based feedforward controller, which proved to be the best choice for the considered industrial plant. It is a safe and real-time feasible control approach, which can

also consider input constraints. Simulation studies showed that this approach has the potential to improve the straightness of the plate centerline by about 33.9 %.

The proposed feedforward controller was implemented in pilot installation at the industrial plant. After safe commissioning, a first test campaign at the industrial plant confirmed that the centerline of the outgoing plate can be clearly improved with the feedforward controller.

## 6.2 Outlook

Currently, the optimization-based feedforward control strategy is used in the industrial pilot installation. The performance is permanently monitored by trained human operators. The acceptance of the control strategy by the operators is promising. If the current tests continue to be successful, permanent use of the strategy will start in the near future.

Until now, the feedforward control is only used in the fifth rolling pass as this is the most essential rolling pass for the final product quality. However, after a new identification campaign, the proposed optimization-based feedforward control strategy can also be used for the third rolling pass. This would also be a necessary preparation for the proposed multi-pass approach. Even though, the optimization-based feedforward control yields promising results, the simulation studies showed that the multi-pass approach has even higher potential to improve the product quality. The multi-pass approach manipulates the shape of the plate in every rolling pass and also minimizes the thickness wedge of the final plate.

So far, the sensitivities of the proposed concept were only determined for one specific product class, but the proposed control concepts can be applied to all product classes. Due to various temperatures and the different metallurgical and geometrical properties of the products, it is expected that individual model parameters have to be identified for every product class. Parameters are expected to vary only in a certain range (without sign changes) and can be adapted based on any input trajectory which yields enough excitation. Thus it is expected that the optimization-based feedforward trajectory calculated for one product class can be used to adapt the model parameters of a new product class. In this case, the product quality is expected to improve with each additional plate of the considered product class.

Accurate measurements of thickness and temperature wedges before and after each rolling pass as well as measuring the roll gap height (under load) would greatly help to improve the model and reduce the model-plant mismatch. Furthermore, such measurements would facilitate a detailed analysis of the individual influences on the shape of the outgoing plate. Based on this knowledge, the (constant) roll gap tilt adjustment could also be used as a control input. A multi-pass control concept suitable for the case where this control input is available was also presented in this work and shows high potential.

Using edger rolls as alternative control inputs (compared to the roll gap tilt) led to new insights and excellent control results in this work. It was found that edger rolls, if active on the entry side of the roll gap, are very useful to correct variations of the camber and to control the lateral plate motion in the roll gap. However, the roll gap tilt is still the better control input if the plate has a constant camber over its whole length. With these insights, the question of a control concept using both, the lateral position of the edger rolls and a roll gap tilt which can be adjusted during the rolling pass, seems natural. Though this is impossible in the considered industrial plant, this can be a useful insight for the design of new reversing roughing mills.

# APPENDIX A

# Appendix

## A.1 Coordinate transformation of plate centerline

This section is dedicated to the rigid-body motion of the centerline $cl(z)$, represented by a rotation with the angle $\gamma$ and a shift with the offset $\mu$ such that the quadratic error between $cl(z)$ and the rotated and shifted centerline $\tilde{cl}(z)$ is minimized. For this, $cl(z)$ is spatially discretized at the positions $z_j = j\Delta z$ with the corresponding values $cl_j = cl(z_j)$, $j = 0, \ldots, k$. The angle $\gamma$ and the offset $\mu$ are the solution of the minimization problem

$$\min_{\gamma,\mu} \sum_{j=0}^{k} (z_j \sin(\gamma) + cl_j \cos(\gamma) + \mu)^2 \, . \tag{A.1}$$

Under the assumption of small angles $\gamma$, (A.1) can be rewritten in the form

$$\min_{\gamma,\mu} \left\| \begin{bmatrix} \mathbf{z} & \mathbf{1} \end{bmatrix} \begin{bmatrix} \gamma \\ \mu \end{bmatrix} + \mathbf{cl} \right\|_2^2 , \tag{A.2}$$

with $\mathbf{z} = \begin{bmatrix} 0, \ldots, k\Delta z \end{bmatrix}^{\mathrm{T}}$, $\mathbf{cl} = \begin{bmatrix} cl_0, \ldots, cl_k \end{bmatrix}^{\mathrm{T}}$ and $\mathbf{1}$ as the vector of ones. The solution of (A.2) reads as

$$\begin{bmatrix} \gamma \\ \mu \end{bmatrix} = -\left( \begin{bmatrix} \mathbf{z} & \mathbf{1} \end{bmatrix}^{\mathrm{T}} \begin{bmatrix} \mathbf{z} & \mathbf{1} \end{bmatrix} \right)^{-1} \begin{bmatrix} \mathbf{z} & \mathbf{1} \end{bmatrix}^{\mathrm{T}} \mathbf{cl} \, . \tag{A.3}$$

The rotated and shifted centerline can thus be calculated as

$$\tilde{\mathbf{cl}} = \mathbf{cl} + \begin{bmatrix} \mathbf{z} & \mathbf{1} \end{bmatrix} \begin{bmatrix} \gamma \\ \mu \end{bmatrix} = \underbrace{\left( \mathbf{I} - \begin{bmatrix} \mathbf{z} & \mathbf{1} \end{bmatrix} \left( \begin{bmatrix} \mathbf{z} & \mathbf{1} \end{bmatrix}^{\mathrm{T}} \begin{bmatrix} \mathbf{z} & \mathbf{1} \end{bmatrix} \right)^{-1} \begin{bmatrix} \mathbf{z} & \mathbf{1} \end{bmatrix}^{\mathrm{T}} \right)}_{\mathbf{S}} \mathbf{cl} \,, \tag{A.4}$$

with the identity matrix $\mathbf{I}$ and the transformation matrix $\mathbf{S}$.

## A.2 Recurring adaptation of the uncertain parameters

The centerline $cl^+$ of the outgoing plate is influenced by the uncertain parameters

- $f_{E_l}$ and $f_{K_\Sigma}$ (control the sensitivity of the control input $u^-$ on $cl_{x,u}$),
- $f_{f\Delta hH}$ (models the correlation between $f_{\Delta hH}^{(5)}$ and $f_{\Delta hH}^{(4)}$), and
- $W_{0,offset}$ (captures possible asymmetries of the plant).

These parameters are estimated with the optimization problems (3.9), (3.10) and the relation (3.11) for a specific material class and for groups of consecutively rolled plates. For other material classes, in particular the parameters $f_{E_l}$ and $f_{K_\Sigma}$ must be newly identified. For this identification step, any trajectory with enough excitation at the input $u^-$ (and thus $cl_{x,u}$) can be used. Furthermore, the parameters $f_{f\Delta hH}$ and $W_{0,offset}$ may change over time due to varying reheating characteristics or damaged or maintained plant equipment (side guides, work rolls, ...). Thus, for permanent use of the mathematical model or model-based control concepts at the industrial plant, recurring adaptation of the parameters in the form

$$\breve{\mathbf{x}}_{par,k+1} = \breve{\mathbf{x}}_{par,k} + \boldsymbol{\chi}_{par}^{-1} (\mathbf{x}_{par,k} - \breve{\mathbf{x}}_{par,k}) \tag{A.5}$$

with $\mathbf{x}_{par} = \begin{bmatrix} f_{E_l} & f_{K_\Sigma} & f_{f\Delta hH} & W_{0,offset} \end{bmatrix}^{\mathrm{T}}$, $\mathbf{x}_{par,k}$ of (3.9), (3.10) and (3.11), the positive definite, diagonal weighting matrix $\boldsymbol{\chi}_{par}$, and the plate index $k$ is recommended. The weighting matrix $\boldsymbol{\chi}_{par}$ is a user-defined design parameter. In case of a step-wise change of the parameters, the entries in the diagonal of $\boldsymbol{\chi}_{par}$ indicate how many plates have to be rolled to change the estimated parameter by about 63 % of the total change. Figure A.1 exemplary shows the estimation of the parameter $W_{0,offset}$. The initial value $\breve{\mathbf{x}}_{par,0}$ is chosen as $\mathbf{0}$ and the corresponding entry of the weighting matrix $\boldsymbol{\chi}_{par}$ as 100. For comparison, the mean value of the histogram in Figure 3.7 is chosen as $W_{0,offset}$, see black line in Figure A.1.

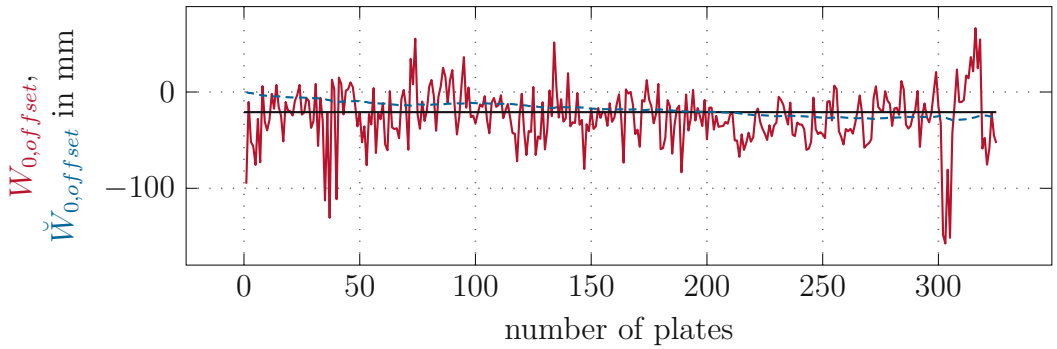


Figure A.1: Offset $W_{0,offset}$, estimated based on (3.9), its mean value in black and recurrently adapted offset $\breve{W}_{0,offset}$ based on (A.5).

## A.3 Constraints for optimization-based feedforward control

In this section, the implementation of the constraints used in the optimization-based approach of Section 4.2 and Section 4.3 is outlined. The limits of the lateral position $u^- \in \begin{bmatrix} -u^-_{max} & u^-_{max} \end{bmatrix}$ are implemented as

$$\begin{bmatrix} u^-_{k-1} \\ u^-_{k-1} \\ \vdots \\ u^-_{k-1} \end{bmatrix} + \begin{bmatrix} 1 & 0 & \dots & 0 \\ 1 & 1 & \ddots & 0 \\ \vdots & \ddots & \ddots & \vdots \\ 1 & 1 & \dots & 1 \end{bmatrix} \Delta\mathbf{U} \leq \begin{bmatrix} u^-_{max} \\ u^-_{max} \\ \vdots \\ u^-_{max} \end{bmatrix}$$

and

$$\begin{bmatrix} u^-_{k-1} \\ u^-_{k-1} \\ \vdots \\ u^-_{k-1} \end{bmatrix} + \begin{bmatrix} 1 & 0 & \dots & 0 \\ 1 & 1 & \ddots & 0 \\ \vdots & \ddots & \ddots & \vdots \\ 1 & 1 & \dots & 1 \end{bmatrix} \Delta\mathbf{U} \geq -\begin{bmatrix} u^-_{max} \\ u^-_{max} \\ \vdots \\ u^-_{max} \end{bmatrix} \tag{A.6}$$

Analogously, constraints on the velocity are implemented as

$$\begin{bmatrix} 1 & 0 & \dots & 0 \\ 0 & 1 & \ddots & 0 \\ \vdots & \ddots & \ddots & \vdots \\ 0 & 0 & \dots & 1 \end{bmatrix} \Delta\mathbf{U} \leq \begin{bmatrix} \frac{v^-_{max}}{v_{en,k}} \\ \frac{v^-_{max}}{v_{en,k+1}} \\ \vdots \\ \frac{v^-_{max}}{v_{en,k+l}} \end{bmatrix} \Delta z^-$$

and

$$\begin{bmatrix} 1 & 0 & \dots & 0 \\ 0 & 1 & \ddots & 0 \\ \vdots & \ddots & \ddots & \vdots \\ 0 & 0 & \dots & 1 \end{bmatrix} \Delta\mathbf{U} \geq - \begin{bmatrix} \frac{v_{max}^-}{v_{en,k}} \\ \frac{v_{max}^-}{v_{en,k+1}} \\ \vdots \\ \frac{v_{max}^-}{v_{en,k+l}} \end{bmatrix} \Delta z^- \ , \tag{A.7}$$

with the absolute maximum lateral velocity $v_{max}^-$ of the edger rolls. The feedforward controller is based on the time-free formulation of the model (2.39) and (2.40) with equidistant spatial grid points. This is why the velocity $v_{en}$ occurs on the right-hand side of (A.7). At the time the feedforward controller is calculated, the planned rolling velocity $u_r$ is known. Using (2.8) and (2.7) according to the Sims model, the velocity $v_{en}$ can be calculated in advance. The acceleration of the edger rolls can also be restricted by

$$\begin{bmatrix} 1 & 0 & \dots & 0 \\ -1 & 1 & \ddots & 0 \\ \vdots & \ddots & \ddots & \vdots \\ 0 & 0 & \dots & 1 \end{bmatrix} \Delta\mathbf{U} \leq \begin{bmatrix} \frac{a_{max}^-}{v_{en,k}^2} \\ \frac{a_{max}^-}{v_{en,k+1}^2} \\ \vdots \\ \frac{a_{max}^-}{v_{en,k+l}^2} \end{bmatrix} \left(\Delta z^-\right)^2$$

and

$$\begin{bmatrix} 1 & 0 & \dots & 0 \\ -1 & 1 & \ddots & 0 \\ \vdots & \ddots & \ddots & \vdots \\ 0 & 0 & \dots & 1 \end{bmatrix} \Delta\mathbf{U} \geq - \begin{bmatrix} \frac{a_{max}^-}{v_{en,k}^2} \\ \frac{a_{max}^-}{v_{en,k+1}^2} \\ \vdots \\ \frac{a_{max}^-}{v_{en,k+l}^2} \end{bmatrix} \left(\Delta z^-\right)^2 \ , \tag{A.8}$$

with the absolute maximum lateral acceleration $a_{max}^-$ of the edger rolls. Because of the definition of $\Delta\mathbf{U}$ in (4.13c) and (4.15b), the formulation (A.8) results in the central difference quotient

$$a_k \propto \frac{\Delta u_{k+1} - \Delta u_k}{\left(\Delta z^-\right)^2} = \frac{u_{k+1} - 2u_k + u_{k-1}}{\left(\Delta z^-\right)^2} \tag{A.9}$$

for the acceleration. Its approximation error is of the order $\mathcal{O}\left(\left(\Delta z^-\right)^2\right)$ [61].

## A.4 Time-varying formulation of the optimal feedforward control

This part of the appendix covers a time-varying formulation of the model (4.13). With this formulation, it is possible to mathematically cover, e. g., the fact that edger rolls are not active at the end of the rolling pass. For the time-varying case, the solution (4.13) for $\mathbf{x}_{k+l}$ and $\mathbf{y}_{k+l}$ can be written as

$$\mathbf{x}_{k+l} = \prod_{i=k}^{k+l-1} \mathbf{\Phi}_i \mathbf{x}_k + \sum_{j=k}^{k+l-1} \prod_{i=j}^{k+l-2} \mathbf{\Phi}_i \mathbf{\Gamma}_{u,j} \left( u_{k-1}^- + \sum_{m=k}^{j} \Delta u_m^- \right) \tag{A.10a}$$

$$\mathbf{y}_{k+l} = \mathbf{C}_{k+l} \mathbf{x}_{k+l} + \mathbf{D}_{k+l} \left( cl_{k+l}^- + cl_{\Delta hH,k+l} \right) , \tag{A.10b}$$

with the left-sided product according to

$$\prod_{i=n}^{m} \mathbf{\Phi}_i = \begin{cases} \mathbf{\Phi}_m \dots \mathbf{\Phi}_{n+1} \mathbf{\Phi}_n , & n \leq m \\ \mathbf{I} , & n > m \end{cases} \tag{A.11}$$

and the identity matrix $\mathbf{I}$. Similar to (4.14), the time-varying counterpart can be written as

$$\mathbf{Y} = \mathbf{F}_{x,k} \mathbf{x}_k + \mathbf{F}_{u,k} u_{k-1} + \mathbf{F}_{\Delta u,k} \Delta \mathbf{U} + \mathbf{F}_{cl,k} \left( \mathbf{C}\mathbf{L}^- + \mathbf{C}\mathbf{L}_{\Delta hH} \right) \tag{A.12a}$$

with

$$\mathbf{F}_{x,k} = \begin{bmatrix} \mathbf{C}_k \\ \mathbf{C}_{k+1} \mathbf{\Phi}_k \\ \vdots \\ \mathbf{C}_{k+l} \prod_{i=k}^{k+l-1} \mathbf{\Phi}_i \end{bmatrix} \tag{A.12b}$$

$$\mathbf{F}_{u,k} = \begin{bmatrix} \mathbf{0} \\ \mathbf{C}_{k+1} \mathbf{\Gamma}_{u,k} \\ \vdots \\ \mathbf{F}_{\Delta u,l,1,k} \end{bmatrix} \tag{A.12c}$$

$$\mathbf{F}_{\Delta u,k} = \begin{bmatrix} \mathbf{0} & \mathbf{0} & \dots & \mathbf{0} \\ \mathbf{C}_{k+1} \mathbf{\Gamma}_u & \mathbf{0} & \dots & \mathbf{0} \\ \vdots & \vdots & \ddots & \vdots \\ \mathbf{F}_{\Delta u,l,1,k} & \mathbf{F}_{\Delta u,l,2,k} & \dots & \mathbf{0} \end{bmatrix} \tag{A.12d}$$

$$\mathbf{F}_{cl,k} = \begin{bmatrix} \mathbf{D}_k & \mathbf{0} & \dots & \mathbf{0} \\ \mathbf{0} & \mathbf{D}_{k+1} & \dots & \mathbf{0} \\ \vdots & \vdots & \ddots & \vdots \\ \mathbf{0} & \mathbf{0} & \dots & \mathbf{D}_{k+l} \end{bmatrix} \tag{A.12e}$$

as well as

$$\mathbf{F}_{\Delta u,n,m,k} = \mathbf{C}_{k+n-1} \sum_{j=k+m-1}^{k+n-1} \prod_{i=j+1}^{k+n-1} \mathbf{\Phi}_i \mathbf{\Gamma}_j \ . \tag{A.12f}$$

## A.5 Second derivative by matrix multiplication

The second derivative of the centerline $cl^+$ at an arbitrary spatial point $k$ can be numerically approximated by the central difference quotient

$$\frac{\mathrm{d}^2}{\mathrm{d}\zeta^2} cl_k^+ \approx \frac{cl_{k+1}^+ - 2cl_k^+ + cl_{k-1}^+}{\Delta\zeta^2} \ . \tag{A.13}$$

At the head (tail) end, the spatial point $cl_{k+1}^+$ ($cl_{k-1}^+$) does not exist. Thus, at the boundaries, the forward

$$\frac{\mathrm{d}^2}{\mathrm{d}\zeta^2} cl_k^+ \approx \frac{cl_{k+2}^+ - 2cl_{k+1}^+ + cl_k^+}{\Delta\zeta^2} \tag{A.14}$$

or backward difference quotient

$$\frac{\mathrm{d}^2}{\mathrm{d}\zeta^2} cl_k^+ \approx \frac{cl_k^+ - 2cl_{k-1}^+ + cl_{k-2}^+}{\Delta\zeta^2} \tag{A.15}$$

is used. In matrix notation, these difference quotients can be assembled as

$$\left[\frac{\mathrm{d}^2}{\mathrm{d}\zeta^2} cl_k^+ \quad \dots \quad \frac{\mathrm{d}^2}{\mathrm{d}\zeta^2} cl_{k+l}^+\right]^{\mathrm{T}} \approx \frac{1}{\Delta\zeta^2} \mathbf{DD} \cdot \mathbf{CL}^+ \ , \tag{A.16}$$

with $\mathbf{CL}^+ = \left[cl_k^+ \quad \dots \quad cl_{k+l}^+\right]^{\mathrm{T}}$ and

$$\mathbf{DD} = \begin{bmatrix} 1 & -2 & 1 & 0 & \dots & 0 \\ 1 & -2 & 1 & 0 & \dots & 0 \\ 0 & 1 & -2 & 1 & \dots & 0 \\ \vdots & \ddots & \ddots & \ddots & \ddots & \vdots \\ 0 & \dots & 0 & 1 & -2 & 1 \\ 0 & \dots & 0 & 1 & -2 & 1 \end{bmatrix} \ . \tag{A.17}$$

The approximation order is $\mathcal{O}(\Delta\zeta^2)$ [61].

# Bibliography


[1] *Sustainable steel – indicators 2020 and steel applications*, report, worldsteel association, Belgium, Brussels, 2020.

[2] F. Schausberger, A. Steinboeck, and A. Kugi, "Optimization-based reduction of contour errors of heavy plates in hot rolling", *Journal of Process Control*, vol. 47, pp. 150–160, 2016.

[3] F. Schausberger, A. Steinboeck, and A. Kugi, "Feedback control of the contour shape in heavy-plate hot rolling", *IEEE Transactions on Control Systems Technology*, vol. 26, no. 3, pp. 842–856, 2018.

[4] D. Xu, Y. Liu, X. Wang, Q. Yang, Z. Dai, and X. Wang, "Research and application on slab camber control model in hot rolling", *Ironmaking and Steelmaking*, vol. 47, no. 7, pp. 781–789, 2020.

[5] S. M. Byon and Y. Lee, "An investigation on the effect of design parameters of side guide on camber in hot slab rolling", *Materials and Manufacturing Processes*, vol. 29, no. 2, pp. 107–114, 2014.

[6] M. Kurz, R. Döll, A. Kainz, T. Pumhössel, and K. Zeman, "Wedge and camber control", in *Proceedings of METEC and 2nd ESTAD*, Düsseldorf, Germany, 2015, pp. 1–10.

[7] A. Kainz, T. Pumhoessel, M. Kurz, M. Widder, L. Aigner, and K. Zeman, "Prediction of camber formation, suppression and control of wedge-shaped hot rolled slabs by analytical concepts and finite elements", *IFAC-PapersOnLine*, vol. 49, no. 20, pp. 238–243, 2016.

[8] H.-K. Hsu and J.-N. Aoh, "The mechanism of position-mode side guide in correcting camber in roughing process of a hot strip mill", *Metals*, vol. 9, no. 5, pp. 504–519, 2019.

[9] D. J. Yun, D. Lee, J. Kim, and S. M. Hwang, "A new model for the prediction of the dog-bone shape in steel mills", *ISIJ International*, vol. 52, no. 6, pp. 1109–1117, 2012.

[10] R. Fabík, "Laboratory and mathematical simulation of slab edging", in *Proceedings of the 19th International Conference on Metallurgy and Materials, METAL 2010*, Roznov Pod Radhostem, Czech Republic, 2010, pp. 339–345.

[11] J. Cao, Y. Liu, F. Luan, and D. Zhao, "The calculation of vertical rolling force by using angular bisector yield criterion and Pavlov principle", *The International Journal of Advanced Manufacturing Technology*, vol. 86, no. 9, pp. 2701–2710, 2016.

[12] A. Pesin and D. Pustovoytov, "Finite element modeling of influence of roll form of vertical scale breaker on decreased formation of surface defects during roughing hot rolling", *Key Engineering Materials*, vol. 685, pp. 181–185, 2016.

[13] Y. Liu, J. Sun, D. Zhang, and D. Zhao, "Three-dimensional analysis of edge rolling based on dual-stream function velocity field theory", *Journal of Manufacturing Processes*, vol. 34, pp. 349–355, 2018.

[14] A. Ettl, K. Prinz, M. Mueller, A. Steinboeck, and A. Kugi, "Mathematical model and stability analysis of the lateral plate motion in a reversing rolling mill stand", *IFAC-PapersOnLine*, vol. 51, no. 2, pp. 73–78, 2018.

[15] F. Schausberger, A. Steinboeck, and A. Kugi, "Mathematical modeling of the contour evolution of heavy plates in hot rolling", *Applied Mathematical Modelling*, vol. 39, pp. 4534–4547, 2015.

[16] A. Steinboeck, A. Ettl, and A. Kugi, "Dynamical models of the camber and the lateral position in flat rolling", *Applied Mechanics Reviews*, vol. 69, no. 4, pp. 1–14, 2017.

[17] K. Prinz, A. Steinboeck, M. Müller, A. Ettl, and A. Kugi, "Automatic gauge control under laterally asymmetric rolling conditions combined with feedforward", *IEEE Transactions on Industry Applications*, vol. 53, no. 3, pp. 2560–2568, 2017.

[18] K. Prinz, F. Schausberger, A. Steinboeck, and A. Kugi, "Feedforward control of lateral asymmetries in heavy-plate hot rolling using vision-based position estimation", *IFAC-PapersOnLine*, vol. 50, no. 1, pp. 11 307–11 312, 2017.

[19] K. Prinz, A. Steinboeck, and A. Kugi, "Optimization-based feedforward control of the strip thickness profile in hot strip rolling", *Journal of Process Control*, vol. 64, pp. 100–111, 2018.

[20] M. Müller, A. Steinboeck, K. Prinz, and A. Kugi, "Optimal parameter identification for a hydrodynamic roll gap model in hot strip rolling", *IFAC-PapersOnLine*, vol. 51, no. 21, pp. 195–200, 2018.

[21] M. Müller, A. Steinboeck, K. Prinz, A. Ettl, A. Kugi, K. Etzelsdorfer, S. Fuchshumer, and H. Seyrkammer, "Asymmetric hydrodynamic roll gap model and its experimental validation", *International Journal of Advanced Manufacturing Technology*, vol. 100, no. 9-12, pp. 3101–3111, 2019.

[22] M. Müller, K. Prinz, A. Steinboeck, F. Schausberger, and A. Kugi, "Adaptive feedforward thickness control in hot strip rolling with oil lubrication", *Control Engineering Practice*, vol. 103, pp. 104584 1–13, 2020.

[23] J. G. Ding, Y. H. C. He, L. P. Kong, and W. Peng, "Camber prediction based on fusion method with mechanism model and machine learning in plate rolling", *ISIJ International*, vol. 61, no. 10, pp. 2540–2551, 2021.

[24] M. S. Kim, Y. J. Choi, I. S. Park, N. W. Kong, M. Lee, and P. G. Park, "Sensitivity analysis on a neural network for analyzing the camber in hot rolling process", in *Proceedings of the 2018 IEEE Industrial Cyber-Physical Systems Conference*, St. Petersburg, Russia, 2018, pp. 212–216.

[25] Y. Tanaka, K. Omori, T. Miyake, K. Nishizaki, M. Inoue, and S. Tezuka, "Camber control techniques in plate rolling", *Kawasaki Steel*, vol. 16, pp. 12–20, 1987.

[26] R. C. González, R. Valdés, and J. A. Cancelas, "Vision based measurement system to quantify straightness defect in steel sheets", in *Proceedings of the 9th International Conference on Computer Analysis of Images and Patterns*, Warsaw, Poland, 2001, pp. 427–434.

[27] H. Hlobil, K. Niel, M. Prinz, G. Trinkl, W. Seyruck, and J. Reisinger, "Camber measurement at hot strip mill at voestalpine by using image processing method", in *Proceedings of SPIE - The International Society for Optical Engineering*, vol. 5679, San Jose, United States, 2005, pp. 140–145.

[28] H. Hlobil, J. Reisinger, G. Trinkl, A. Wurm, and M. Traugott, "Optical measurement systems for quality improvement in hot strip mill and plate mill technology", in *Proceedings of 14th International Metallurgical & Material Conference*, Hradec nad Moravicí, Czech Republic, 2005, pp. 1–5.

[29] R. J. Montague, J. Watton, and K. J. Brown, "A machine vision measurement of slab camber in hot strip rolling", *Journal of Materials Processing Technology*, vol. 168, pp. 172–180, 2005.

[30] J. W. Yoo, N. W. Kong, J. Song, and P. G. Park, "Camber detection algorithm using the image stitching technique in hot-rolling process", in *Proceedings of the International Conference on Robotics*, Phuket, Thailand, 2010, pp. 74–77.

[31] J. Lee, N. Kong, J. Yoo, and P. Park, "A fast image stitching algorithm in the endless hot rolling process", in *Proceedings of the 11th International Conference on Control, Automation and Systems*, Gyeonggi-do, Korea, 2011, pp. 1264–1268.

[32] N. W. Kong, J. W. Yoo, J. S. Lee, S. W. Yun, J. Bae, and P. G. Park, "Vision-based camber measurement system in the endless hot rolling process", *Optical Engineering*, vol. 50, no. 10, pp. 1–11, 2011.

[33] J. Canny, "A computational approach to edge detection", *IEEE Transactions on Pattern Analysis and Machine Intelligence*, vol. 8, pp. 679–698, 1986.

[34] B. N. Carruthers-Watt, Y. Xue, and A. J. Morris, "A vision based system for strip tracking measurement in the finishing train of a hot strip mill", in *Proceedings of the 2010 IEEE International Conference on Mechatronics and Automation*, Xi'an, China, 2010, pp. 1115–1120.

[35] I. Malloci, J. Daafouz, C. Iung, R. Bonidal, and P. Szczepanski, "Robust steering control of hot strip milling", *IEEE Transactions on Control Systems Technology*, vol. 18, no. 4, pp. 908–917, 2010.

[36] H. Furumoto, S. Kanemori, and T. Takeguchi, "Reduction of off-centering at tail end caused by unstable work roll position with mill stabilizing device in hot rolling", *Procedia Engineering*, vol. 207, pp. 1373–1378, 2017.

[37] F. Schausberger, C. Pietschnig, A. Ettl, A. Steinboeck, and A. Kugi, "Optimization-based estimator for the lateral strip position in tandem hot rolling", *IFAC-PapersOnLine*, vol. 54, no. 11, pp. 7–12, 2021.

[38] U. Knechtelsdorfer, A. Steinboeck, F. Schausberger, and A. Kugi, "A novel mass flow controller for tandem hot rolling mills", *Journal of Process Control*, vol. 104, pp. 168–177, 2021.

[39] F. Schausberger, A. Steinboeck, and A. Kugi, "Optimization-based estimator for the contour and movement of heavy plates in hot rolling", *Journal of Process Control*, vol. 29, pp. 23–32, 2015.

[40] A. Sun, "Development of an interactive virtual environment for training manufacturing operators", Ph.D. dissertation, Purdue University Graduate School, Purdue, USA, 2020.

[41] C. Pietschnig, A. Ettl, U. Knechtelsdorfer, A. Steinboeck, and A. Kugi, "Optimal control of plate motion and camber in a reversing rolling mill", *IFAC-PapersOnLine*, vol. 53, no. 2, pp. 11 962–11 967, 2020.

[42] C. Pietschnig, A. Steinboeck, and A. Kugi, "Are edger rolls useful to control the plate motion and camber in a reversing rolling mill?", *Journal of Process Control*, vol. 114, pp. 71–81, 2022.

[43] C. Pietschnig, A. Steinboeck, and A. Kugi, "Optimal control of motion and camber of steel plates in a multi-pass reversing rolling process", *IFAC-PapersOnLine*, vol. 55, no. 21, pp. 180–185, 2022.

[44] J. Lenard, *Primer on Flat Rolling*, 2nd. Oxford: Elsevier, 2014.

[45] S. Timoshenko and J. N. Goodier, *Theory of Elasticity*, 3rd. New York: McGraw-Hill, 1969.

[46] R. B. Sims, "The calculation of roll force and torque in hot rolling mills", en, *Proceedings of the Institution of Mechanical Engineers*, vol. 168, no. 1, pp. 191–200, 1954.

[47] D. R. Bland and H. Ford, "The calculation of roll force and torque in cold strip rolling with tensions", *Proceedings of the Institution of Mechanical Engineers*, vol. 159, no. 1, pp. 144–163, 1948.

[48] U. Knechtelsdorfer, M. Müller, A. Steinboeck, and A. Kugi, "Slip model adaptation based on measurements of the strip velocity", *IFAC-PapersOnLine*, vol. 52, no. 14, pp. 42–47, 2019.

[49] C. T. Chen, *Linear System Theory and Design*. USA: Oxford University Press, 1984.

[50] C. W. José Hol, J. de Roo, L. Kampmeijer, T. Dirkson, G. Schipper, M. La Maire, and J. van der Lugt, "Model predictive controller for strip-tracking during tail-out of the finishing mill", *IFAC-PapersOnLine*, vol. 46, no. 16, pp. 397–402, 2013.

[51] A. Hensel and T. Spittel, *Kraft- und Arbeitsbedarf bildsamer Formgebungsverfahren*. Leipzig: VEB Deutscher Verlag für Grundstoffindustrie, 1978.

[52] M. Spittel and T. Spittel, *Metal Forming Data of Ferrous Alloys - Deformation Behaviour*, H. Warlimont, Ed. Berlin, Heidelberg: Springer, 2009.

[53] K. Johnson, *Contact Mechanics*. New York: Cambridge University Press, 1992.

[54] A. Savitzky and M. J. Golay, "Smoothing and differentiation of data by simplified least squares procedures.", *Analytical chemistry*, vol. 36, no. 8, pp. 1627–1639, 1964.

[55] S. Flixeder, T. Glück, and A. Kugi, "Force-based cooperative handling and lay-up of deformable materials: Mechatronic design, modeling, and control of a demonstrator", *Mechatronics*, vol. 47, pp. 246–261, 2017.

[56] F. Schausberger, A. Steinboeck, A. Kugi, M. Jochum, D. Wild, and T. Kiefer, "Vision-based material tracking in heavy-plate rolling", *IFAC-PapersOnLine*, vol. 49, no. 20, pp. 108–113, 2016.

[57] L. Wang, *Model Predictive Control System Design and Implementation Using MATLAB®*. London: Springer, 2009.

[58] S. Bajtela, "Regelung des Einlaufes in das Vorgerüst unter Verwendung von Staucherwalzen", Bachelor Thesis, TU Wien, Vienna, Austria, 2022.

[59] N. Abe and K. Yamanaka, "Smith predictor control and internal model control - A tutorial", in *Proceedings of SICE Annual Conference*, Fukui, Japan, 2003, pp. 1383–1387.

[60] J.E. Normey-Rico and E.F Camacho, *Control of Dead-time Processes*. London: Springer, 2007.

[61] U. M. Ascher and C. Greif, *A First Course in Numerical Methods*. USA: Society for Industrial and Applied Mathematics, 2011.

# Eidesstattliche Erklärung

Ich erkläre an Eides statt, dass die vorliegende Arbeit nach den anerkannten Grundsätzen für wissenschaftliche Abhandlungen von mir selbstständig erstellt wurde. Alle verwendeten Hilfsmittel, insbesondere die zugrunde gelegte Literatur, sind in dieser Arbeit genannt und aufgelistet. Das Thema dieser Arbeit wurde von mir bisher weder im In- noch Ausland einer Beurteilerin/einem Beurteiler zur Begutachtung in irgendeiner Form als Prüfungsarbeit vorgelegt. Diese Arbeit stimmt mit der von den Begutachterinnen/Begutachtern beurteilten Arbeit überein.

Wien, November 2022 Christopher Pietschnig